RATIONAL TARGETING OF SURVIVIN'S NUCLEAR EXPORT SIGNAL BY SUPRAMOLECULAR LIGANDS – ENHANCEMENT OF NES BINDER SPECIFICITY

Dissertation

zur Erlangung des Doktorgrades

Dr. rer. nat.
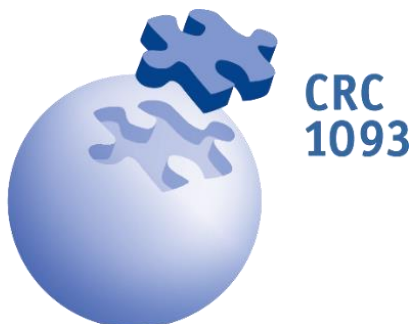
der Fakultät für Biologie

an der Universität Duisburg-Essen

vorgelegt von

Annika Meiners

aus Ratingen

Oktober 2020

Die der vorliegenden Arbeit zugrundeliegenden Experimente wurden am Zentrum für Medizinische Biotechnologie (ZMB) in der Abteilung für Molekularbiologie II der Universität Duisburg-Essen durchgeführt.

1. Gutachter: Prof. Dr. Shirley Knauer

2. Gutachter: Prof. Dr. Hemmo Meyer

3. Gutachter: Prof. Dr. Aphrodite Kapurniotu

Vorsitzender des Prüfungsausschusses: Prof. Dr. Stefan Westermann

Tag der mündlichen Prüfung: 25.02.2021

In the context of this doctoral work, the following articles were submitted for publication:

Meiners, Annika;‡ Bäcker, Sandra;‡ Heid, Christian;‡ Hadrovic, Inesa;‡ Beuck, Christine; Ruiz-Blanco, Yasser; Mieres-Perez, Joel; Pörschke, Marius; Grad, Jean-Noël; Vallet, Cecilia; Hofmann, Daniel; Bayer, Peter; Sanchez-Garcia, Elsa; Schrader, Thomas; Knauer, Shirley (2020): **Targeting a protein epitope: Specific inhibition of the Survivin-CRM1-interaction by peptide-modified Molecular Tweezers.** *Nature Communications*, in revision.
‡ equal contribution

van der Meer, Selina; Hadrovic, Inesa; Meiners, Annika; Heggen, Marc; Loza, Kateryna; Knauer, Shirley K.; Bayer, Peter; Schrader, Thomas; Beuck, Christine; Epple, Matthias (2020): **New Tools to Probe the Protein Surface: Ultrasmall Gold Nanoparticles carry Amino Acid Binders.** *Chemistry – A European Journal*, submitted.

TABLE OF CONTENT

SUMMARY

The protein Survivin is overexpressed in most types of cancer and considered a cytoprotective factor, correlating with resistance against chemo- and radiotherapy. As Survivin is mostly absent in normal resting tissues, it is a very cancer-specific protein and its increased occurrence in tumor cells has been associated with poor patient prognosis. Survivin features a nuclear export signal (NES) [89]VKKQFEELTL[98], which is recognized by the export receptor Crm1. This protein-protein interaction is not only required for the cytoprotective activity of Survivin, but also pivotal for its mitotic function. Thus, it represents a promising target for cancer research and therapy. Since Crm1 does not only serve as an export receptor for Survivin but has many different cargos, targeting Crm1 does not specifically inhibit the interaction with Survivin. So far, most Crm1 inhibitors revealed dose-limiting toxicity and severe side effects as they interfere with a variety of cargo proteins. Instead, this thesis aimed to specifically target the NES on Survivin's surface using amino acid-selective, supramolecular tweezers. Although the basic tweezer molecules already selectively bind to surface-exposed lysine residues, additional modifications were introduced to shield Survivin's NES region, thereby blocking Crm1.

First, tweezers were modified with small peptides (ELTL and ELTLGEFL) that were derived from Survivin's homodimerization interface, which partly overlaps with the NES. Binding of the peptide-modified tweezers to lysines in and near Survivin's NES was verified by NMR titrations and further strengthened by MD and QM/MM calculations. The peptide modifications of the tweezer did not only increase its affinity for Survivin as evidenced by ITC, but also enhanced its inhibitory effect on the Survivin/Crm1 interaction as shown in pull-down and fluorescence anisotropy experiments. The regioselectivity and signal-specificity of the peptide-modified tweezers were further confirmed using a Survivin point mutant (K90/103T) lacking putative anchor lysines of the tweezer and additionally by using a tweezer with the scrambled peptide sequence LFEEGLLT.

Furthermore, bivalent tweezer molecules were developed based on oligomer scaffolds that connected two tweezer units. These molecules aimed to target one lysine on each side of the NES simultaneously. ITC and pull-down experiments confirmed that the oligomer double tweezers bind to Survivin and impair the interaction between Survivin and Crm1 even better than the peptide-modified tweezers. Last, tweezers were attached to the surface of cell-permeable ultra-small gold nanoparticles. ITC experiments revealed binding of the tweezer-modified nanoparticles to Survivin with low micromolar affinity and, thus, demonstrated the integrity of the tweezers after fixation on the particle. Hence, they might be further explored to

facilitate cellular uptake of other tweezer molecules, e.g. the peptide-modified or double oligomer tweezers.

In sum, the molecular tweezer seems to be well suited to address the NES epitope on Survivin's surface and to interfere with the Survivin/Crm1 interaction. Thus, it might indeed be a promising approach for the development of novel supramolecular cancer therapies.

ZUSAMMENFASSUNG

Das Protein Survivin wird in nahezu allen Krebsarten überexprimiert und als zytoprotektiver Faktor betrachtet, der mit einer Resistenz gegenüber Chemo- und Strahlentherapie einhergeht. Da Survivin in den meisten normalen, ausdifferenzierten Zellen nicht vorkommt, ist es ein sehr krebsspezifisches Protein und sein erhöhtes Vorkommen in Tumorzellen wird mit schlechten Prognosen für den Patienten assoziiert. Survivin verfügt über ein Kernexportsignal ^{89}VKKQFEELTL^{98}, welches von dem Exportrezeptor Crm1 erkannt wird. Diese Protein-Protein-Interaktion ist nicht nur für die zytoprotektive Aktivität von Survivin notwendig, sondern auch für seine mitotische Funktion. Daher stellt sie ein vielversprechendes Ziel für die Krebsforschung und –therapie dar. Da Crm1 nicht nur als Exportrezeptor für Survivin dient, sondern viele verschiedene Proteine exportiert, inhibiert eine Therapie, die auf Crm1 abzielt, nicht spezifisch die Survivin-Interaktion. Die meisten bisherigen Crm1-Inhibitoren zeigen dosislimitierende Toxizität und drastische Nebenwirkungen, da sie viele verschiedene Frachtproteine von Crm1 beeinflussen. Ziel dieser Arbeit war es stattdessen, das Kernexportsignal von Survivin spezifisch mit Aminosäure-selektiven, supramolekularen Pinzetten zu addressieren. Obwohl die einfachen Pinzettenmoleküle bereits selektiv an Oberflächen-exponierte Lysine binden, wurden zusätzliche Modifizierungen vorgenommen, um das Kernexportsignal abzuschirmen und die Interaktion mit Crm1 zu inhibieren.

Als erstes wurden die Pinzetten mit kleinen Peptiden (ELTL und ELTLGEFL) ausgestattet, die von Survivins Dimerisierungsregion inspiriert wurden, welche teilweise mit dem Kernexportsignal überlappt. Die Bindung der Peptid-Pinzetten an Lysine in und neben dem Kernexportsignal wurde mit NMR verifiziert und mithilfe von MD und QM/MM Berechnungen bestärkt. Die Peptidmodifizierung hat nicht nur die Affinität der Pinzetten für Survivin erhöht, wie mit ITC gezeigt wurde, sondern auch deren inhibitorisches Potential für die Interaktion mit Crm1 in Pulldown- und Fluoreszenzanisotropie-Experimenten verbessert. Die Regioselektivität und Signalspezifität der Peptid-Pinzetten wurden mithilfe einer Survivin-Mutante (K90/103T), bei welcher die vermutlichen Anker-Lysine für die Pinzetten fehlen, sowie einer Pinzette, deren Aminosäuresequenz durchmischt wurde (LFEEGLLT), nachgewiesen.

Zusätzlich wurden bivalente Pinzettenmoleküle auf Basis von Oligomergerüsten entwickelt, welche zwei Pinzetteneinheiten verbinden. Diese Moleküle zielen darauf ab, je ein Lysin auf beiden Seiten des Kernexportsignals gleichzeitig zu binden. ITC und Pulldown-Experimente zeigten, dass diese Oligomer-Doppelpinzetten an Survivin binden und die Interaktion mit Crm1 sogar stärker als die Peptid-Pinzetten schwächen. Als letztes wurden Pinzettenmoleküle auf der Oberfläche von zellgängigen Goldnanopartikeln verankert. ITC-Experimente zeigten eine

Bindung mit niedriger, mikromolarer Affinität der Pinzetten-modifitierten Nanopartikel an Survivin und somit die Intaktheit der Pinzetten nach der Fixierung auf den Partikeln. Daher könnten sie in Zukunft verwendet werden, um die zelluläre Aufnahme anderer Pinzettenmoleküle, z.B. der Peptid- oder Oligomer-Doppelpinzetten, zu ermöglichen.

Zusammengefasst scheinen die Pinzetten gut geeignet zu sein, um das Kernexportsignal von Survivin zu addressieren und die Survivin-Crm1-Interaktion zu stören. Daher stellen sie einen vielversprechenden Ansatz für die Entwicklung von neuartigen supramolekularen Krebstherapien dar.

1 INTRODUCTION

1.1 SURVIVIN

Survivin (also known as BIRC5) was first identified in 1997 and described as a uniquely structured inhibitor of apoptosis protein (Ambrosini et al., 1997). Since then it has arisen more and more interest as a target in cancer therapies due to its involvement in two major processes linked to carcinogenesis: mitosis and apoptosis (Wheatley and Altieri, 2019). Survivin is present during fetal development, but absent in normal resting tissues (Ambrosini et al., 1997; Li et al., 1998). However, it is highly overexpressed in almost all types of cancer cells and its upregulation correlates with poor patient prognosis including increased tumor recurrence and resistance against chemo- and radiotherapies (Adida et al., 1998; Adida et al., 2000; Capalbo et al., 2007; Chen et al., 2014; Wheatley and Altieri, 2019).

The importance of Survivin in cell proliferation, and thus potentially in tumor progression, is supported by the findings that depletion of Survivin or interference with its functions leads to mitotic defects including incorrectly aligned chromosomes, cytokinesis failure, mitotic catastrophe, multinucleated cells, and increased apoptosis (Li et al., 1998; Carvalho et al., 2003; Lens et al., 2003; Castedo et al., 2004; Wheatley and Altieri, 2019; Vallet et al., 2020). Furthermore, Survivin has recently been linked to angiogenesis (Sanhueza et al., 2015; Li et al., 2016) and autophagy (Humphry and Wheatley, 2018). With these multiple tasks in major cellular processes, Survivin promotes cancer progression and tumor cell survival through many different routes, most of which are not fully understood yet (Wheatley and Altieri, 2019).

Survivin's overexpression in cancer cells and its severe consequences have indicated a high potential as a tumor marker and as a target in cancer therapies (Peery et al., 2017). So far, a Survivin-specific anti-cancer agent has not yet reached the clinic (Wheatley and Altieri, 2019). This is possibly caused by the fact that Survivin has no enzymatic activity and only few small pockets, which can hardly be targeted by small molecules (Wheatley and Altieri, 2019). Survivin fulfills its tasks in protein complexes, often by regulating the localization of its partners.

1.1.1 SURVIVIN'S CELLULAR FUNCTIONS

Survivin is a multifunctional protein playing several important roles in apoptosis and mitosis. As a mitotic regulator, Survivin ensures proper chromosome segregation and as an inhibitor of apoptosis protein (IAP), Survivin reduces caspase activity and protects cells against apoptosis (Wheatley and Altieri, 2019). Key to Survivin's multiple functions are protein-protein interactions with a multitude of cell cycle and apoptosis-relevant proteins.

1.1.1.1 SURVIVIN'S ROLE IN MITOSIS

The cell cycle's purpose is to divide a cell into two genetically identical daughter cells (Alberts et al., 2017). In eukaryotes, it comprises four phases: gap 1 (G1), synthesis (S), gap 2 (G2) and mitosis (M), with G1, S and G2 phases belonging to the interphase (Figure 1-1). During gap phases, the cell grows and prepares for cell division (Alberts et al., 2017). DNA is replicated in S phase, while nuclear (mitosis) and cell (cytokinesis) division are executed during M phase (Alberts et al., 2017).
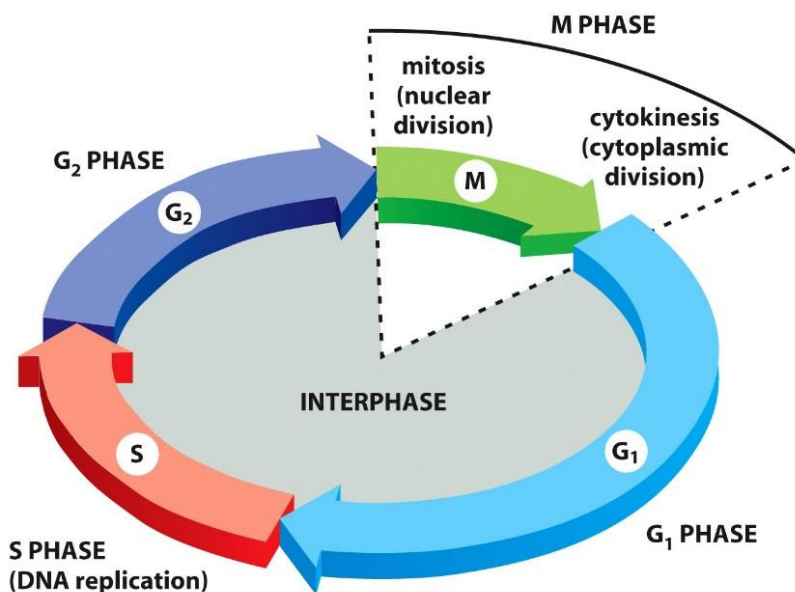
Figure 1-1: Cell cycle phases.

The cell cycle is divided into G1 (gap 1), S (synthesis), G2 (gap 2) and M phase (mitosis). The G1, S and G2 phases comprise the interphase. DNA is replicated in S phase, cells grow in gap phases and cell division in two daughter cells occurs during mitosis (Alberts et al., 2017).

Mitosis can be divided into five stages: prophase, prometaphase, metaphase, anaphase and telophase (Figure 1-2). It begins with chromosome condensation and the formation of a compact pair of sister chromatids in prophase. When the nuclear envelope breaks down in

prometaphase, sister chromatids are attached to the microtubules of the mitotic spindle. In metaphase, the chromosomes are aligned at the equator of the mitotic spindle and their kinetochores attach to microtubules of the opposed pole as preparation for subsequent segregation. In anaphase, chromosomes move to opposite spindle poles. Once they arrive, the mitotic spindle breaks down, chromosomes decondense and nuclei are reformed. Afterwards, in cytokinesis, the cell is separated into two daughter cells each with identical chromosomes. (Alberts et al., 2017)
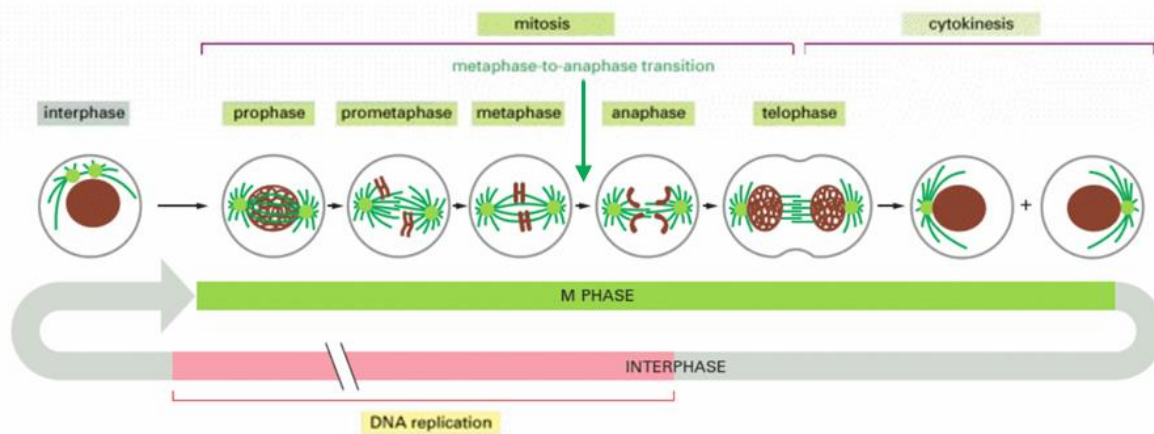
Figure 1-2: Stages of mitosis.
The M phase is divided into mitosis (nuclear division) and cytokinesis (cell division). Mitosis consists of five stages: prophase, prometaphase, metaphase, anaphase and telophase (Alberts et al., 2017).

The cell cycle underlies a strict control system and several checkpoints ensure that one stage is completed correctly before the next phase begins. The first checkpoint is located at the end of G1, the second at G2/M transition, where mitosis starts, and the third checkpoint is located within mitosis at the metaphase-to-anaphase transition. The cell cycle control system is driven by cyclin-dependent kinases (CDKs), which require cyclin binding for their enzymatic activity and then phosphorylate cell cycle relevant proteins. Cyclin levels fluctuate depending on the cell cycle phase, regulating CDK activation and, thus, the whole cell cycle. (Alberts et al., 2017)

Survivin is a key regulator of cell proliferation and its cell cycle-dependent expression is ensured by four transcriptional elements on the BIRC5 gene (chromosome 17) (Ambrosini et al., 1997; Li and Altieri, 1999; Wheatley and Altieri, 2019). It features three cycle-dependent elements and a cell cycle homology region (Li et al., 1998; Li and Altieri, 1999). Therefore, Survivin's expression is maximal in G2/M phase (Li et al., 1998), where it acts as a member of the chromosomal passenger complex (CPC). The CPC is involved in major mitotic events such as chromosome condensation, kinetochore-microtubule attachment, and activation of the spindle assembly checkpoint as well as in the formation and regulation of the contractile

3

apparatus during cytokinesis (Carmena et al., 2012). The CPC consists of one enzymatic subunit, the Aurora B kinase, and three regulatory subunits, Survivin, the inner centromere protein (INCENP) and Borealin (Carmena et al., 2012). Survivin's C-terminal α-helix forms a three-helical bundle with the N-terminal helices of INCENP and Borealin (Jeyaprakash et al., 2007). The latter is required for Survivin binding to INCENP and probably stabilizes the protein complex (Ruchaud et al., 2007a). The Aurora B kinase binds near the C-terminus of INCENP and is able to phosphorylate the other CPC members as well as different target proteins (e.g. Histone H3), and thus mediates the CPC's functions (Ruchaud et al., 2007a).

Survivin contributes significantly to the correct localization of the CPC in mitosis (Figure 1-3) (Ruchaud et al., 2007a, 2007b). In prophase, it targets the CPC to the chromosome arms, where Aurora B phosphorylates histone H3 on S10 and S28, as well as to the centromeres, thus ensuring proper alignment of the chromosomes (Lens et al., 2003; Ruchaud et al., 2007a; Wheatley and Altieri, 2019). Phosphorylation of Survivin (T117) is essential for its correct localization and binding to INCENP (Wheatley et al., 2004), while ubiquitination and de-ubiquitination of K63 ensure Survivin's dynamic association with the centromeres (Vong et al., 2005; Ruchaud et al., 2007a). However, the CPC's localization to the centromeres might be mediated by Survivin binding to histone H3 phosphorylated at T3 at the inner centromere via a small hydrophobic pocket and its surrounding acidic environment involving D7, L64, D70/71, E76 and W67 of Survivin (Wang et al., 2010; Niedzialkowska et al., 2012). Furthermore, the interaction between Survivin and the export receptor chromosome region maintenance 1 (Crm1) seems to be essential for tethering the CPC to the centromeres (Knauer et al., 2006).

The CPC remains at the centromeres throughout metaphase, where it regulates kinetochore-microtubule attachments (Ruchaud et al., 2007a). In cells lacking Survivin, Aurora B kinase is not recruited to the centromeres and thus cannot participate in the reorientation of misattached kinetochores (Lens et al., 2003). Hence, these cells fail to properly segregate their chromatids (Lens et al., 2003). Furthermore, the CPC is involved in the formation of the bipolar spindle and stabilizes it from prophase/prometaphase to anaphase (Ruchaud et al., 2007a). In anaphase, the CPC localizes to the spindle midzone and subsequently accumulates at the cleavage furrow and midbody in telophase, and thus enables cytokinesis (Ruchaud et al., 2007a; Wheatley and Altieri, 2019).
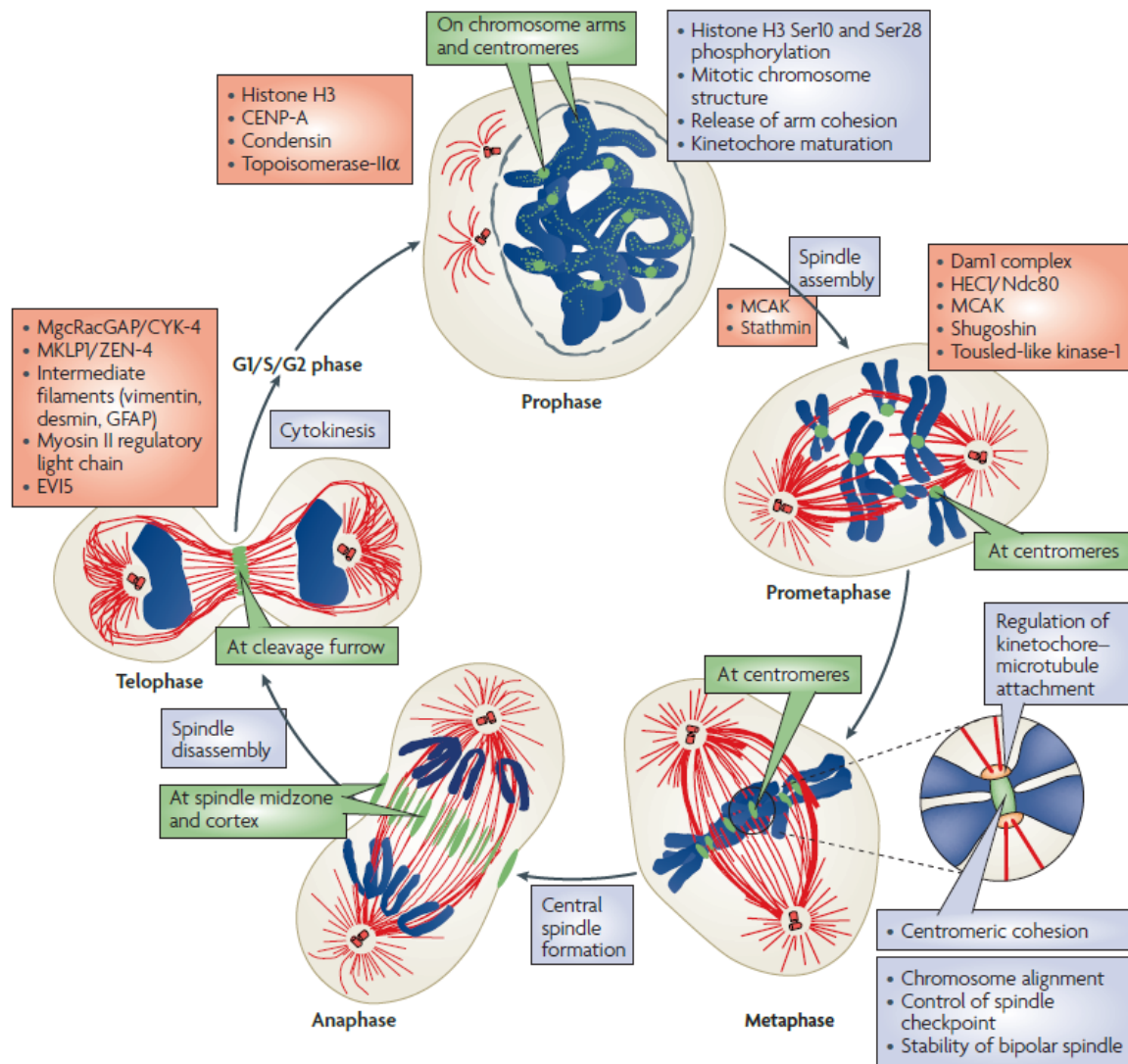
Figure 1-3: CPC localization during mitosis.

Schematic representation of the chromosomal passenger complex (CPC) localization (green boxes) and corresponding functions (grey boxes) during mitosis (Ruchaud et al., 2007a). Target proteins of the CPC in the respective phases are listed in red boxes. Chromosomes are depicted in blue, tubulin in red and the nuclear envelope in grey. A detailed description can be found in the main text.

1.1.1.2 *SURVIVIN'S ROLE IN APOPTOSIS*

Apoptosis is a common type of programmed cell death, which can be considered as the opposite of mitosis. It is necessary to maintain the balance between cell proliferation and death (Kerr et al., 1972; Cotter, 2009). Apoptosis eliminates unnecessary, misplaced, or tumorigenic cells to protect the organism and therefore plays an important role in cancer development and progression (Kerr et al., 1972; Ashkenazi, 2008; Cotter, 2009). In contrast to necrosis, which

5

is a passive and uncontrolled type of cell death characterized amongst others by cell swelling or formation of cytoplasmic vacuoles and affects multiple cells, apoptosis removes distinct, single cells or clusters of cells (Elmore, 2007). Specific morphological hallmarks characterize apoptosis, including cell shrinkage, chromatin condensation, as well as cell and nuclear fragmentation (Kerr et al., 1972; Cotter, 2009). Apoptotic bodies containing cytoplasm and tightly packed but still intact organelles are formed and subsequently phagocytosed, resulting in the removal of the apoptotic cell without inflammatory reactions and damage of the surrounding tissue (Elmore, 2007).

Apoptosis can be initiated or inhibited by environmental stimuli and hence is a regulated process (Kerr et al., 1972). Factors that initiate apoptosis can either be intrinsic e.g. DNA damages upon irradiation, or extrinsic by extracellular signals like tumor necrosis factor-related apoptosis-inducing ligand (TRAIL), which binds to receptors in the cell membrane (Hengartner, 2000; Ashkenazi, 2008). These two major apoptotic pathways are characterized by the activation of multiple cysteinyl-aspartate-specific proteases (caspases) resulting in a cascade of events (Figure 1-4) that trigger apoptosis (Hengartner, 2000; Elmore, 2007). Often expressed as inactive proenzymes, caspases are activated by cleavage and then able to activate other proenzymes, which starts a protease cascade (Cohen, 1997; Elmore, 2007). Caspases are categorized in initiators (caspase-2,-8,-9,-10) and effectors (caspase-3,-6,-7), depending on their major function (Cohen, 1997). At the beginning of the apoptotic process, the intrinsic and extrinsic pathways differ in stimuli, localization and protein involvement. The extrinsic, also called death receptor pathway is activated by ligand binding to a specific receptor (Elmore, 2007). This initiates receptor clustering and formation of a death-inducing signaling complex, which recruits several procaspase-8 and results in the caspase cascade (Hengartner, 2000). The intrinsic or mitochondrial pathway is characterized by recruitment of pro-apoptotic members of the Bcl-2 family to the mitochondria, where cytochrome c release is triggered (Hengartner, 2000; Elmore, 2007). Together with Apaf-1 and procaspase-9, cytochrome c forms the apoptosome, which activates further caspases. Both pathways converge at the cleavage of caspase-3 and result e.g. in DNA fragmentation, degradation of proteins, and formation of apoptotic bodies and hence cell death (Elmore, 2007).
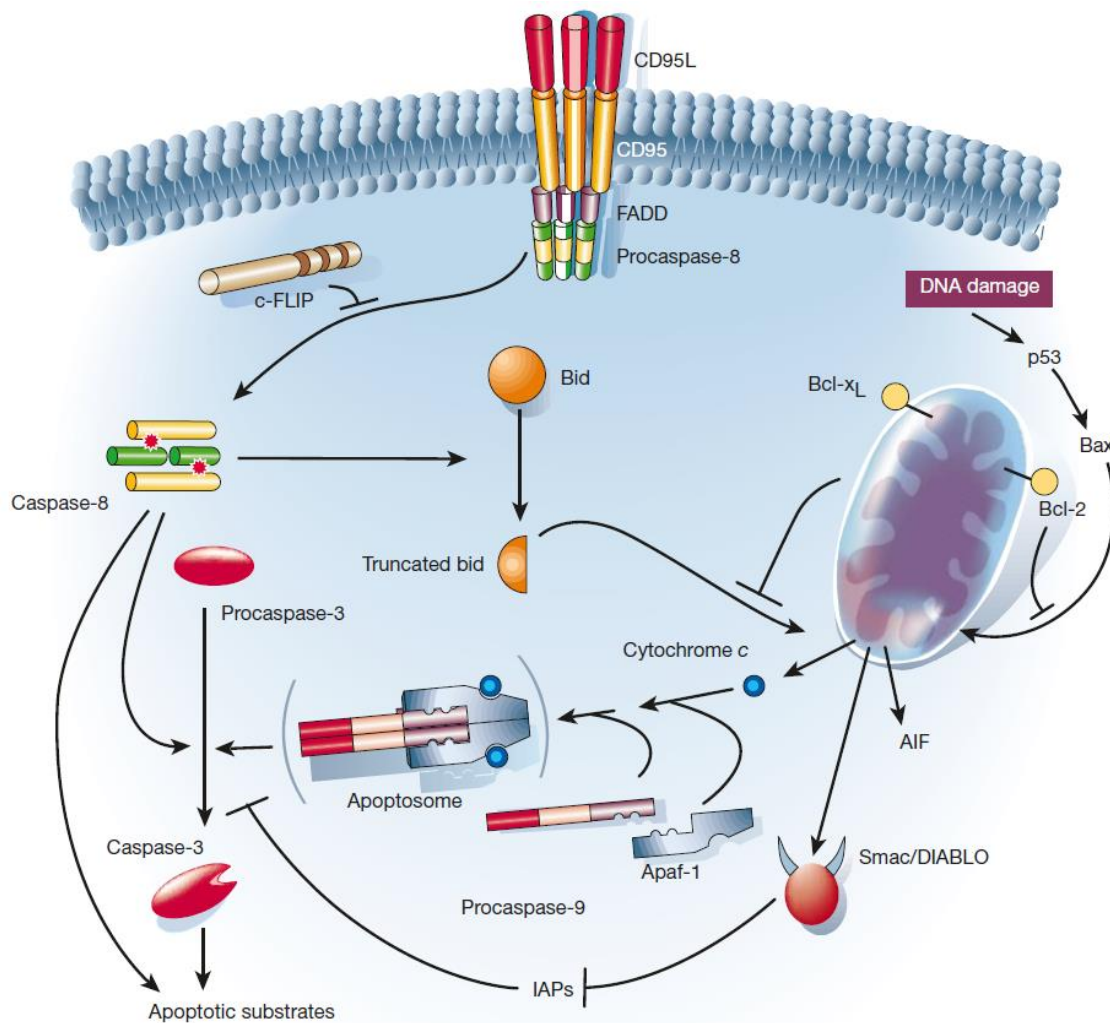
Figure 1-4: The extrinsic and intrinsic apoptotic pathways.

The extrinsic pathway (left) is initiated by members of the death receptor superfamily (such as Fas-receptor, also called cluster of differentiation 95 (CD95), and tumor necrosis factor (TNF) receptor I) (Hengartner, 2000). Binding of a ligand induces receptor clustering and formation of a death-inducing signaling complex, which then recruits several procaspase-8 molecules via the adaptor molecule Fas-associated death domain protein (FADD). Caspase-8 is then activated, which can be blocked by c-FLIP. The intrinsic pathway (right) is triggered e.g. by DNA damage, which activates the p53 tumor suppressor protein. Next, pro-apoptotic members of the Bcl-2 family (e.g. Bcl-2-associated X protein (BAX)) are recruited to the mitochondria, where they trigger cytochrome c release. Cytochrome c associates with the apoptotic protease-activating factor 1 (Apaf-1) and procaspase-9 to form the apoptosome. This activates caspase-3, where both pathways converge, and triggers apoptosis. Caspase-3 activation can be inhibited by inhibitor of apoptosis proteins (IAPs). However, IAPs are antagonized by the protein Smac/Diablo. (Hengartner, 2000)

Caspases are the key executioners of apoptosis (Cohen, 1997) and their natural inhibition is mediated by proteins belonging to the IAP family. Thus, IAPs can protect cells from apoptosis and regulate spontaneous caspase activation (Hengartner, 2000). The IAP family comprises eight members (Figure 1-5): Bruce/Apollon, Livin/inhibitor of apoptosis protein-link protein 2

(ILP2), melanoma-IAP (ML-IAP), Survivin, neuronal apoptosis-inhibitory protein (NAIP), cellular IAP1 und IAP2 (c-IAP1, c-IAP2) and X-linked inhibitor of apoptosis protein (XIAP) (Eckelman et al., 2006; Srinivasula and Ashwell, 2008).
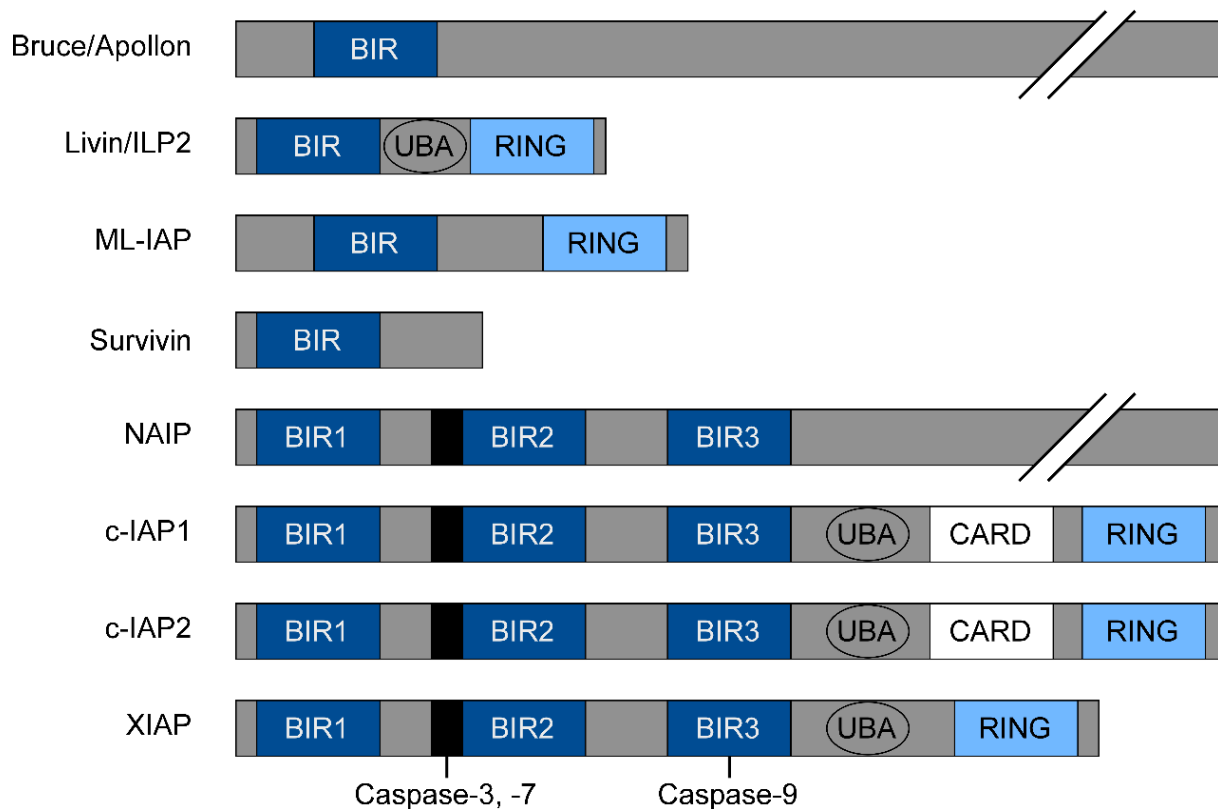
Figure 1-5: Members of the human inhibitor of apoptosis protein (IAP) family.
The IAP family consists of the proteins Bruce/Apollon, Livin/ILP2, Survivin, NAIP, c-IAP1, c-IAP2 and XIAP. All IAPs contain one or more N-terminal BIR domains (dark blue) and, in some cases, an additional CARD (white) and RING domain (light blue). Binding of caspases 3 and 7 occurs via an upstream region (18 aa) of BIR2 (black). BIR3 of XIAP is able to inhibit caspase 9.

IAPs are characterized by an approximately 70 amino acid (aa) long baculovirus inhibitor of apoptosis repeats (BIR) domain, a zinc finger domain, which occurs at least once and up to three times at their N-termini (Altieri, 2010). Several IAPs contain additional domains like c-terminal really interesting new gene (RING) motifs, ubiquitin-associated domains (UBA) or caspase recruitment domains (CARD) (Altieri, 2010). The RING domain serves as E3 ubiquitin ligase and the UBA domain is considered as binding site for ubiquitinated proteins (Altieri, 2010). BIR domains mediate several protein-protein interactions. BIR2 and BIR3 of XIAP and other relatives contain acidic grooves, which can interact with caspases via their IAP binding motif (IBM) (Srinivasula and Ashwell, 2008; Altieri, 2010). Binding of caspase-3 and -7 for example is achieved by an upstream of BIR2 located region of 18 aa that serves as "sinker",

whilst a helix c-terminal of BIR2 serves as an additional binding unit or "hook" for caspases-3 and -7 (Riedl et al., 2001; Srinivasula and Ashwell, 2008). However, only XIAP is considered as direct inhibitor of caspases *in vivo* (Eckelman et al., 2006; Altieri, 2010).

As the smallest member of the IAP family (142 aa), Survivin only possesses one BIR domain and does not feature other typical IAP motifs (Ambrosini et al., 1997). Furthermore, Survivin's single BIR domain has no IBM-binding groove, and thus does not directly interact with caspases (Altieri, 2010). Instead, its cytoprotective function seems to be based on interactions with partner proteins, and therefore an indirect inhibition of apoptosis. Survivin binds to XIAP, probably via interactions of its BIR domain with BIR2 and BIR3 of XIAP (Dohi et al., 2004; Altieri, 2010). The Survivin/XIAP complex possesses a higher stability against proteasomal destruction and an enhanced inhibitory effect on caspase-9 activation compared to sole XIAP (Dohi et al., 2004). Besides, the complexation of Survivin and XIAP might affect binding of XIAP-antagonists like the second mitochondria-derived activator of caspases (Smac), also called direct IAP-binding protein with low pI (DIABLO), (Dohi et al., 2004). These IAP inhibitors are usually located in the mitochondria and released into the cytoplasm together with cytochrome C during the apoptotic pathway to counteract IAPs (Du et al., 2000; Hengartner, 2000). Furthermore, Survivin is also able to directly bind to Smac/DIABLO (Song et al., 2003). Thereby, this antagonist is sequestered from XIAP, which is then able to inhibit caspases and fulfill its anti-apoptotic function (Song et al., 2003; Wheatley and Altieri, 2019). Survivin may also bind to hepatitis B X-interacting protein (HBXIP) to form a complex, which prevents caspase-9 binding to the apoptotic protease-activating factor 1 (Apaf-1), and therefore the formation of the apoptosome (Marusawa et al., 2003). Taken together, Survivin is associated with several apoptosis-relevant proteins and processes, and might fulfill its cytoprotective role via various routes.

1.1.2 SURVIVIN'S STRUCTURE AND DOMAIN ORGANIZATION

Survivin is a small (142 aa and 16.5 kDa) multifunctional protein, which possesses a well-defined structure and domain organization (Figure 1-6 A) (Ambrosini et al., 1997). As a member of the IAP family, Survivin contains a BIR domain. However, unlike the other IAPs who consist of several BIR domains, Survivin only features one, which is located at its N-terminus (aa 15–89) (Ambrosini et al., 1997). The BIR domain consists of a three-stranded β-sheet and four short α-helices, and thus comprises a zinc-binding motif, which coordinates the Zn^{2+} ion by C57, C60, H77 and C84 (Verdecia et al., 2000). Survivin has a c-terminal α-helix

(aa 98–142) with hydrophobic clusters (Chantalat et al., 2000; Verdecia et al., 2000). Borealin and INCENP can associate with the long α-helix of Survivin, and thus form a tight three-helix bundle, which is the regulatory basis of the CPC (Jeyaprakash et al., 2007).
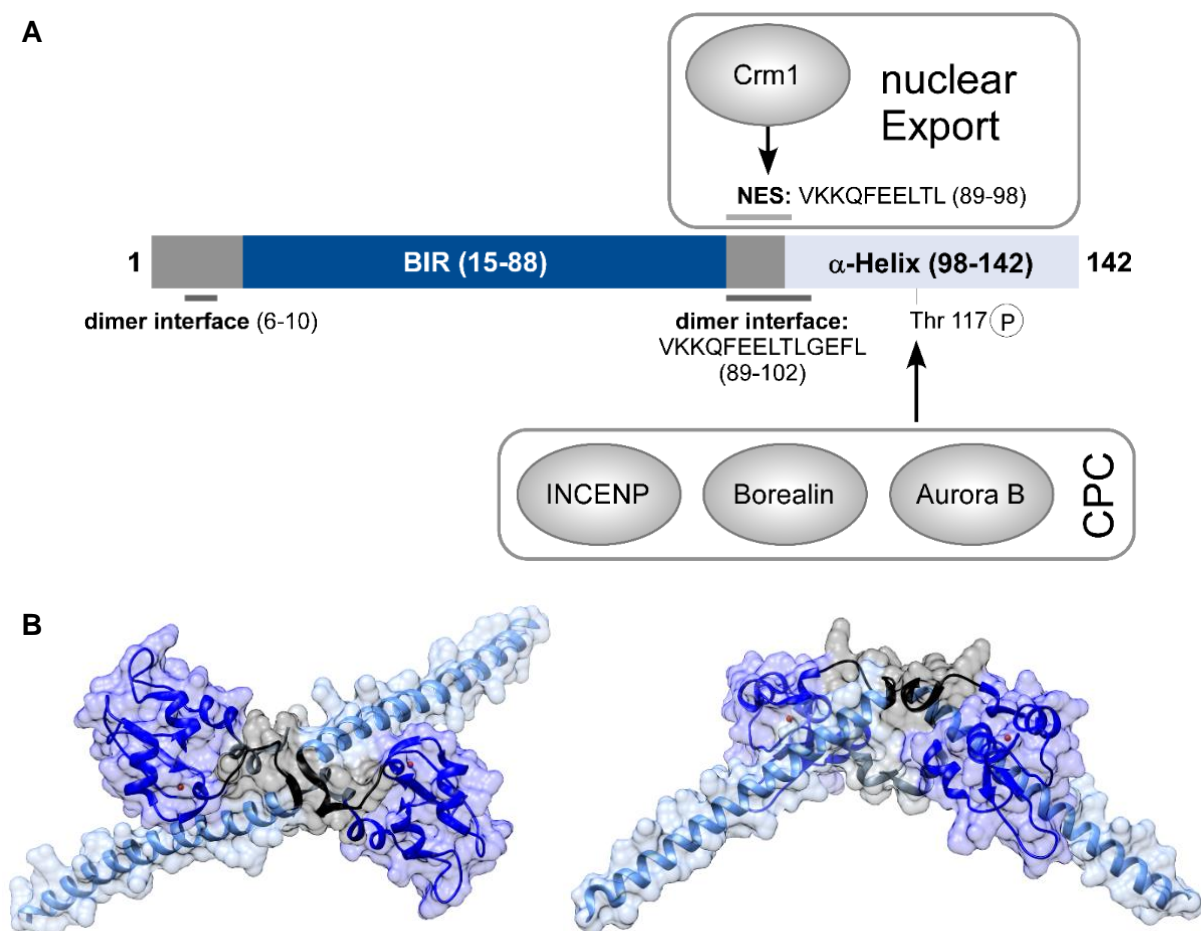
Figure 1-6: Domain organization and structure of Survivin.

A) Survivin contains an N-terminal BIR domain (dark blue) and a c-terminal α-helix (light blue), which can interact with the proteins INCENP, Borealin and Aurora B from the CPC. In between, Survivin possesses a nuclear export signal (NES), which partly overlaps with the dimer interface. B) Representation of Survivin's structure with the BIR domain (dark blue), α-helix (light blue) and NES (black) based on PDB ID: 1E31. The zinc ion is colorized in orange. Survivin occurs as a bow tie-shaped homodimer in solution (Chantalat et al., 2000).

X-ray crystallography revealed a dimeric arrangement of Survivin (Figure 1-6 B) with a dimer interface mainly constituted by hydrophobic amino acids (Chantalat et al., 2000; Verdecia et al., 2000). Specifically, L98 of one monomer protrudes into a hydrophobic pocket formed by L6 and L102, W10 as well as F93 and F101 on the second protomer (Verdecia et al., 2000). Whilst sole Survivin occurs as a homodimer, it has been shown to interact in the monomeric state with its partner proteins in mitosis and apoptosis (Jeyaprakash et al., 2007; Pavlyukov et al., 2011). However, Survivin dimerization seems to prevent protein degradation by the

proteasome, since its highly hydrophobic dimer interface is protected in the dimeric state, and thus stabilized (Qi et al., 2016). Moreover, Survivin possesses a nuclear export signal (NES, aa 89–98), which mediates its active export to the cytoplasm by the export receptor Crm1 (Rodríguez et al., 2002; Stauber et al., 2006). This interaction is not only important for Survivin's active transport into the cytoplasm, but also essential for targeting the CPC to the centromeres, and thus its function in mitosis (Knauer et al., 2006; Knauer et al., 2007). Notably, Survivin's NES partly overlaps with the dimer interface. Furthermore, homodimerization has been shown to antagonize nuclear export (Engelsma et al., 2007).

Survivin's anti-apoptotic functions are executed in the cytoplasm, where the caspase cascade proceeds. For the mitotic function, Survivin needs to be in the nucleus to aid localizing the CPC to centromeres, and subsequently to the mitotic spindle. Hence, Survivin's correct localization needs to be controlled depending on its intended role. This is mediated by the cell's major export receptor, which on the one hand tethers the CPC to the centromeres and on the other hand exports Survivin via an active transport mechanism (Knauer et al., 2006; Knauer et al., 2007).

1.1.3 SURVIVIN'S NUCLEOCYTOPLASMIC TRANSLOCATION

In eukaryotic cells, nucleus and cytoplasm are separated by the nuclear membrane, which contains nuclear pore complexes (NPCs). NPCs are large macromolecular assemblies of approximately 120 MDa that form channels to ensure the transfer of molecules across the membrane (Reichelt et al., 1990; Beck and Hurt, 2017). NPCs are composed of several subcomplexes and contain around 500–1000 nuclear pore proteins, called nucleoporins (NUPs) (Kabachinski and Schwartz, 2015; Beck and Hurt, 2017). Key structural elements comprise the inner pore ring, the nuclear and cytoplasmic rings, the nuclear basket and the cytoplasmic filaments (Figure 1-7) (Beck and Hurt, 2017). Furthermore, NUPs can be divided into different groups: transmembrane, scaffold and barrier-forming NUPs, as well as the cytoplasmic filaments and the nuclear basket (Sakiyama et al., 2017). NPCs are anchored to the nuclear envelope by transmembrane NUPs, while scaffold NUPs connect transmembrane and barrier-forming NUPs (Grossman et al., 2012a; Sakiyama et al., 2017). The latter contain phenylalanine- and glycine-rich repeats (FG), which are natively unfolded, form the central channel and mediate the transport function of the NPC (Denning et al., 2003; Alber et al., 2007).

Large molecules of more than 40–60 kDa, e.g. proteins and RNAs, must be actively transported through the NPC, while small molecules can pass the membrane by diffusion (Izaurralde et al., 1997; Mattaj and Englmeier, 1998; Görlich and Kutay, 1999; Kabachinski and Schwartz, 2015). However, even small molecules often cross the membrane in an active, carrier-dependent and, thus, controlled manner (Görlich and Kutay, 1999). The active export or import of proteins results from interactions between the cargo, transport receptors (karyopherins (Kaps), e.g. importin, exportin) and the small GTPase Ras-related nuclear protein (Ran) (Kabachinski and Schwartz, 2015). Ran exists either as guanosine triphosphate (GTP)- or hydrolyzed guanosine diphosphate (GDP)-bound form, and thus is switched on and off (Bourne et al., 1991).

A RanGTP gradient with a lower concentration in the cytoplasm than in the nucleus, drives the nuclear transport (Izaurralde et al., 1997; Kabachinski and Schwartz, 2015). The asymmetric distribution of RanGTP is maintained by several exchange factors, such as the chromatin-bound Ran guanine nucleotide exchange factor (RanGEF), also called regulator of chromosome condensation 1 (RCC1), the Ran-GTPase-activating protein (RanGAP) and Ran-binding proteins (RanBP1 and 2) (Izaurralde et al., 1997). RanGEF catalyzes the exchange of Ran-bound GDP to GTP in the nucleus (Bischoff and Ponstingl, 1991), while RanGAP converts RanGTP to RanGDP (Bischoff et al., 1994; Izaurralde et al., 1997). The nucleoporin RanBP2 and cytoplasmic RanBP1 aid GTP hydrolysis and are crucially involved in import and export processes (Bischoff et al., 1995; Mahajan et al., 1997; Kehlenbach et al., 1999; Monecke et al., 2014).
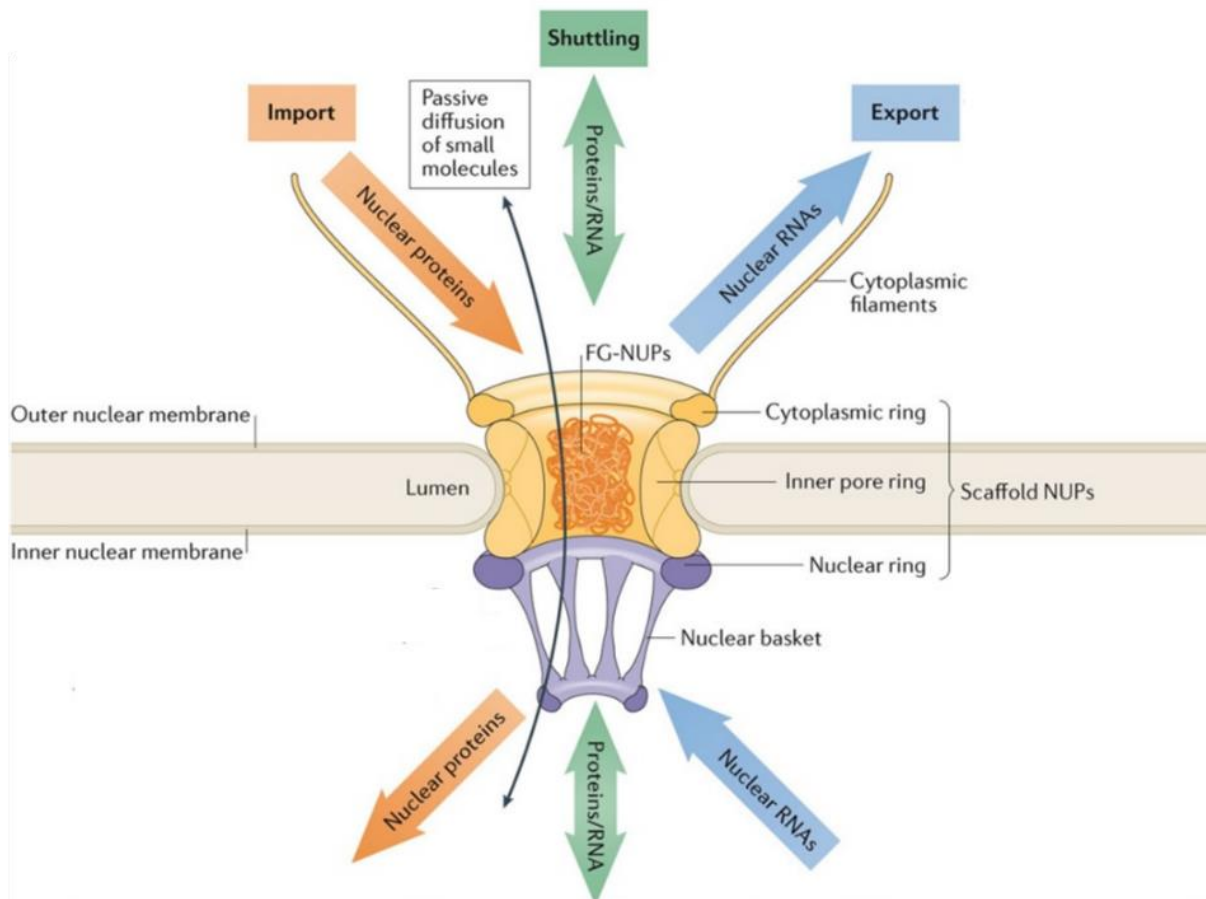
Figure 1-7: The nuclear pore complex.

The nuclear pore complex (NPC) is integrated into the nuclear membrane. Substructures of the NPC are the cytoplasmic ring, the inner pore ring, the nuclear ring, the nuclear basket as well as the cytoplasmic filaments, and all are composed of nucleoporins (NUPs). The central channel is formed by NUPs that contain phenylalanine- and glycine-rich repeats (FG-NUPs). In both directions, small molecules can diffuse passively, whereas larger RNAs and proteins are actively transported through the NPCs. Modified after Beck and Hurt (2017).

Nucleocytoplasmic shuttling is a fast process with approximately 1000 translocations per second (Ribbeck and Görlich, 2001). However, the transport is strictly selective, since relatively large receptor proteins and their cargo complexes can pass the NPC, whilst other proteins of lower sizes are kept out (Weis, 2007). The import or export of these protein complexes is mediated by interactions of the transport receptors with the FG-repeats of nucleoporins in the central channel of the NPC (Sakiyama et al., 2017). Karyopherins have been shown to directly interact with FG-repeats (Rexach and Blobel, 1995), and thus enable transport through the NPC. The exact mechanism of the translocation and the involvement of the FG-NUPs is not yet fully understood and a matter of debate (Weis, 2007; Sakiyama et al., 2017). Several models have been proposed on how FG-NUPs ensure selective transport of karyopherins like importin-β and exportin1 and form barriers for other proteins (Figure 1-8). One prominent

model is the "selective-phase model" suggested by Görlich and coworkers (Ribbeck and Görlich, 2001; Ribbeck and Görlich, 2002; Frey and Görlich, 2007). In this model, the barrier results from hydrophobic interactions between the phenylalanine-rich NUPs in the central channel, which form a meshwork like a hydrogel that restricts the movement of molecules through the pore (Ribbeck and Görlich, 2001; Frey et al., 2006). Transport receptors, which are generally more hydrophobic than other proteins (Ribbeck and Görlich, 2002), can interact with the FG-repeats and are incorporated in the channel (Ribbeck and Görlich, 2001). Hence, the receptor proteins locally disrupt the hydrogel as they compete with the mutual attraction of FG-repeats for each other, and therefore cross the channel with their cargo (Ribbeck and Görlich, 2001; Frey et al., 2006).
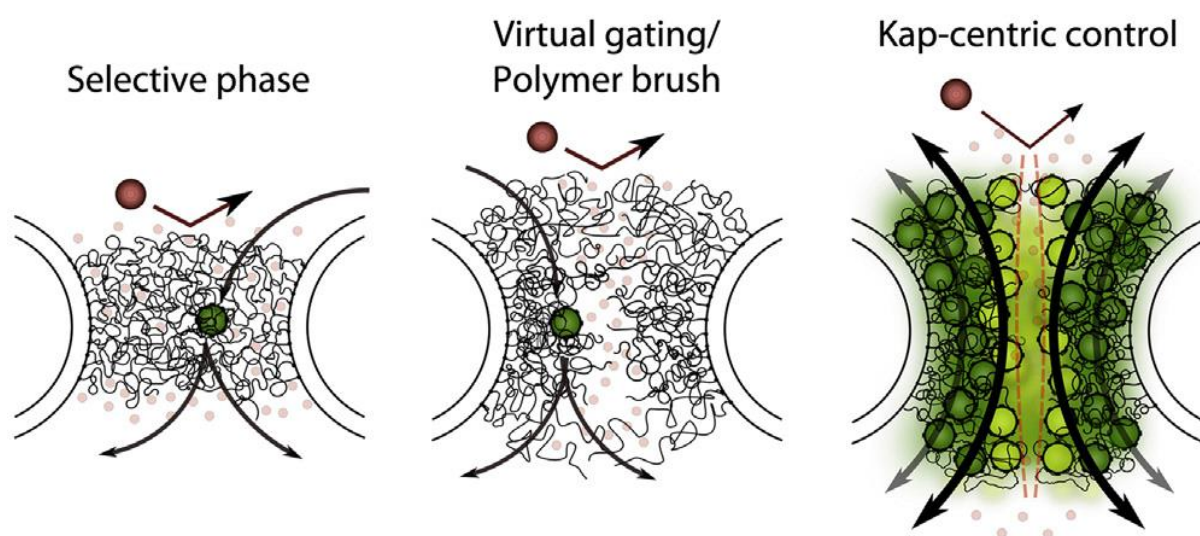
Figure 1-8: Overview of NPC barrier models.

Different explanations for the selective barrier of the NPC by the selective phase model (left), virtual gating/polymer brush model (center) and Kap-centric control model (right) (Sakiyama et al., 2017). Small molecules (pale red dots) diffuse freely, whereas large non-specific molecules (red dots) are restrained. Kaps (slow-phase: green dots; fast-phase: light green dots) pass the barrier by interacting with FG-repeats.

The "virtual gate" model was proposed by Rout and colleagues (Rout et al., 2000; Rout et al., 2003). This model suggests that the barrier, which keeps out molecules, is not mechanical but entropic (Rout et al., 2003; Weis, 2007). The narrow tube of the central channel packed with FG-repeats and the filamentous FG-NUPs at both ends of the NPC restrict molecular movements, and thus require a decrease in the entropy of the molecule that wants to enter the NPC (Rout et al., 2000; Rout et al., 2003). For this, the molecule needs to directly bind to the NPC as export receptors do. The resulting binding energy overcomes the entropic barrier and allows the receptor molecule to pass with its cargo (Rout et al., 2003). In fact, this model was

supported by findings that FG-repeats can extend or collapse and might act as polymer brushes, which contribute to the entropic barrier (Lim et al., 2006; Weis, 2007).

Recently, another model stressing the involvement of karyopherins themselves in the selective barrier, the "Kap-centric control" model, has been proposed by Lim and coworkers (Kapinos et al., 2014; Kapinos et al., 2017). They consider a slowly exchanging karyopherinβ1 (Kapβ1) phase as integral component of the barrier, whereby Kapβ1 is tightly bound to FG-repeats in the periphery of the channel (Kapinos et al., 2014). A fast phase coexists along the pre-occupied FG-repeats and forms a narrow tunnel for further Kaps, which bind much weaker than the already integrated Kaps and thus can move rapidly along the channel (Kapinos et al., 2014). Even though the exact mechanism of how the barrier of the NPC works is unclear, it is common ground that karyopherins mediate the translocation of their cargos through the NPC. This transport is strongly dependent on the GTPase Ran (Melchior et al., 1993; Görlich et al., 1996; Richards et al., 1997).

For nuclear import, proteins need to feature a nuclear localization signal (NLS), which classically contains several basic amino acids, especially lysines (Kalderon et al., 1984; Dingwall et al., 1988). The NLS is recognized by the adaptor protein importin-α, which then forms a trimeric import complex with Kapβ1, also called importin-β (Figure 1-9). Subsequently, importin-β carries the cargo through the membrane via interactions with the FG-NUPs in the central channel of the NPC (Görlich and Kutay, 1999). Once the import complex has reached the nucleus, RanGTP binds to importin-β, the importin heterodimer disassociates and the cargo is released (Rexach and Blobel, 1995; Kabachinski and Schwartz, 2015). The importin-β-RanGTP complex is transported to the cytoplasm, where GTP hydrolysis by RanGAP leads to its disassembly and releases the importins for further import cycles (Stewart, 2007).

For nuclear export, the cargo protein needs to contain a nuclear export signal, which is usually composed of a hydrophobic and leucine-rich amino acid sequence (Wen et al., 1995). The most prominent NESs originate from the protein kinase A inhibitor (PKI; NES: aa 37–46, LALKLAGLDI) and the human immunodeficiency virus 1 (HIV-1) Rev protein (NES: aa 75–83, LPPLERLTL) (Fischer et al., 1995; Wen et al., 1995). The NES consensus sequence is L-X_{2-3}-L-X_{2-3}-L-X-L, where L represents a hydrophobic amino acid, most likely leucine but also isoleucine, phenylalanine, methionine or valine, and X_{2-3} can be two or three arbitrary amino acids (Kosugi et al., 2008; Kim et al., 2017). This signal is recognized by Crm1, one of the major export receptors, also called exportin 1, which cooperatively binds to RanGTP and the cargo in the nucleus (Fornerod et al., 1997). The ternary export complex passes the NPC and disassembles in the cytoplasm upon GTP hydrolysis (Figure 1-9).
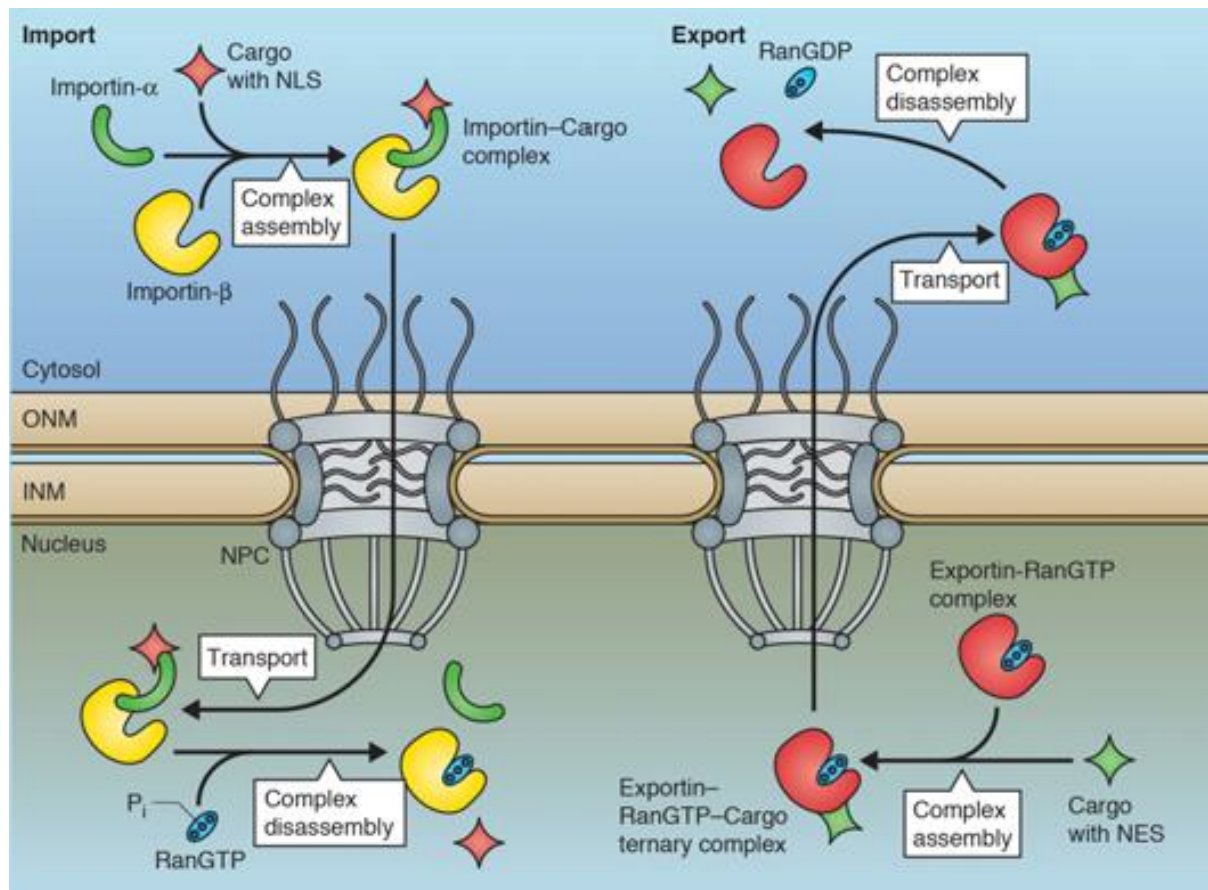
Figure 1-9: Nuclear import and export cycles through the nuclear pore complex.

Left: For nuclear import, the NLS-bearing cargo (red) is recognized by the adaptor protein importin-α (green), which then forms a trimeric import complex with importin-β (yellow) (Kabachinski and Schwartz, 2015). Importin-β carries the cargo through the membrane. In the nucleus, RanGTP (blue) binds to importin-β, which then releases the cargo. Right: For nuclear export, the NES of the cargo protein is recognized by the export receptor Exportin (red), which cooperatively binds to RanGTP (blue) and the cargo (green) in the nucleus. The ternary export complex passes the NPC and disassembles in the cytoplasm upon GTP hydrolysis (Kabachinski and Schwartz, 2015).

Survivin is small enough to diffuse across the membrane, and thus can enter the nucleus even though it does not feature a nuclear localization signal (Stauber et al., 2007). However, Survivin's export is mediated in an active manner. Since Survivin possesses a leucine-rich nuclear export signal [89]VKKQFEELTL[98] between its BIR domain and the C-terminal helix, it is targeted by Crm1 (Knauer et al., 2007).

1.1.3.1 CRM1 MEDIATED NUCLEAR EXPORT

Crm1 is an export receptor for a variety of proteins containing a leucine-rich NES (Fornerod et al., 1997; Xu et al., 2012). It consists of 21 HEAT repeats (H1–21), which are composed of a pair of anti-parallel helices A and B connected by a short linker loop (Figure 1-10 A) (Andrade and Bork, 1995; Monecke et al., 2014). This rather hydrophobic motif was named after the first proteins it was identified in, namely **H**untington **e**longation factor 3, the regulatory subunit **A** of protein phosphatase 2A and the P3 kinase **T**OR1 (Andrade and Bork, 1995). Crm1's HEAT repeats are arranged in a toroid (Figure 1-10 B), resulting in an overall super-helical shape with a hydrophobic core (Monecke et al., 2009; Monecke et al., 2014). While A helices form the outer surface and may interact with the FG-rich NUPs in the nuclear membrane, B helices form the inner surface and ensure binding of RanGTP (Monecke et al., 2009; Monecke et al., 2014).
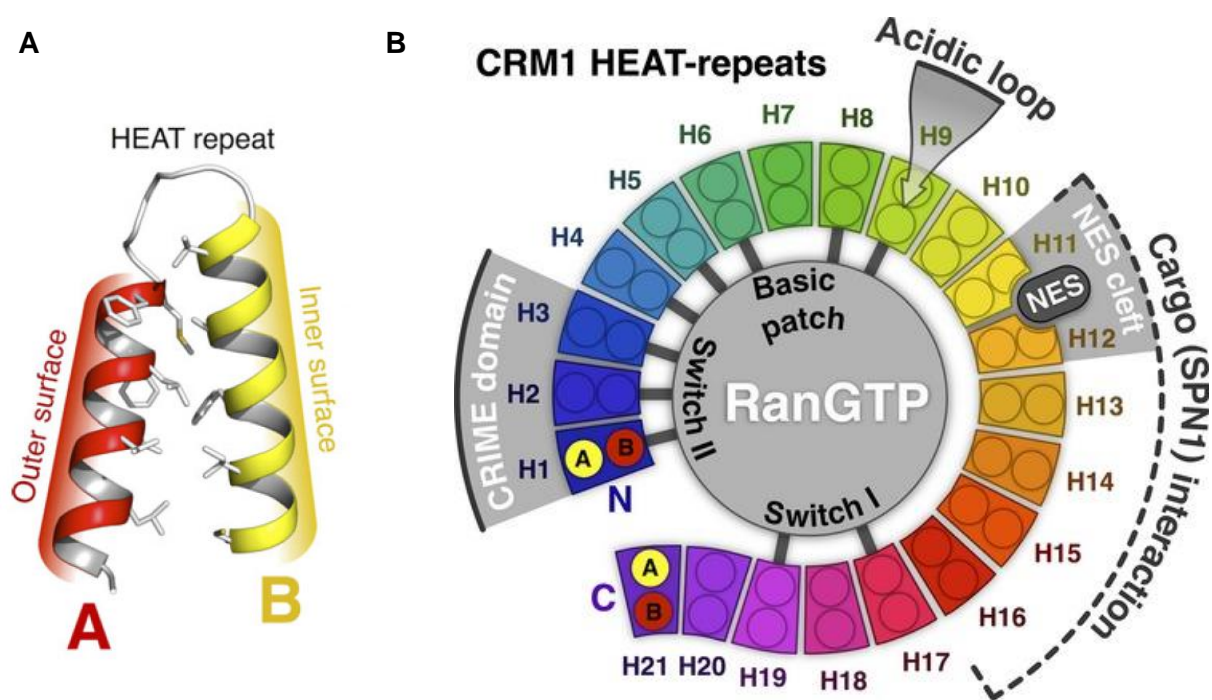
Figure 1-10: HEAT repeat architecture and domain organization of Crm1.

A) Each HEAT repeat contains a pair of helices A and B, which are connected by a short linker loop (Monecke et al., 2014). B) Crm1 consists of 21 HEAT repeats (H1–21), which form a toroid-like structure. The CRIME domain and acidic loop at H9 are involved in RanGTP binding. HEAT repeats 11 and 12 form a NES cleft, which binds to cargo proteins (Monecke et al., 2014).

Especially the N-terminal CRIME domain, named after importin-β type transport receptors (**Cr**m1-**im**portin β **e**tc.), is essential for the association with Ran, as it binds to the GTP-triggered switch II region of RanGTP by hydrophilic and hydrophobic interactions of the

B helices (Vetter et al., 1999; Monecke et al., 2014). The binding site for NES-bearing cargos is a hydrophobic groove formed by HEAT repeats 11 and 12 and is called NES cleft (Dong et al., 2009a; Dong et al., 2009b; Monecke et al., 2009). This binding site is rather rigid, contains five hydrophobic pockets and recognizes a variety of different NESs, which adapt their conformations to the NES cleft and may bind to the groove in both orientations (Güttler et al., 2010; Fung et al., 2015). A stretch of 26 residues at HEAT repeat 9, which connects helices A and B, forms a β-hairpin called the acidic loop, and is important for Ran binding as well as for cargo binding and release (Monecke et al., 2009; Koyama and Matsuura, 2010; Monecke et al., 2014). This loop adopts a seatbelt-like conformation by interacting with HEAT repeats at the opposite side of the Crm1 toroid, and thus locks Ran to the CRIME domain (Monecke et al., 2009; Monecke et al., 2014). Changes in the local conformation of the acidic loop, e.g. upon RanGTP binding, cause rearrangement of the HEAT repeats 11 and 12, and thus open or close the NES cleft (Koyama and Matsuura, 2010).

In several crystal structures of free or RanGTP- and cargo-bound Crm1, HEAT repeat 21 shows an atypical arrangement and two major conformations, which result in two different overall conformations of the protein: an extended and a compact form (Monecke et al., 2013; Monecke et al., 2014). In absence of Ran, the helix 21B spans over the Crm1 toroid and interacts with the bases of HEAT repeat 9 (Figure 1-11 A) (Dickmanns et al., 2015). The acidic loop binds to the inner side of HEAT repeats 11 and 12, which form the NES cleft, and thus is oriented in a "flipped back" conformation (Dickmanns et al., 2015). In this extended, superhelical conformation, the NES binding groove is closed (Figure 1-11 C) and Crm1's affinity for potential cargos is low (Monecke et al., 2014). In complex with RanGTP, the B helix of HEAT repeat 21 stacks to the other HEAT repeats and the C- and N-termini of Crm1 can tightly interact with each other by several salt bridges and hydrogen bonds resulting in a compact toroidal form of Crm1 (Figure 1-11 B) (Monecke et al., 2014). The NES cleft is open in this conformation (Figure 1-11 D) and NES-bearing cargos can be bound (Monecke et al., 2014; Dickmanns et al., 2015). Furthermore, the C-terminal acidic tail adjacent to helix 21B plays also an important role in NES binding and release, as electrostatic interactions occur with basic residues on helix B of HEAT repeat 12 on the inner surface beneath the NES cleft that mediate opening and closing of the groove (Fox et al., 2011).
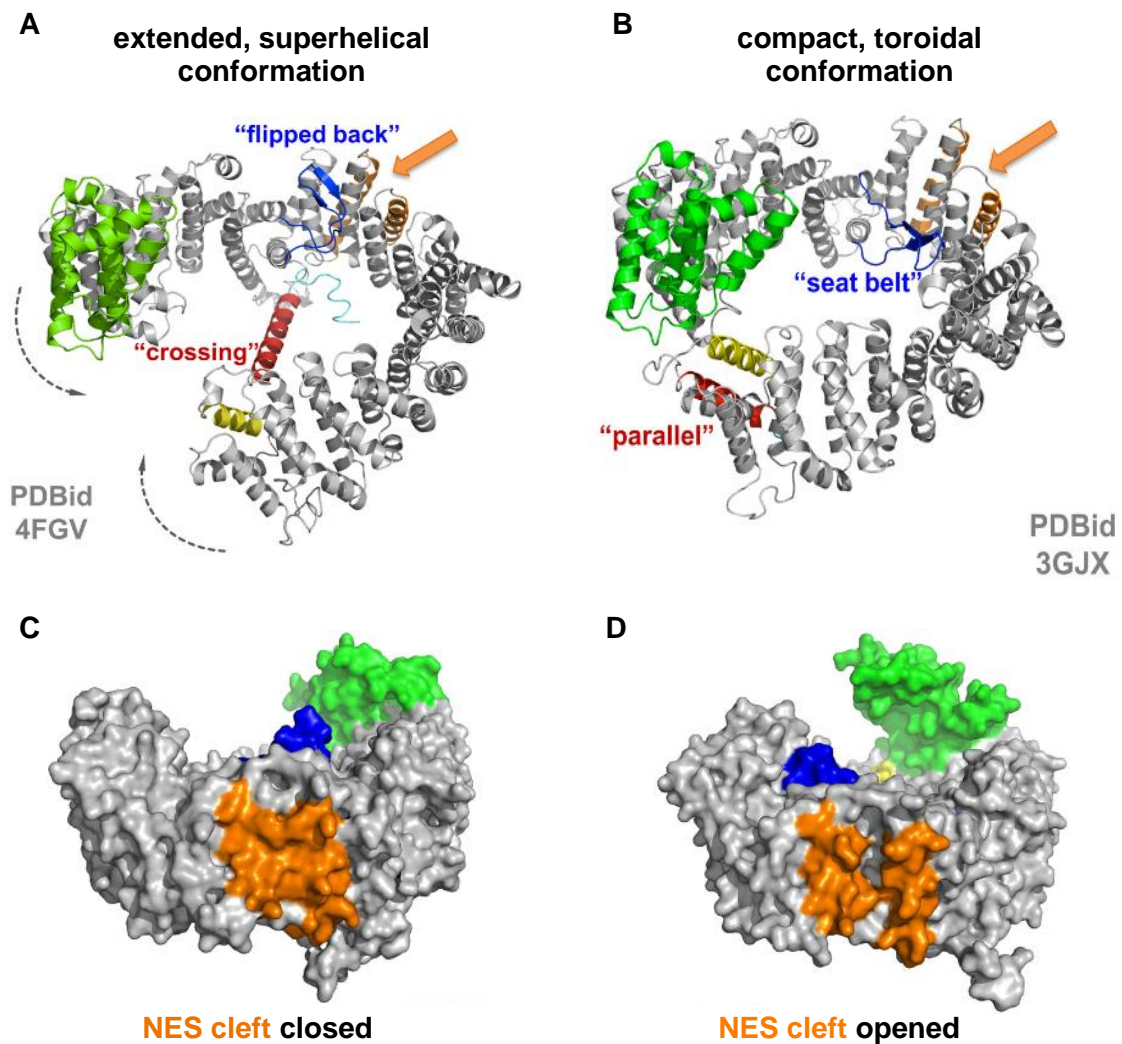
Figure 1-11: Structural changes between the main conformations of Crm1.

The overall conformation of Crm1 (grey) changes between the extended, superhelical (A) and compact, toroidal (B) conformation. The CRIME domain (green), acidic loop (blue), the C-terminal B-helix of HEAT repeat 21 (red) and the NES cleft (orange) undergo positional changes during nuclear export cycles upon RanGTP binding. The NES cleft is either closed (C) or opened (D) for cargo proteins. Structures are labeled with the PDB ID they were derived from. Modified after Dickmanns et al. (2015). See main text for details.

The whole Crm1-mediated export cycle is driven by Ran binding and release, as well as resulting local conformational changes. The overall movements, positional changes and important interaction sites between Crm1 and its cargo, Ran and disassembly factors such as Ran-binding proteins (Ran-BPs) are depicted in Figure 1-12 (Monecke et al., 2014). Especially the acidic loop (depicted in light green) and C-terminal helix (blue) mediate these conformational changes (Fox et al., 2011; Dölker et al., 2013; Monecke et al., 2013; Monecke et al., 2014). In the nucleus, helix 21B and the acidic c-terminal tail of free Crm1 lie across the toroid and interact with HEAT repeats on the opposed side (H9-12) (Fox et al., 2011; Monecke

et al., 2014). Besides, the acidic loop at HEAT repeat 9 binds to the HEAT repeats 11 and 12 that form the NES cleft. These interactions stabilize the closed NES cleft (Fox et al., 2011; Monecke et al., 2014). Thus, unbound Crm1 exhibits the extended, superhelical conformation with low affinity for cargo proteins (Monecke et al., 2014). The C- and N-termini are not interacting with each other and the CRIME domain is easily accessible for RanGTP. (Monecke et al., 2014)
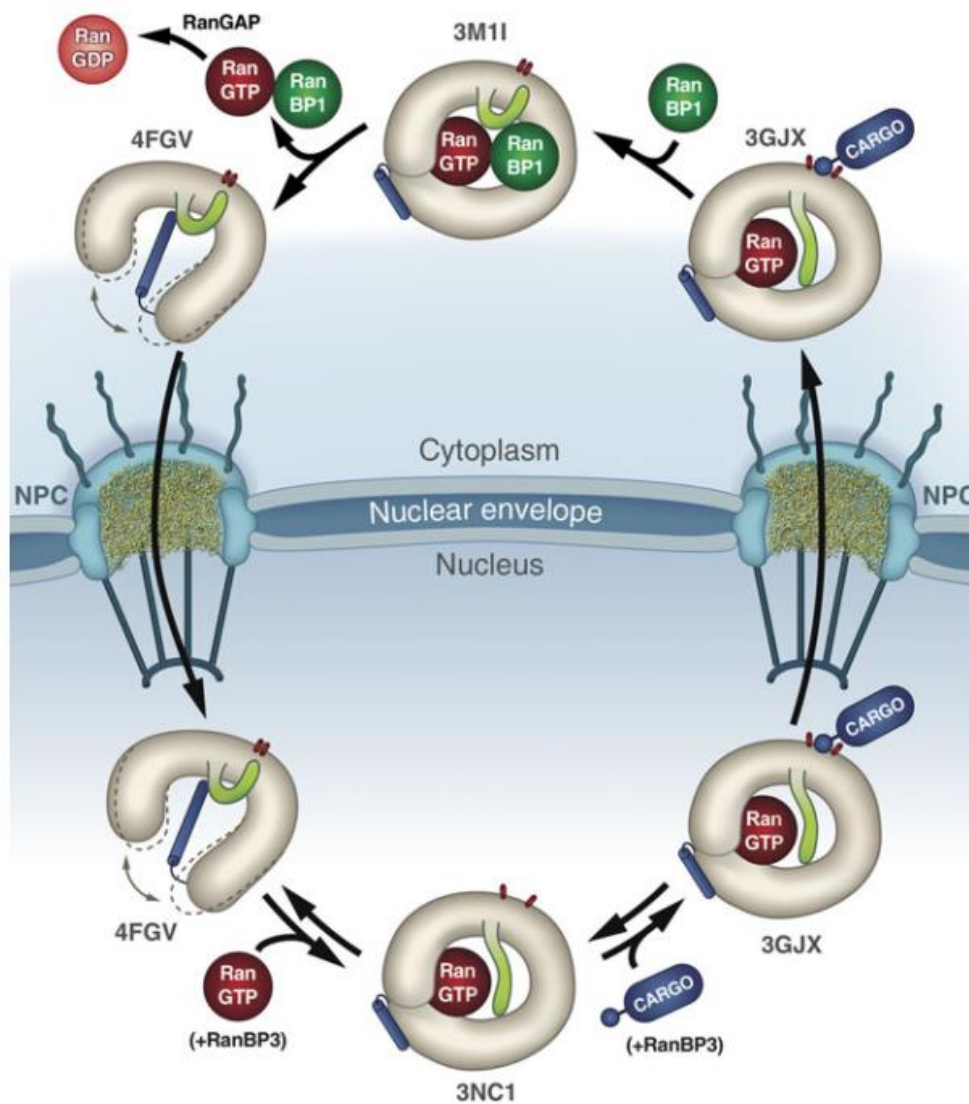
Figure 1-12: Overview of Crm1's conformational changes during an export cycle.

The conformation of Crm1 (grey) changes during the transport cycle. Especially the positions and local conformations of the acidic loop (light green), the C-terminal B-helix of HEAT repeat 21 (blue) and the NES cleft (red) change (Monecke et al., 2014). The dashed line based on free Crm1 shows its structural flexibility. The PDB ID for each structure is stated. See main text for details.

Upon RanGTP binding, the local positions of the acidic tail (H21) and loop (H9) change and lead to overall rearrangements of Crm1 resulting in the compact form, in which RanGTP is encircled by the toroid. Here, helix 21B stacks parallel to the other C-terminal HEAT repeats and the acidic loop locks Ran to the CRIME domain (Monecke et al., 2009; Monecke et al., 2014). Hence, the effects that maintained the closed NES cleft are reversed and the hydrophobic groove opens for cargos. The assembly factor RanBP3 seems to stabilize the Crm1-Ran-complex, as well as the ternary complex with the cargo in the nucleus (Englmeier et al., 2001; Lindsay et al., 2001).

After transport through the membrane, the complex disassembles as GTP is hydrolyzed by the RanGAP (Dahlberg and Lund, 1998; Monecke et al., 2014). This process is aided by cytoplasmic RanBP1, which induces rearrangements in the protein complex (Bischoff et al., 1995; Koyama and Matsuura, 2010; Monecke et al., 2013; Monecke et al., 2014). Upon RanBP1 binding, the HEAT 9 loop moves to the inner surface of Crm1 behind the NES cleft and causes changes in the conformations of HEAT 11 and 12, which release the cargo as the NES cleft is constricted (Koyama and Matsuura, 2010). Furthermore, the hydrolysis of GTP to GDP by RanGAP reduces the affinity of Ran for Crm1, which disassembles the whole complex, and free Crm1 diffuses to the nucleus to mediate the next export cycle (Monecke et al., 2014).

1.1.3.2 INHIBITORS OF CRM1 MEDIATED NUCLEAR EXPORT

The export receptor Crm1 is overexpressed in various cancer cells and exports several (proto-)oncogenes and tumor suppressors such as p53, Cyclin D1 or breast cancer 1 (BRCA1), and thus arose interest as potential target in cancer therapies (Monecke et al., 2014; Ferreira et al., 2020). Leptomycin B (LMB), a natural product from *Streptomyces* and originally discovered as antifungal antibiotic (Hamamoto et al., 1983), is the first identified and most prominent Crm1 inhibitor (Dickmanns et al., 2015). It binds covalently to Crm1's NES cleft at cysteine 528, and thus blocks it for cargo proteins (Figure 1-13) (Kudo et al., 1999). LMB is modified by Crm1, which renders its binding irreversible (Sun et al., 2013). Phase I clinical trials with LMB revealed dose-limiting toxicity and severe side effects, which made it unsuitable as a therapeutic (Newlands et al., 1996).

In the last decade, *in silico* docking methods have been used to develop new small molecules that bind to Crm1's cysteine 528 and were called selective inhibitors of nuclear export (SINEs) (Lapalombella et al., 2012; Ferreira et al., 2020). Their interaction with Crm1 is also covalent but in contrast to LMB it is slowly reversible and SINEs occupy less space in the NES groove as they are smaller (Sun et al., 2013; Sun et al., 2016; Ferreira et al., 2020). These second

generation export inhibitors have been studied in several preclinical models and showed potent activity against cancer cells, such as growth inhibition or increased apoptosis, and only minor toxicity for normal cells (Sendino et al., 2018). The most prominent SINE is Selinexor, which has been tested in a large number of clinical studies either as single agent or in combination with other cancer drugs, and showed a broad activity in several types of solid tumors (reviewed in Sendino et al. (2018)). In fact, it has been approved for the treatment of refractory multiple myeloma under the name XPOVIO™ (Karyopharm Therapeutics, Newton, USA) by the U.S. Food and Drug Administration (FDA) in 2019, as it showed clinical benefit when co-administered with dexamethasone (Chari et al., 2019; U.S. Food and Drug Administration, 2019). However, in this study patients suffered from severe side effects including thrombocytopenia (73 %), nausea (72 %), fatigue (73 %), anemia (67 %) and neutropenia (40 %) (Chari et al., 2019).
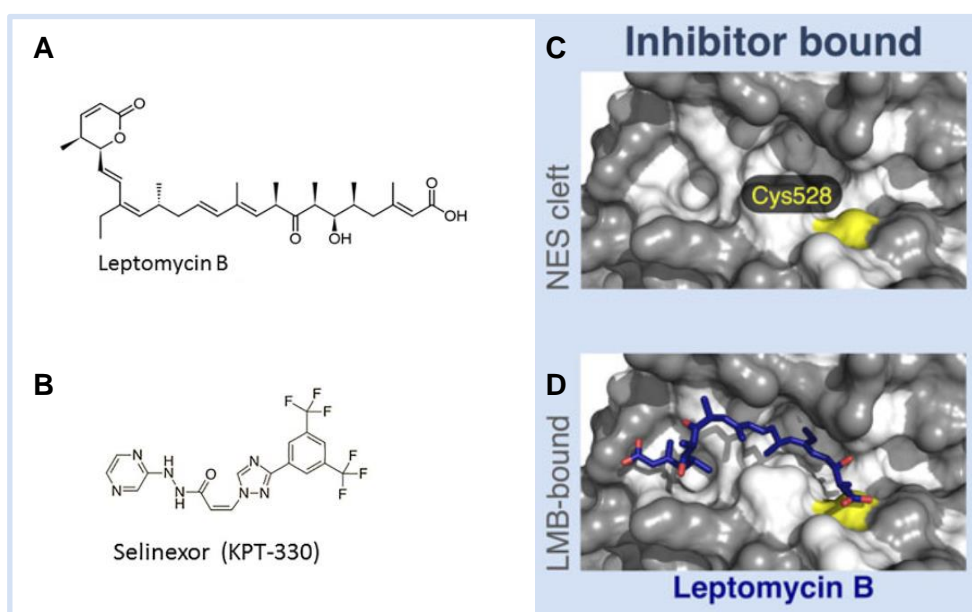
Figure 1-13: Export inhibitors of Crm1 bind covalently at cysteine residue 528 in the NES cleft.
Chemical structures of inhibitors Leptomycin B (LMB) (A) and Selinexor (B) (Ferreira et al., 2020). Binding of export inhibitors is mostly reliant on cysteine residue 528 (yellow) in Crm1's NES cleft (C). LMB binds covalently to C528 and blocks the NES cleft (Monecke et al., 2014).

Even though Crm1's overexpression is associated with cancer, it nevertheless fulfills important roles such as nuclear export or export-independent regulation of mitosis in normal cells (Arnaoutov et al., 2005; Sendino et al., 2018). As it serves as export receptor for a variety of proteins, its inhibition likely results in toxic effects for healthy tissues. Transport inhibitors that target a cancer-specific cargo itself might be more appropriate for a well-tolerated treatment. As Survivin is upregulated in most tumor cells and absent in normal resting tissues (Ambrosini

et al., 1997), it is a more specific target in tumor therapies and its inhibition might cause lower toxicities than Crm1's.

1.1.4 SURVIVIN AS TARGET IN CANCER THERAPY

For a long time, Survivin has been considered "undruggable" and no Survivin-specific cancer drug has yet reached the clinic (Peery et al., 2017; Wheatley and Altieri, 2019). Lacking catalytic activity and deep pockets, Survivin can hardly be targeted by conventional small molecules (Peery et al., 2017; Wheatley and Altieri, 2019). Nevertheless, several different strategies are pursued to develop treatments, which specifically target cancer cells overexpressing Survivin (Figure 1-14).

Survivin has often been targeted on its expression level using antisense oligonucleotides and small interfering (si)RNAs (Peery et al., 2017). The single strand antisense oligonucleotide LY2181308 developed by Eli Lilly, which targets Survivin's mRNA, has been clinically tested with patients suffering from acute myeloid leukemia (AML; Phase I) and prostate cancer (Phase II) (Peery et al., 2017). For AML, synergistic effects with the chemotherapeutics cytarabine and idarubicin could be observed in a small cohort (Erba et al., 2013). However, for solid tumors, LY2181308 did not have additional benefits when co-administered with docetaxel and prednisone (Wiechno et al., 2014; Peery et al., 2017). Other antisense oligonucleotides did not exceed phase I studies and showed disadvantages like instability and low availability, and exhibited dose-limiting toxicities (Raetz et al., 2014; Peery et al., 2017). Furthermore, small molecules that interfere with the Survivin expression have been tested in preclinical and phase I and II clinical studies (Khanna et al., 2007; Nakahara et al., 2007; Giaccone et al., 2009; Grossman et al., 2012b; Peery et al., 2017). The most prominent small molecule transcription inhibitor YM155 has been identified as suppressor of the Survivin promotor via high-throughput screening (Nakahara et al., 2007). However, it has shown only mixed effects in clinical phase I and II studies and its exact mechanism remains unclear, as DNA damaging effects were observed in addition to the suppression of Survivin's expression (Peery et al., 2017).
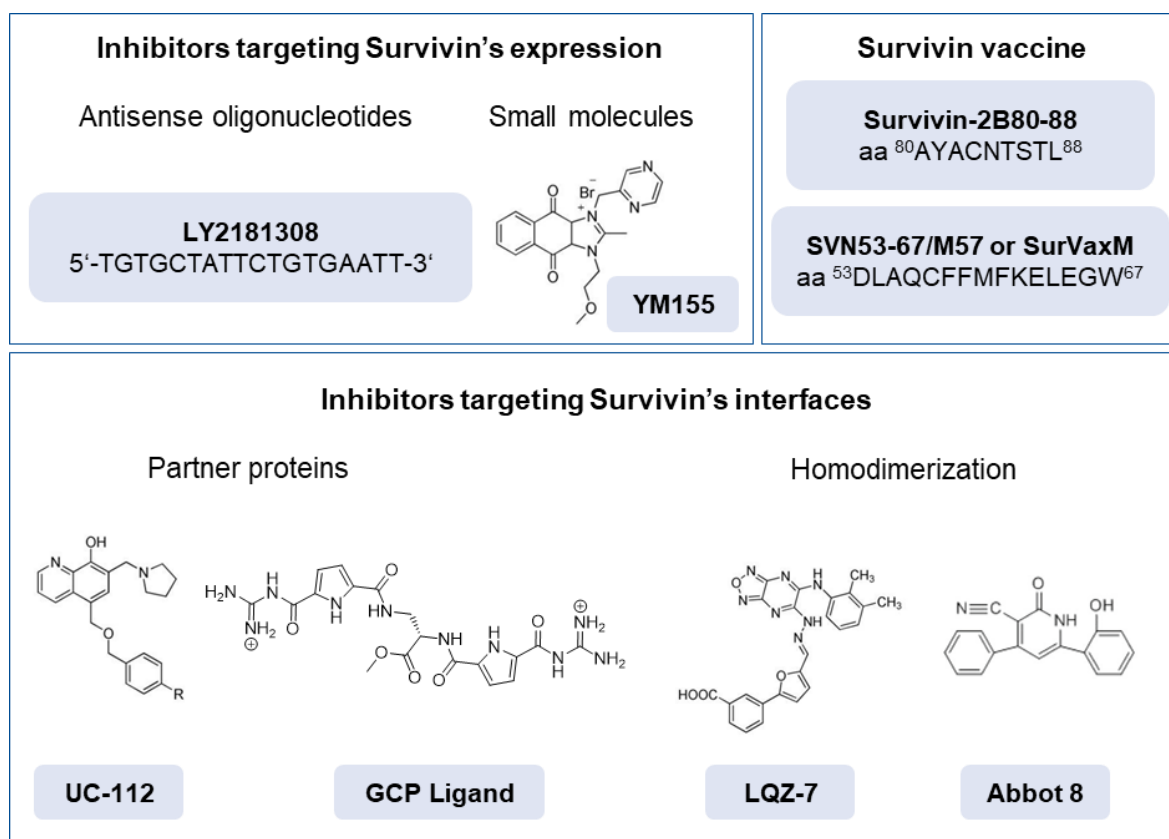
Figure 1-14: Overview of different strategies to target Survivin in cancer therapies.

Survivin has been targeted during the development of new cancer therapies via many different routes. Either its expression, or alternatively protein-protein interactions as well as homodimerization have been inhibited with antisense oligonucleotides, small molecules or peptide mimetics. Furthermore, Survivin has been tested as cancer vaccine. The most prominent approaches and recently identified ligands are depicted. Several interactions with partner proteins are targeted by ligands: a Smac mimetic, UC-112, interferes with the Survivin/Smac interaction, and the depicted guanidiniocarbonyl pyrrole (GCP) ligand disrupts the Survivin/Histone H3 interaction. Modified after Peery et al. (2017), Bäcker (2018), Wang et al. (2018), Li et al. (2019) and Vallet et al. (2020).

Survivin has also arose interest as cancer vaccine. Peptide mimetics (e.g. survivin-2B80-88 or SVN53-67/M5, also called SurVaxM), derived from Survivin's amino acid sequence, have been used to induce cytotoxic T lymphocyte responses by binding to human leukocyte antigens (HLAs), e.g. HLA-24A (Hirohashi et al., 2002; Ciesielski et al., 2010). The cytotoxic T cells were then able to recognize cancer cells expressing HLA-A24 and presenting endogenous Survivin peptides (Peery et al., 2017). The vaccine SurVaxM decelerated the cancer progression and prolonged the survival of patients with recurrent malignant glioma in first studies, and thus has entered phase II clinical trials (Fenstermaker et al., 2016).

Targeting Survivin on the protein level is challenging since it has no enzymatic activity and lacks deep pockets. However, attempts have been made to inhibit Survivin protein interactions

or the homodimerization of Survivin with small molecules or peptide mimetics (Peery et al., 2017). A structure-based screening for Smac mimetics identified a compound (UC-112), which increased caspase (3, 7 and 9) activity and was predicted to bind to Survivin's BIR domain (Wang and Li, 2014; Xiao et al., 2015). UC-112 decreased protein levels of Survivin and XIAP, probably by increasing their degradation via the proteasome. Nevertheless, its specificity for Survivin needs to be enhanced, even though this has already been partly achieved with the analog 4g (Xiao et al., 2015), and its mechanism of action requires further elucidation (Wang and Li, 2014; Peery et al., 2017). Especially the question, whether the inhibition of tumor growth is really due to interference of UC-112 (and its analog) with the Survivin/Smac interaction, remains open (Li et al., 2019). Small molecules inhibiting the dimerization of Survivin might increase degradation of the protein as the hydrophobic interface becomes exposed (Qi et al., 2016; Peery et al., 2017). The first compounds binding to Survivin's dimer interface were Abbot 8, identified via NMR-based screening, and compound LQZ-7, found by computational screening, which were both further improved by the generation of analogs (LLP3/LLP9 and LQZ-7F) to efficiently disrupt homodimerization and promote Survivin degradation (Wendt et al., 2007; Qi et al., 2016; Peery et al., 2017). However, none of these Survivin compounds has been clinically tested yet.

Recently, Survivin has been targeted using protein-derived small INCENP peptides (Fuchigami et al., 2020) and ligands based on the artificial amino acid-receptor guanidiniocarbonyl pyrrole (GCP) (Vallet et al., 2020). These Survivin ligands are based on supramolecular interactions and might represent a new class of drugs, which overcome obstacles such as the lack of enzymatic activity and deep pockets that conventional small molecules face. However, improvements concerning the specificity, cellular uptake ability and availability or solubility of the ligands are still required (Bäcker, 2018; Vallet, 2019; Fuchigami et al., 2020). One of the most interesting surface areas of Survivin is its NES, as it is pivotal for Survivin's dual role in mitosis and apoptosis and represents the interface for Crm1 (Knauer et al., 2007). Indeed, first efforts towards specific Survivin NES binders have been taken using supramolecular chemistry within the Knauer group (Bäcker, 2018; Heid, 2018; Vallet, 2019).

1.2 SUPRAMOLECULAR CHEMISTRY

Supramolecular chemistry was defined as "chemistry beyond the molecule" by Jean-Marie Lehn, who received the Nobel Prize in chemistry in 1987 together with Donald J. Cram and Charles J. Pedersen (Lehn, 1988). While molecular chemistry deals mainly with covalent bonds, supramolecular chemistry is based on non-covalent intermolecular forces between two or more molecules (Lehn, 1988; Steed et al., 2007). It makes use of a toolbox of molecular building blocks, which are held together by intermolecular bonds including electrostatic interactions, hydrogen bonding and π–π interactions (Steed et al., 2007).

1.2.1 SUPRAMOLECULAR INTERACTIONS

Supramolecular interactions are generally weaker than covalent interactions (Steed et al., 2007). However, electrostatic interactions represent the strongest non-covalent interactions and reach strengths only slightly lower then covalent interactions (Albrecht, 2007; Steed et al., 2007). They are based on the attraction of opposite charges of ions or dipoles (Albrecht, 2007). The second highest strength is exerted with hydrogen bonding, which involves proton donors and acceptors (Steed et al., 2007). Proton donors consist of a hydrogen atom attached to an electronegative atom like oxygen, resulting in a dipole and, thus, a positive charge at the hydrogen atom, whereas proton acceptors are dipoles carrying a strong negative charge accessible for the positively charged hydrogen (Steed et al., 2007). Further types of non-covalent interactions comprise van der Waals and π-π interactions. The latter are based on ring-systems, and thus on the attraction of their negatively charged π-electron cloud and the positively charged σ-framework of a neighboring ring-system (Steed et al., 2007).

Weak van der Waals interactions result from fluctuations in the electron distribution between nearby molecules. Upon electron movements within one molecule, instantaneous dipoles are generated, which can attract dipoles with opposed charge from another molecule (Steed et al., 2007). Last, hydrophobic interactions, which occur amongst others when a guest molecule replaces water molecules within a cavity of a host molecule, play a role in supramolecular chemistry (Steed et al., 2007). Even though a single non-covalent interaction, e.g. one hydrogen bond, is rather weak, in combination with several others, the bond energy accumulates and renders the binding stable (Albrecht, 2007). This cooperativity effect is crucial, when molecular building blocks form preorganized receptor molecules, which use

"molecular recognition" based on well-defined interaction patterns such as sequences of donor and acceptor groups or hydrogen bonding arrays (Lehn, 2002).

1.2.2 SUPRAMOLECULAR CHEMISTRY FOR PROTEIN TARGETS

Proteins are crucially involved in key processes in cells. Their functions include signaling, transportation or catalysis, and are often mediated via protein-protein interactions (PPI) (Peczuh and Hamilton, 2000; Keskin et al., 2008; van Dun et al., 2017). Unfortunately, PPIs can also be associated with diseases including cancer, and the development of small molecules, which recognize and target involved protein surface regions with high affinity and selectivity, is challenging (Kar et al., 2009; Kubota and Hamachi, 2015). Since the interaction between proteins is often conducted by larger surfaces (van Dun et al., 2017), targeting with conventional small molecules is not sufficient. Therefore, specific, tailor-made molecules, which cover larger protein areas, are required. Supramolecular chemistry can provide a solution to this problem, since it enables the combination of several binders for diverse protein surface elements. Artificial host molecules, which recognize their target through non-covalent host-guest interactions (van Dun et al., 2017), can be expanded by additional molecular recognition units that might enhance affinity or specificity for one protein.

Host-guest chemistry plays an important role in supramolecular chemistry and implies the interactions between a large host and a smaller guest molecule, which can be enclosed by the host via non-covalent interactions (Steed et al., 2007). For this purpose, both molecules must have appropriate interaction sites and the selectivity of the host can be achieved amongst others by complementarity or cooperativity of binding groups (Steed et al., 2007). Artificial host molecules can be used to recognize biological targets such as specific amino acids or peptide fragments, and thereby modulate their functions (Figure 1-15) (van Dun et al., 2017). Examples are crown ethers, curcubiturils, calixarenes (Zadmard and Alavijeh, 2014) or molecular tweezers (van Dun et al., 2017).
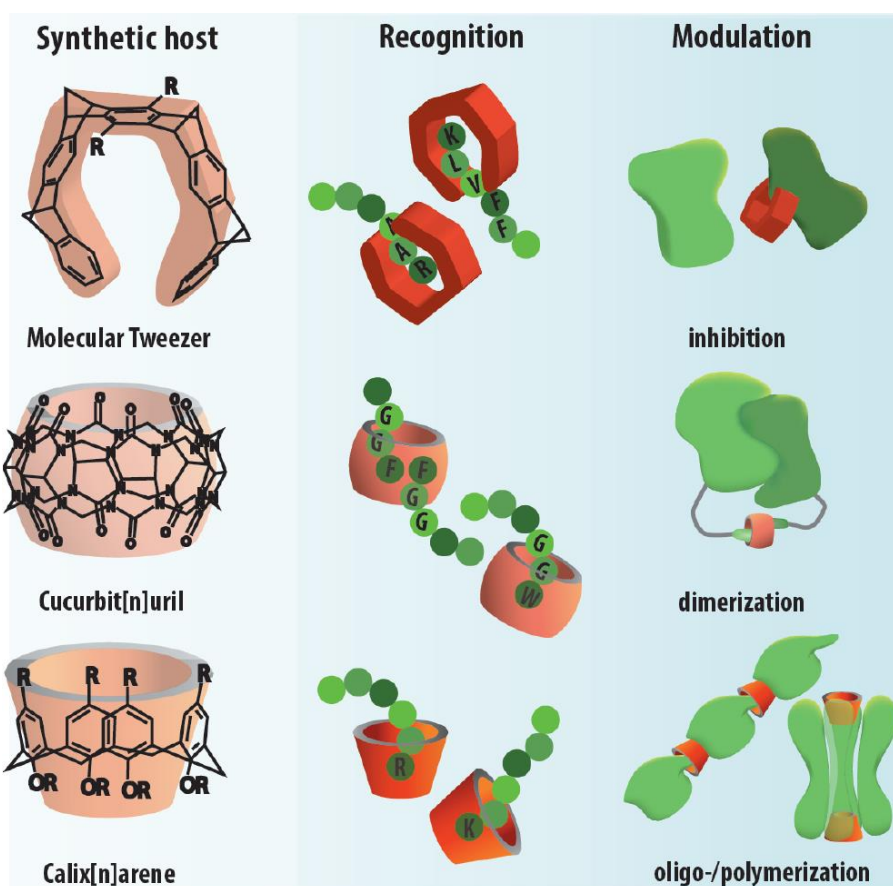
Figure 1-15: Artificial host molecules recognize and modulate their biological targets.

Artificial host molecules can selectively recognize amino acids and peptides, and thus modulate protein functions. Scheme of supramolecular hosts, their peptide sequence recognition and protein modulation mechanisms (van Dun et al., 2017).

1.2.2.1 *AMINO-ACID SELECTIVE MOLECULAR TWEEZER*

An artificial host receptor for selective binding of lysine and arginine residues is the water-soluble molecular tweezer (Fokkens et al., 2005). In 1978 Chen and Whitlock first introduced the term "molecular tweezer" for a bifunctional derivate of caffeine (C. W. Chen and H. W. Whitlock Jr.). Two caffeine molecules were linked by a rigid diyne unit, which prevents self-association and keeps the two units at a distance of ~ 7 Å. This and the resulting *syn* conformation enables insertion of π-systems between the rings (Figure 1-16 A). During the next years, the original molecular tweezer was modified several times. Zimmerman and co-workers (Zimmerman and VanZyl, 1987) enhanced the insertion of guest molecules through a more rigid structure (Figure 1-16 B). Klärner and co-workers developed tweezer molecules

consisting of alternating norbornadiene and benzene rings, rendering it an enhanced binder for aromatics (Figure 1-16 C) (Klärner et al., 1996).

A   **B**   **C**

$R^1 = CH_3$

$R^2 = CO_2CH_3$

First molecular tweezer **Rigid molecular tweezer** **Molecular tweezer**
by Whitlock et al. **by Zimmerman et al.** **by Klärner et al.**
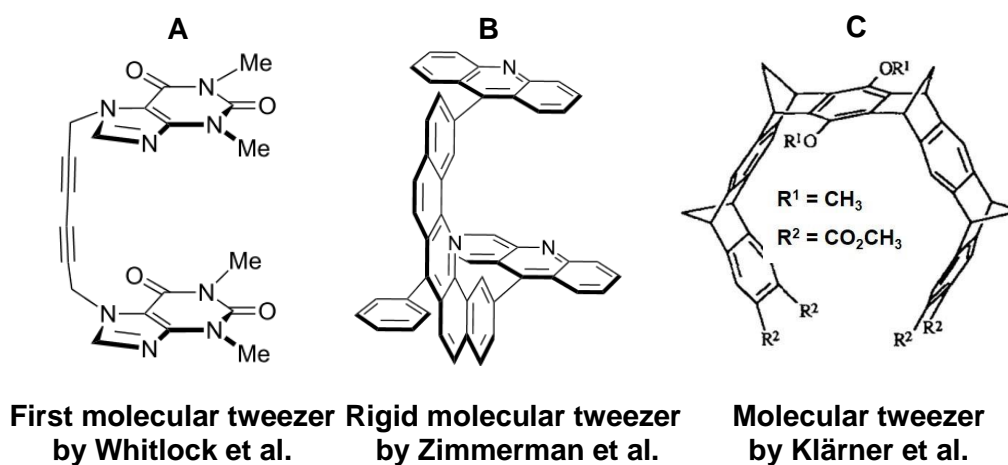
Figure 1-16: Development of molecular tweezers.

Structures of Whitlock's first molecular tweezer (A) and its successors: the rigid tweezer by Zimmermann and coworkers (B) and a molecular tweezer for aromatics by Klärner et al. (C). Modified after Klärner et al. (1996) and Zimmerman (2016).

For the use in biological systems, the molecular tweezer was further improved by Frank-Gerrit Klärner and Thomas Schrader. In 2005, they developed a water-soluble host molecule featuring a torus-shaped unpolar cavity and two rotatable peripheral anionic phosphonate groups (Figure 1-17 A) (Fokkens et al., 2005). As its predecessor, this tweezer consists of alternating norbornadiene and benzene rings forming a hydrophobic cavity. The bi-phosphonate tweezer is capable of binding amino acids with positive side chains, making it selective for lysine and arginine residues as indicated by high binding constants of up to 5000 M^{-1} (Figure 1-17 B). The host threads its guest molecules lysine (Figure 1-17 C) as well as arginine (Figure 1-17 D) in the cavity, where it is bound non-covalently (Fokkens et al., 2005). The bi-phosphonate groups form salt bridges with the ammonium or guanidinium cation of the guest molecule (Fokkens et al., 2005). Van der Waals and electrostatic interactions as well as hydrophobic effects facilitate binding of the guest into the cavity (Hadrovic et al., 2019). The phosphonate groups were exchanged by two phosphate groups, which has further enhanced the tweezer's affinity for lysines and arginines (Heid, 2018).

Since its development, the bi-phosphate tweezer (which will hereinafter be referred to as TW) has been tested as inhibitior for virus infections (Röcker et al., 2018), fibril formation associated to amyloidosis (Sinha et al., 2011; Prabhudesai et al., 2012; Hadrovic et al., 2019) and single protein-protein interactions (Bier et al., 2013; Trusch et al., 2016), and thus proven its potential

for biological applications. Although the molecular tweezer is selective for lysines and arginines, it is not specific for a certain area on a protein surface. To achieve the required specificity, it needs to be equipped with additional recognition units. Indeed, first steps were already taken to make the amino acid-selective tweezer more specific for one protein binding site, namely Survivin's NES, via peptide-modification (Bäcker, 2018; Heid, 2018).
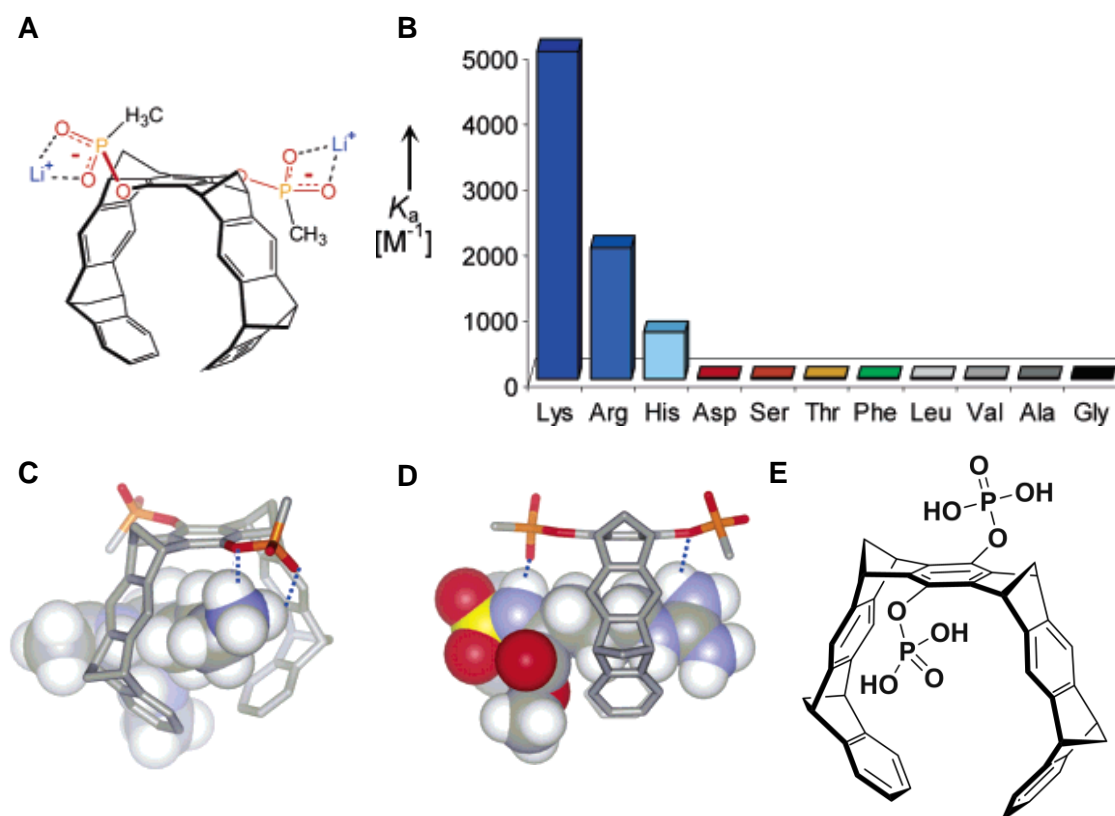
Figure 1-17: Lysine- and arginine-selective molecular tweezer.
A) Chemical structure of the bi-phosphonate tweezer. B) The bi-phosphonate tweezer is selective for positive amino acids as indicated by high binding constants and favors lysine. Monte Carlo simulations show how the side chains of lysine (C) and arginine (D) are threaded in the tweezer's cavity. A-D) Modified after Fokkens et al. (2005). E) The chemical structure of the bi-phosphate tweezer was provided by Dr. Christian Heid (Schrader group, University of Duisburg-Essen).

1.3 AIM OF THIS THESIS: ENHANCEMENT OF SURVIVIN NES BINDER SPECIFICITY

The protein Survivin is mostly absent in differentiated tissues, but highly upregulated in cancer cells (Ambrosini et al., 1997; Adida et al., 1998; Adida et al., 2000). It fulfills roles in mitosis as well as apoptosis, which are mediated via the interaction between Survivin's NES and the export receptor Crm1 (Knauer et al., 2007). Therefore, this PPI is an attractive target for cancer research and therapy. As inhibiting Crm1 interferes also with a variety of other cargo proteins besides Survivin, and produces severe side effects for patients, a Survivin-specific approach is required. However, Survivin has no enzymatic activity nor deep pockets for small-molecules and, thus, can hardly be targeted with conventional strategies. Recently, a novel approach based on non-covalent, supramolecular ligands has been explored involving amino acid-selective tweezers (Bäcker, 2018; Heid, 2018), which were further examined in this thesis.

1.3.1 ASSESSMENT OF PEPTIDE-MODIFIED TWEEZERS

As part of the collaborative research center for supramolecular chemistry on proteins (CRC1093), peptide-modified tweezers were developed by the groups of Prof. Dr. Thomas Schrader and Prof. Dr. Shirley Knauer. Asymmetric basic molecular tweezers were developed and equipped with peptides derived from Survivin's homodimerization interface (Figure 1-18 A) (Bäcker, 2018; Heid, 2018). The sequences of the attached peptides ELTL (Figure 1-18 B) and ELTGEFL (Figure 1-18 C) were chosen in order to represent a second recognition unit for the dimer interface and should increase the specificity of the basic tweezer for Survivin's surface (Bäcker, 2018; Heid, 2018). The dimer interface is mainly constituted by hydrophobic amino acids (Chantalat et al., 2000; Verdecia et al., 2000). Especially, L98 of one monomer protrudes into a hydrophobic pocket formed by L6 and L102, W10 as well as F93 and F101 on the second protomer (Verdecia et al., 2000). Therefore, the sequence [95]ELTLGEFL[102] on Survivin's surface is essential for dimerization and conjugation of this sequence to the tweezer should direct the supramolecular ligand to the dimer interface and, thus, the NES as they partly overlap.
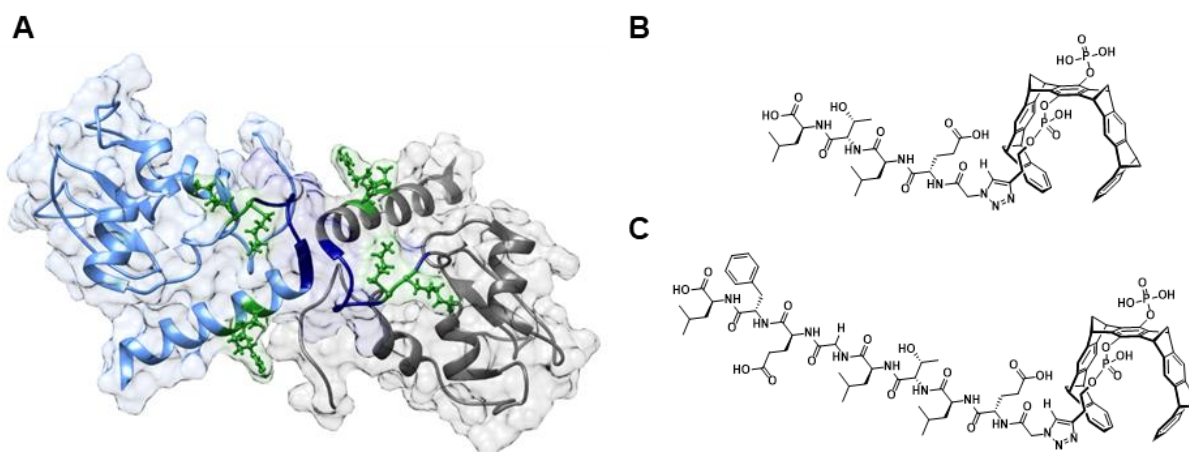
Figure 1-18: Peptides derived from Survivin's dimer interface were conjugated to molecular tweezers.

A) Survivin features a dimerization interface that partly overlaps with its NES. The NES is highlighted in dark blue, basic amino acids in the proximity of the NES are colored in green and depicted as sticks (PDB ID: 1XOX). A short peptide ELTL (B) and the longer sequence ELTLGEFL (C) were derived from the dimer interface and conjugated to the molecular tweezer.

So far, it was shown that the unmodified tweezer (TW) and the short peptide-modified tweezer (TW-ELTL) bind to basic amino acids in and near Survivin's NES (K90/91/103 and R106) and interfere with the interaction with the export receptor Crm1 (Bäcker, 2018). However, the exact binding site of the tweezers needs to be further confirmed and the regioselectivity and signal-specificity of the peptide-tweezers should be examined in this thesis.

1.3.2 DEVELOPMENT OF TWEEZER-EQUIPPED PRECISION MACROMOLECULES

The generation of asymmetric tweezer molecules, which have already successfully been conjugated with peptides (Heid, 2018), paved the way for the combination of several tweezer units in one ligand and their modification with other types of molecules. This thesis addressed this issue by developing molecular double-tweezers (dTWs). These molecules contain two tweezer units that are supposed to bind to the protein surface simultaneously. Survivin's NES is enclosed by several basic amino acids (K90, K91 K103 as well as R106; Figure 1-18 A) and, thus, offers anchor residues for tweezer units on both sides of the NES epitope. The question whether the combination of two tweezer units in one ligand and the correct choice of a suitable linker can enhance the specificity for Survivin's NES, should be investigated. Therefore, the use of precision macromolecules based on monodisperse, sequence-defined oligomers was explored for the development of tailor-made ligands for Survivin's surface. These ligands consisted of different functional monomeric building blocks, which can be combined with

tweezers, peptides, nanoparticles or any other ligand carrying reactive groups, creating unique structures.
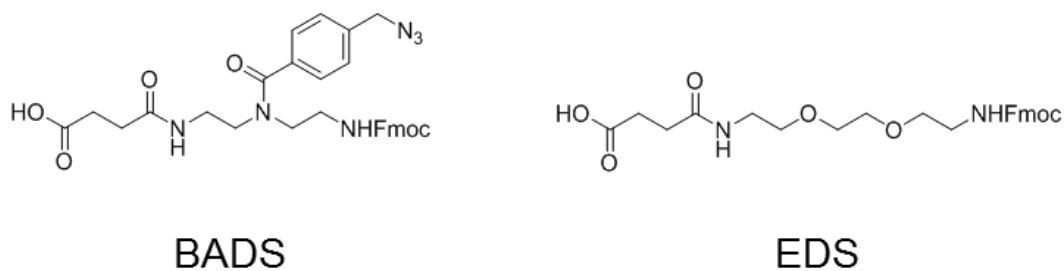
Figure 1-19: Building blocks for precision macromolecules.
Monomeric building blocks can be combined to create a scaffold for amino acid-selective ligands. The building block BADS (p-(azidomethyl)benzoyl diethylenetriamine succinic acid) contains an azide group and, thus, can be clicked to tweezers. The building block EDS, which is based on 2,2'(Ethylenedioxy)bis(ethylamine) and succinic acid, can be used as spacer to maintain specific distances between tweezer units. Images were provided by Theresa Seiler (Hartmann group, Heinrich Heine University Düsseldorf).

The precision oligomers used in this work contain two different building blocks that differ in their arrangement and quantity (Figure 1-19). The building block EDS serves as spacer in this arrangement, while the building block BADS contains an azide group for the addition of tweezers via click reaction (Ebbesen et al., 2016; Baier et al., 2018). The oligomer dTWs were developed together with the groups of Prof. Dr. Laura Hartmann (Heinrich Heine University, Düsseldorf) and Prof. Dr. Thomas Schrader (University of Duisburg-Essen, Essen).Three macromolecules with different lengths, each containing two tweezer units in different distances, were designed based on the building blocks BADS and EDS (Figure 1-20). The shortest precision macromolecule contains only two BADS blocks, enabling the attachment of two tweezers at a distance of approx. 8 Å. The middle macromolecule is composed of two BADS blocks separated by one EDS block, resulting in a distance of 32 Å between the two azides for click coupling. The longest macromolecule is equipped with two BADS blocks and three EDS blocks in between, enabling a distance of the azides of approx. 67 Å.

Furthermore, tweezer molecules were conjugated to cell-permeable ultra-small gold nanoparticles as an alternative scaffold to the oligomeric macromolecules. As they might enable cellular uptake of potential inhibitors of the Survivin/Crm1 interaction, the ability of the modified nanoparticles to bind to Survivin should be assessed.
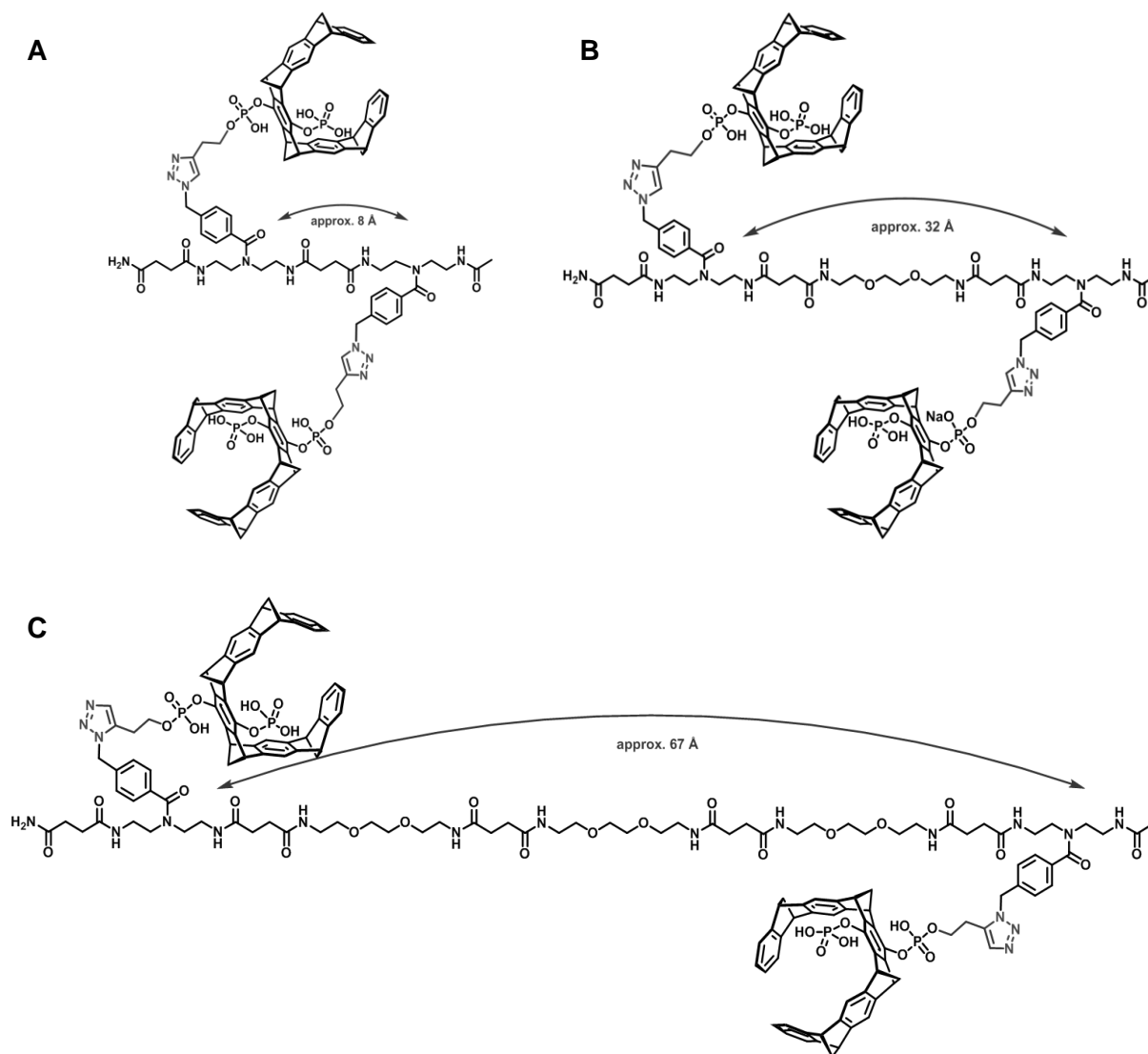
Figure 1-20: Oligomer double-tweezers.

Monomeric building blocks BADS and EDS were combined to develop three oligomer dTWs with different lengths. A short (A), middle (B) and long (C) oligomer scaffold was conjugated with two tweezer units. The images were provided by Inesa Hadrovic (Schrader group, University of Duisburg-Essen).

Taken together, this thesis aimed to analyze the effects of different mono- or multivalent tweezers on the Survivin/Crm1 interaction. As this PPI is pivotal for both functions of Survivin, in mitosis and apoptosis, its inhibition with the supramolecular ligands would set the ground for other tailor-made molecules in novel anti-cancer approaches.

2 MATERIAL AND METHODS

2.1 MATERIALS

2.1.1 LABORATORY DEVICES

All laboratory devices and instruments used in this work are listed in Table 2-1.

Table 2-1: Laboratory devices.

Laboratory device	Manufacturer
Agarose gel electrophoresis chamber	Peqlab Biotechnologie GmbH, Erlangen
Analytical balance CP124S	Sartorius AG, Göttingen
BioPhotometer® Plus	Eppendorf AG, Hamburg
Calorimeter MicroCal iTC200	Malvern Panalytical GmbH, Kassel
Centrifuge Sorvall™ RC 6 Plus	Thermo Fisher Scientific, Waltham
Centrifuge 5417 C/R	Eppendorf AG, Hamburg
Centrifuge Allegra X-22	Beckman Coulter GmbH, Krefeld
Centrifuge ROTINA 380/380 R	Andreas Hettich GmbH & Co. KG, Tuttlingen
ChemiDoc Imaging System	Bio-Rad Laboratories GmbH, Munich
Chemistry pumping unit	Vacuubrand GmbH & Co. KG, Wertheim
CO_2 incubator	Binder GmbH, Tuttlingen
CO_2 incubator	Memmert GmbH & Co. KG, Schwabach
Confocal laser scanning microscope (inverse) TCS SP8	Leica Microsystems GmbH, Mannheim
Gel caster	Bio-Rad Laboratories GmbH, Munich
Gel documentation system E-Box VX2	Vilber Lourmat Deutschland GmbH, Eberhardzell
GrantBio 360° vertical multi-function rotator PTR-30	Grant Instruments Ltd, Cambridge
GrantBio orbital shaking platform POS-300	Grant Instruments Ltd, Cambridge
Heating plate	Medax GmbH & Co. KG, Rendsburg
Liquid chromatography (LC) system ÄKTApurifier™	GE Healthcare Life Sciences, Freiburg
Magnetic stirrer Hei-Mix L	Heidolph Instruments GmbH & Co. KG, Schwabach
Magnetic stirrer HI 180	Hanna Instruments Deutschland GmbH, Kehl
Microscope Primo Vert	Carl Zeiss, Oberkochen

Laboratory device	Manufacturer
Mini centrifuge Spectrafuge	Labnet International Inc, Edison
NMR spectrometer (700 MHz Ultrashield)	Bruker Corporation, Rheinstetten
Orbital benchtop shaker MaxQ™ 4000	Thermo Fisher Scientific, Waltham
Orbital shaker POS-300	Grant Instruments Ltd, Royston
Orbital tabletop shaker Forma 420 Series	Thermo Fisher Scientific, Waltham
Peristaltic pump P-1	GE Healthcare Life Sciences, Freiburg
Pipettes Research Plus	Eppendorf AG, Hamburg
Pipetting aid Pipetus®	Hirschmann Laborgeräte GmbH & Co. KG, Eberstadt
FiveEasy Plus pH meter FP20	Mettler Toledo, Gießen
PAGE chamber Mini-PROTEAN® Tetra Cell	Bio-Rad Laboratories GmbH, Munich
Power supply peqPOWER 300	PEQLAB Biotechnologie GmbH, Erlangen
Power supply PowerPac Basic	Bio-Rad Laboratories GmbH, Munich
Precision balances 440-21A/440-47N	Kern & Sohn GmbH, Balingen
Rotator PTR-30	Grant Instruments Ltd, Royston
Safety cabinet NuAire NU-437-400E	Integra Biosciences GmbH, Fernwald
Safety cabinets HERAsafe	Thermo Fisher Scientific, Waltham
Spectrofluorometer FP-8300 equipped with a CTU-100 circulating thermostat unit	Jasco Corporation, Tokyo
Spectrophotometer NanoDrop™ 2000c	Thermo Fisher Scientific, Waltham
Tank electro blotter PerfectBlue™	PEQLAB Biotechnologie GmbH, Erlangen
Thermal mixer ThermoMixer Comfort	Eppendorf AG, Hamburg
Thermal mixer MHR 11	HLC BioTech, Bovenden
Thermocycler TProfessional standard gradient 96	Biometra GmbH, Göttingen
Ultrasonic homogenizer mini20	Bandelin electronic GmbH & Co. KG, Berlin
Ultrasonic homogenizer Sonopuls HD 2070	Bandelin electronic GmbH & Co. KG, Berlin
UV Sterilizing PCR Workstation	Peqlab Biotechnologie GmbH, Erlangen
Vortexer Vortex-Genie 2	Scientific Industries, Bohemia
Water bath 1002-1013	Gesellschaft für Labortechnik mbH, Burgwedel
Water purification system Milli-Q® Advantage A10	Merck KGaA, Darmstadt

2.1.2 CONSUMABLES

Consumables used in this work are listed in Table 2-2. All other disposables, which are not stated in this table, were obtained from Sarstedt AG & Co. KG (Nümbrecht).

Table 2-2: Consumables.

Item	Supplier
Affinity chromatography column GSTrap™ 4B, 5 ml	GE Healthcare Life Sciences, Freiburg
Affinity chromatography column HisTrap™ FF, 5 ml	GE Healthcare Life Sciences, Freiburg
Anion exchange chromatography column HiTrap™ Q HP, 5 ml	GE Healthcare Life Sciences, Freiburg
Centrifugal Concentrators VivaSpin® 500/6/Turbo 15 (MW cutoff 10/30 kDa)	Sartorius AG, Göttingen
Chromatography column size exclusion HiLoad 26/600 Superdex 75 pg	GE Healthcare Life Sciences, Freiburg
Millex AA filter unit (0.22/0.45/0.8 µm)	Merck Millipore, Tullagreen
PCR tubes (0.2 ml)	Bio-Rad Laboratories GmbH, Munich
Polyvinylidene difluoride (PVDF) transfer membrane Amersham Hybond™ P 0.2	GE Healthcare Life Sciences, Freiburg
Hellma™ Suprasil™ Quartz Ultra-Micro Cell Cuvettes (light path 3x3 mm, center 15 mm)	Hellma Analytics, Müllheim
Rotilabo®-Blotting Papers	Carl Roth GmbH & Co. KG, Karlsruhe
µ-Slide 8 well	ibidi GmbH, Planegg
Slide-A-Lyzer™ G2 Dialysis Cassettes (MW cutoff 10 kDa, 0.5/3 ml)	Thermo Fisher Scientific, Waltham
Slide-A-Lyzer™ Mini Dialysis Device (MW cutoff 10 kDa, 0.1 ml)	Thermo Fisher Scientific, Waltham
Syringe without needle (50 ml)	Terumo, Laguna

2.1.3 CHEMICALS

If not stated otherwise, chemicals and reagents were obtained from Applichem GmbH (Darmstadt). All other chemicals used in this thesis are listed in Table 2-3.

Table 2-3: Chemicals.

Chemical / Reagent	Supplier
^{15}N-ammonium chloride	Sigma-Aldrich Chemie Gmbh, Munich
Antibiotic-Antimycotic	Life Technologies GmbH, Darmstadt
Bio-Rad Protein Assay Dye Reagent (5x)	Bio-Rad Laboratories GmbH, Munich
Cobalt (II) chloride hexahydrate	Sigma-Aldrich Chemie Gmbh, Munich
Copper (II) sulfate pentahydrate	Sigma-Aldrich Chemie Gmbh, Munich
Deoxyguanosine triphosphate (dGTP) sodium salt	Peqlab Biotechnologie GmbH, Erlangen
Deoxynucleotide triphosphate (dNTP) Solution Mix	New England BioLabs (NEB) GmbH, Frankfurt am Main
Disodium hydrogen phosphate heptahydrate	Sigma-Aldrich Chemie Gmbh, Munich
Dulbecco's Modified Eagle Medium (DMEM), high glucose, GlutaMax supplement	Life Technologies GmbH, Darmstadt
Dulbecco's Phosphate-Buffered Saline (DPBS)	Life Technologies GmbH, Darmstadt
Ethanol	VWR International GmbH, Darmstadt
Fetal calf serum (FCS)	Life Technologies GmbH, Darmstadt
Glutathione Sepharose 4B beads	GE Healthcare Life Sciences, Freiburg
HCS CellMask™ Deep Red Stain	Life Technologies GmbH, Darmstadt
HDGreen™ Plus	INTAS Science Imaging Instruments GmbH, Göttingen
Normal goat serum	Dako Deutschland GmbH, Hamburg
Optimized Minimum Essential Medium (Opti-MEM™)	Life Technologies GmbH, Darmstadt
cOmplete™ Protease Inhibitor Cocktail	Roche, Mannheim
Sodium dihydrogen phosphate monohydrate	Carl Roth GmbH & Co. KG, Karlsruhe
Thiamine (Vitamin B1) hydrochloride	Sigma-Aldrich Chemie Gmbh, Munich
TrypLE™ Express	Life Technologies GmbH, Darmstadt

2.1.4 KITS

All kits relevant for this work are listed in Table 2-4 and were used according to the manufacturer's instructions.

Table 2-4: Kits.

Kit	Application	Manufacturer
Atto 488 Protein Labeling Kit	Labeling of cysteines with a fluorophore	Jena Bioscience, Jena
NucleoBond™ Xtra Midi	Plasmid isolation	Macherey-Nagel, Düren
NucleoSpin™ Gel and PCR Clean-Up	Plasmid purification	Macherey-Nagel, Düren
Phusion™ High-Fidelity PCR Kit	Polymerase chain reaction	Thermo Fisher Scientific, Waltham
Pierce™ ECL Plus Western Blotting Substrate	Substrate for the horseradish peroxidase (HRP)	Thermo Fisher Scientific, Waltham
Q5® Site-Directed Mutagenesis Kit	Site-directed mutagenesis	New England BioLabs, Ipswich
SuperSignal™ West Femto Maximum Sensitivity Substrate	Substrate for the horseradish peroxidase	Thermo Fisher Scientific, Waltham

2.1.5 BUFFERS, SOLUTIONS AND MEDIA

The composition of buffers, solutions and media frequently used in this work are listed in Table 2-5. Unless stated otherwise, they were prepared in ultra-pure water (ddH$_2$O) generated by the water purification system Milli-Q® Advantage A10 and the pH was adjusted at room temperature.

Table 2-5: Buffers, solutions and media.

Buffer/ Solution/ Medium	Ingredients	Final concentration
Coomassie destaining solution	Acetic acid	10 % (v/v)
	Ethanol	40 % (v/v)
Coomassie staining solution	Acetic acid	10 % (v/v)
	Ethanol	40 % (v/v)
	Coomassie brilliant blue G250	0.1 % (w/v)

Buffer/ Solution/ Medium	Ingredients	Final concentration
DNase I		10 g/l in 150 mM sodium chloride
DNA loading dye (10x)	Bromophenol blue	0.25 % (w/v)
	EDTA	100 mM
	Glycerol	20 % (w/v)
	Xylene cyanol	0.25 % (w/v)
DMEM++	Antibiotic-Antimycotic	1x
	FCS	10 % (v/v)
		in DMEM
GSH-elution buffer	L-GSH reduced	20 mM
		in PBS
		pH 7.4
Gel filtration buffer	DTT	2 mM
	Potassium chloride	150 mM
	Potassium phosphate	50 mM
		pH 7.4
High salt buffer	Sodium Chloride	500 mM
		in PBS
Hoechst solution	Ethanol	25 % (v/v)
	Hoechst 33342	1 mg/ml
		in PBS
Ion exchange chromate-graphy (IEC) buffer A	DTT	1 mM
	Sodium chloride	25 mM
	Tris-HCl	50 mM
		pH 7.5
IEC buffer B	DTT	1 mM
	Sodium chloride	1 M
	Tris-HCl	50 mM
		pH 7.5
LB agar	LB agar powder	40 g/l
LB medium	LB medium powder	25 g/l
Lysis buffer	Sodium chloride	150 mM
	Tris-HCl	50 mM
		pH 7.5

Buffer/ Solution/ Medium	Ingredients	Final concentration
Lysozyme		50 g/l in 10 mM Tris-HCl pH 7.5
Nickel-Nitrilotriacetic acid (Ni-NTA) binding buffer	Sodium dihydrogen phosphate Sodium chloride Imidazole	50 mM 300 mM 20 mM pH 8.0
Ni-NTA elution buffer	Disodium hydrogen phosphate Sodium chloride Imidazole	50 mM 300 mM 500 mM pH 8.0
NMR buffer	DTT KPi Potassium chloride	2 mM 50 mM 90 mM pH 6.5
Phosphate-buffered saline (PBS)	Disodium hydrogen phosphate Potassium chloride Potassium dihydrogen phosphate Sodium chloride	10 mM 2.7 mM 2 mM 137 mM pH 7.4
PMSF		0.2 M in ethanol
Potassium phosphate buffer	DTT KPi Potassium chloride	2 mM 50 mM 150 mM pH 7.4
PreScission protease cleavage buffer (PCB)	DTT EDTA Sodium chloride Tris-HCl	1 mM 1 mM 25 mM 50 mM pH 7.5
PreScission protease storage buffer	DTT EDTA Glycerol Sodium chloride Tris-HCl	1 mM 10 mM 20 % (v/v) 150 mM 50 mM pH 8.0

Buffer/ Solution/ Medium	Ingredients	Final concentration
Pull-down blocking buffer	BSA	1 % (w/v)
		in pull-down buffer
Pull-down buffer	DTT	1 mM
	Triton X-100	0.02 % (v/v)
		in PBS pH 7.4
Radioimmunoprecipitation assay (RIPA) buffer	DTT	1 mM
	EDTA	5 mM
	NP-40	1 % (v/v)
	PMSF	1 mM
	cOmplete™ Protease Inhibitor Cocktail tablet (Roche, Basel)	1x
	Sodium chloride	150 mM
	Sodium deoxycholate	1 % (w/v)
	Tris-HCl	50 mM
		pH 7.4
SDS-PAGE running buffer	Glycine	192 mM
	SDS	0.1 % (w/v)
	Tris	25 mM
SDS sample buffer (5x)	Bromophenol blue	0.1 % (w/v)
	EDTA	5 mM
	Glycerol	30 % (v/v)
	β-Mercaptoethanol	7.5 % (v/v)
	SDS	15 % (w/v)
	Tris-HCl	60 mM
		pH 6.8
Size exclusion chromatography (SEC) buffer	Potassium phosphate	50 mM
	Potassium chloride	150 mM
	DTT	2 mM
		pH 7.4
Separation gel buffer (4x)	SDS	0.8 % (w/v)
	Tris	1.5 M
		pH 8.8
Stacking gel buffer (4x)	SDS	0.8 % (w/v)
	Tris-HCl	0.5 M
		pH 6.8
Stripping buffer	Sodium dihydrogen phosphate	20 mM

Buffer/ Solution/ Medium	Ingredients	Final concentration
	Sodium chloride	500 mM
	EDTA	50 mM
		pH 7.4
TEV Dialysis buffer	Tris-HCl	50 mM
	Sodium chloride	25 mM
	DTT	1 mM
	EDTA	0.5 mM
		pH 7.5
Transfer buffer	Glycine	192 mM
	Methanol	20 % (v/v)
	SDS	0.01 % (v/v)
	Tris	25 mM
		pH 7.5
Tris-acetate-EDTA (TAE) buffer	EDTA	1 mM
	Tris acetate	40 mM
		pH 8.3
Tris-buffered saline (TBS)	Sodium chloride	150 mM
	Tris-HCl	50 mM
		pH 7.4
Tris-buffered saline with Tween® 20 (TBST)	Tween® 20	0.1 % (v/v) in TBS
Western blotting (WB) blocking buffer	Milk powder	5 % (w/v) in TBST
Wet blot buffer	Glycine	192 mM
	Methanol	20 % (v/v)
	SDS	0.01 % (w/v)
	Tris	25 mM
		pH 8.3

2.1.6 ANTIBODIES

Primary and secondary antibodies (Table 2-6) were used for western blotting (WB, section 2.4.8).

Table 2-6: Antibodies.

Antigen	Origin	Dilution	Application	Manufacturer
Anti-mouse IgG-HRP	Sheep	1:10000	WB	GE Healthcare Life Sciences, Freiburg (NXA931)
GST-tag	Mouse monoclonal	1:1000	WB	Santa Cruz Biotechnology Inc, Heidelberg (sc-57753)
HA-tag	Mouse monoclonal	1:1000	WB	BioLegend Inc, Koblenz (901501)

2.1.7 PLASMIDS

The plasmids for eukaryotic expression are listed in Table 2-7 and those for expression in bacteria can be found in Table 2-8.

Table 2-7: Eukaryotic expression plasmids used in this work.

Plasmid	Features	Reference
pcDNA^{TM}3.1(+); pc3	Empty vector with amp^r, neo^r	Invitrogen
pc3-Crm1-GFP	Crm1 C-terminally fused with green fluorescent GFP, amp^r	Knauer group, University of Duisburg-Essen
pc3-Survivin-HA	Survivin wildtype (WT) C-terminally fused with HA, amp^r	Knauer group, University of Duisburg-Essen

Table 2-8: Prokaryotic expression plasmids used in this work.

Plasmid	Features	Reference
pET41-GST-PreSc-Survivin120	C-terminally truncated Survivin, N-terminally fused with GST and PreScisson protease cleavage site	Sandra Bäcker, Knauer group, University of Duisburg-Essen
pET41-GST-PreSc-Survivin120K90/103T	C-terminally truncated Survivin K90/103T mutant, N-terminally fused with GST and PreScisson protease cleavage site	This work
pET41-GST-PreSc-Survivin120K90/103S	C-terminally truncated Survivin K90/103S mutant, N-terminally fused with GST and PreScisson protease cleavage site	This work
pET41-GST-PreSc-Survivin120K90/91/103A	C-terminally truncated Survivin K90/91/103A mutant, N-terminally fused with GST and PreScisson protease cleavage site	This work
pET41-GST-PreSc-Survivin120K90/91/103S	C-terminally truncated Survivin K90/91/103S mutant, N-terminally fused with GST and PreScisson protease cleavage site	Sandra Bäcker, Knauer group, University of Duisburg-Essen
pET41-GST-PreSc-Survivin120K103S	C-terminally truncated Survivin K103S mutant, N-terminally fused with GST and PreScisson protease cleavage site	Stefanie Sichelschmidt, Knauer group, University of Duisburg-Essen
pTGA20-His-TEV-Crm1-1-1062VLV430AAA	C-terminally truncated Crm1 1062VLV430AAA mutant, N-terminally fused with His-tag, zz-domain and TEV cleavage site	Rodriguez group, University of the Basque Country, Spain

2.1.8 BACTERIAL STRAINS AND EUKARYOTIC CELL LINES

The bacterial strains used in this work are listed in Table 2-9. *Escherichia coli* (*E. coli*) XL2-Blue, NEB® 5-alpha or NEB® 10-beta were used for plasmid amplification. *E. coli* SoluBL21 or *E. coli* Codon Plus DE3 (RIL) were used for heterologous protein expression. The respective

bacteria were grown at 37 °C in LB medium or on dishes with LB agar, supplemented with the respective antibiotics (Table 2-9). The eukaryotic cell lines used in this work are listed in Table 2-10. All cell lines were cultivated in DMEM++.

Table 2-9: Characteristic of used bacterial strains.

Bacterial strain	Genotype	Supplier
E. coli XL2-Blue	endA1 supE44 thi-1 hsdR17 recA1 gyrA96 relA1 lac [F' proAB lacIqZΔM15 Tn10 (TetR) Amy CamR]	Agilent Technologies, Waldbronn
E. coli NEB® 5-alpha	fhuA2 Δ(argF-lacZ)U169 phoA glnV44 Φ80Δ (lacZ)M15 gyrA96 recA1 relA1 endA1 thi-1 hsdR17	New England BioLabs, Ibswich
E. coli NEB® 10-beta	Δ(ara-leu) 7697 araD139 fhuA ΔlacX74 galK16 galE15 e14- φ80dlacZΔM15 recA1 relA1 endA1 nupG rpsL (StrR) rph spoT1 Δ(mrr-hsdRMS-mcrBC)	New England BioLabs, Ibswich
E. coli SoluBL21	F- ompT hsd SB (rB- mB-) gal dcm (DE3) + further uncharacterized mutations	Genlantis, San Diego
E. coli Codon Plus DE3 (RIL)	E. coli B F– ompT hsdS(rB– mB–) dcm+ Tet^r gal λ(DE3) endA metA::Tn5(kan^r) Hte [argU ileY leuW Cam^r]	Agilent Technologies

Table 2-10: Characteristics of used eukaryotic cell lines.

Cell line	Origin	Growth property	Reference
HEK 293T	*Homo sapiens*, embryonic kidney	adherent	Research resource identifier: CVCL_1926 American type culture collection: CRL-11268
HeLa (Henrietta Lacks) Kyoto	*Homo sapiens*, cervical adenocarcinoma	adherent	Research resource identifier: CVCL_1922

2.2 MOLECULAR BIOLOGICAL METHODS

2.2.1 POLYMERASE CHAIN REACTION (PCR)

The polymerase chain reaction (PCR) is used to amplify DNA segments based on a template. For this purpose, specific primers, DNA polymerase and deoxynucleotide triphosphates (dNTPs) are required (Mullis and Faloona, 1989). One PCR cycle consists of three steps, which are repeated 25 to 30 times. First, the double-stranded DNA is denatured at 98 °C. Next, specific primers anneal to the DNA template at 2 to 5 °C below their melting temperature. Afterwards, DNA polymerase elongates the new DNA strand at 72 °C by incorporating dNTPs. Prior to the first step, an initial denaturation (30 s) and after the last cycle an additional elongation of 2 min at 72 °C were performed to ensure the correct amplification of the DNA.

In this work, PCR was performed according to the Q5® Site-Directed Mutagenesis Kit protocol from New England BioLabs when generating Survivin mutants. 25 µl of the reaction mixture were prepared (Table 2-11). The PCR program (Table 2-12) was carried out in a Thermocycler TProfessional standard gradient 96 from Biometra.

Table 2-11: PCR reaction mixture for site-directed mutagenesis.

Reagent	Volume	Final concentration
Q5 Hot Start High-Fidelity 2X Master Mix	12.5 µl	1x
10 µM forward/ reverse primer	1.25 µl each	0.5 µM
Template DNA (1–25 ng/µl)	1 µl	1–25 ng
Nuclease-free water	9.0 µl	

Table 2-12: PCR program.

Step	Temperature	Time
Initial denaturation	98 °C	30 s
Denaturation	98 °C	10 s
Annealing	50–72 °C	30 s
Elongation	72 °C	30 s/ kb
Final elongation	72 °C	2 min
Pause	15° C	Hold

2.2.2 AGAROSE GEL ELECTROPHORESIS

Agarose gel electrophoresis is widely used to separate DNA fragments according to their size. DNA is negatively charged and thus migrates through agarose gels in an electric field. The movement of fragments is affected by their size. Small DNA fragments move faster through the gel matrix than large ones. Visualization of fragments is achieved with a fluorescent DNA-binding dye.

For gel preparation, agarose (1–2 % (w/v)) was dissolved by heating in 1 x TAE buffer and supplemented with DNA-binding dye HDGreen™ PLUS from INTAS in a 1:10,000 dilution. The gel was cast with a comb to form sample wells. After it had become solid, the gel was transferred into a gel chamber filled with 1 x TAE buffer. DNA samples were mixed with 10 x DNA loading dye and loaded onto the gel. The DNA ladder GeneRuler™ 1 kb PLUS from Thermo Fisher Scientific was used as size standard. Electrophoresis was performed at 90 V for 45–60 min. DNA bands were visualized with UV-light in an E-Box VX2 documentation system (Vilber Lourmat).

2.2.3 ISOLATION AND PURIFICATION OF DNA

Plasmids were propagated in *E. coli* XL2blue, NEB® 5-alpha or NEB® 10-beta cells. DNA isolation from bacterial cultures was performed with the NucleoBond™ Xtra Midi kit from Macherey-Nagel according to the manufacturer's protocol. During cloning processes, the NucleoSpin™ Gel and PCR Clean-Up kit from Macherey-Nagel was used to remove contaminations like PCR additives, DNA dyes and enzymes.

2.2.4 DETERMINATION OF DNA CONCENTRATION

DNA concentrations were calculated with the NanoDrop™ 2000c (Thermo Fisher Scientific) by measuring the absorbance at 260 nm, the absorbance maximum of nucleic acids. Purity of the DNA was assessed using the A260/280 and A260/230 absorbance ratios. Protein impurities have an impact on the A260/280 ratio due to the absorbance maximum of aromatic amino acids at 280 nm and DNA samples with ratios above 1.8 are considered pure. Especially organic components influence A260/230 ratios, which ideally are 2.0–2.2. Prior to DNA quantification, a blank measurement with HPLC-H_2O or elution buffer from the respective purification kit was performed.

2.2.5 RESTRICTION

Plasmids and PCR products were digested with restriction enzymes from New England Biolabs. For restriction double digest, the NEBcloner® tool was used to determine digestion conditions and buffer requirements. 1 µg DNA and 10 units of respective restriction enzymes were incubated for 15 min to 4 h at 37 °C. Fragments were separated by agarose gel electrophoresis and purified (section 2.2.3).

2.2.6 LIGATION

Ligation of digested DNA fragments was performed using the T4 DNA ligase (New England Biolabs). It catalyses the formation of phosphodiester bonds in the DNA backbone and is able to connect blunt ends as well as cohesive ends. The ligation mix contained 50 ng vector and inserts in ratios of 1:1 and 1:3 in 1x T4 DNA ligase buffer. Ligation was carried out for 30 min at RT. Afterwards, the ligated construct was transformed into competent *E. coli* XL2-Blue or NEB® 10-beta.

2.2.7 SITE-DIRECTED MUTAGENESIS

For substitution of amino acids, the Q5® Site-Directed Mutagenesis Kit from NEB was used. After PCR (section 2.2.1), 1 µl of PCR product was mixed with 5 µl of 2 x Kinase-Ligase-DpnI (KLD) reaction buffer, 1 µl of 10 x KLD enzyme mix and 3 µl of HPLC-H_2O and incubated for 5 min at RT. This step was performed to remove template DNA and to circulate the PCR product prior to transformation in *E. coli* NEB® 5-alpha included in the kit.

2.2.8 DNA SEQUENCING

DNA sequencing was carried out by LGC Genomics. For this, 40 µl plasmid DNA with a concentration of 100 ng/µl were sent to LGC Genomics. Sequencing primers (Table 2-13) were provided by the company. Sequencing results were analyzed with SnapGene and Clustal Omega (EMBL-EBI).

Table 2-13: Sequencing primers.

Name	Sequence
T7prom	TAATACGACTCACTATAGGG
T7term	GCTAGTTATTGCTCAGCGG

2.3 MICROBIOLOGICAL METHODS

2.3.1 TRANSFORMATION OF CHEMICALLY COMPETENT *E. COLI*

Transformation of plasmids in *E. coli* was used for either propagation of plasmids or expression and further isolation of recombinant proteins. For this, 50 µl of chemically competent *E. coli* XL2-Blue, NEB® 5-alpha or NEB® 10-beta for plasmid propagation or *E. coli* SoluBL21 or Codon Plus DE3 (RIL) for protein expression were thawed on ice (10 min). When using the Q5® Site-Directed Mutagenesis protocol, 5 µl of the KLD reaction mix (section 2.2.7) were added to *E. coli* NEB® 5-alpha. For all other transformations, 50–100 ng of DNA were used. Cells were incubated on ice for 30 min. Afterwards, a heat shock at 42 °C was performed for 30 s (or 45 s in case of *E. coli* soluBL21). Bacteria were placed on ice for 5 min before preheated SOC or LB medium was added (250–950 µl). After shaking (300 rpm) at 37 °C for 1–2 h bacteria were spread (50–200 µl) onto LB agar plates with the appropriate antibiotics and incubated overnight at 37 °C. Colonies were picked to inoculate liquid cultures.

2.3.2 CULTIVATION OF BACTERIA

Bacteria were cultivated in LB medium with either 50 µg/ml kanamycin or 100 µg/ml carbenicillin. For plasmid isolation with the NucleoBond® Xtra Midi kit (section 2.2.3) or as pre-culture for protein expression (section 2.3.5), 200 ml cultures were prepared from glycerol stocks or single colonies from an agar plate. When picking a colony, a small culture of 6 ml was prepared of which 500 µl were used to inoculate the 200 ml cultures. Bacteria were grown overnight at 37 °C in a 500 ml baffled Erlenmeyer flask at 120 rpm in a Forma 420 Series shaker (Thermo Fisher Scientific).

2.3.3 BACTERIAL GLYCEROL STOCK

For long-term storage of transformed *E. coli* (section 2.3.1), 800 µl of a bacterial culture were mixed with 200 µl of sterile 87 % glycerol. The obtained bacterial stocks were stored at -80 °C and used to inoculate new cultures (section 2.3.2.).

2.3.4 DETERMINATION OF OPTICAL DENSITY

Bacterial growth of liquid cultures was monitored by measuring the optical density (OD_{600}) with the BioPhotometer® Plus from Eppendorf. For this, 100 µl of bacterial suspension was mixed with 900 µl of MilliQ-H_2O in a disposable cuvette and measured. 100 µl LB medium with the appropriate antibiotic diluted with 900 µl MilliQ-H_2O was used as blank.

2.3.5 EXPRESSION OF RECOMBINANT PROTEINS

For the expression of recombinant proteins *E.coli* SoluBl21 were mainly used. For this, 2–4x 1 l LB media with 50 µg/ml kanamycin in 2 l Erlenmeyer flasks with chicane were inoculated with 50 ml of an overnight culture (section 2.3.2) and shaken at 37 °C and 120 rpm. Bacteria were grown until an OD_{600} of 1.0–1.2 for $Survivin_{120}$ or 0.6–0.8 for all other GST-fusions was reached. Next, protein expression was induced with 0.2 mM IPTG for $Survivin_{120}$ or 1 mM for other proteins. The cultures were incubated at 30 °C and 120 rpm for 20 h in a MaxQ™ 4000 shaker (Thermo Fisher Scientific), harvested by centrifugation (7,000 x g, 4 °C, 20 min), resuspended in PBS ($Survivin_{120}$) or lysis buffer, shock frozen in liquid nitrogen and stored at -80 °C until further protein purification steps were performed (section 2.4).

The $Crm1_{1062}VLV430AAA$ mutant was expressed in *E. coli* Codon Plus DE3 (RIL). Bacteria were cultivated in LB media containing 100 µg/ml carbenicillin for the pTGA20 vector and 50 µg/ml chloramphenicol for maintaining the pACYC plasmid in the BL21-Codon Plus strain. The expression was induced with 0.1 mM IPTG at an OD_{600} of 0.5 and carried out at 20 °C for 20 h at 120 rpm.

2.4 BIOCHEMICAL METHODS

2.4.1 PURIFICATION OF RECOMBINANT PROTEINS

To isolate recombinant GST-tagged fusion proteins e.g. $Survivin_{120}$ or His-tagged $Crm1_{1062}VLV430AAA$ mutant from *E. coli* several purification steps were performed including bacterial lysis, affinity chromatography and anion exchange or size exclusion chromatography (SEC). The chromatography steps vary for the proteins used in this work (Table 2-14) but were all carried out at 4 °C. Purification of $Survivin_{120}$ included GSH-affinity and SEC. Other GST-tagged fusions were purified via GSH-affinity and anion exchange chromatography. The fused GST-tag was optionally cleaved by PreScission protease. His-tagged $Crm1_{1062}VLV430AAA$ mutant was purified by Nickel-NTA and subsequent anion exchange chromatography. The fused His-tag was cleaved by Tobacco Etch Virus (TEV) protease.

Table 2-14: Overview of protein purification steps.

	GST-Survivin$_{120}$	GST-fusions	His-Crm1$_{1062}$VLV430AAA
Step 1	GSH-affinity with ÄKTApurifier™	GSH-affinity manually	Ni-NTA-affinity manually
Step 2 (optionally)	GST-tag cleavage in solution by PreScission protease	GST-tag cleavage on column by PreScission protease	His-tag cleavage in solution by TEV protease
Step 3	SEC with ÄKTApurifier	Anion exchange with ÄKTApurifier	Anion exchange with ÄKTApurifier

2.4.1.1 BACTERIAL CELL LYSIS

Heterologous expression of GST-fusion proteins was performed in *E. coli* SoluBL21. The culture (2 l for Survivin$_{120}$, 4 l for all other proteins) was pelleted, resuspended in 40 ml PBS buffer (Survivin$_{120}$) or lysis buffer and stored at -80 °C. After thawing, the protease inhibitor PMSF was added (1 mM) and the suspension was incubated on ice for 10 min. Next, 50 µg/ml lysozyme was added with subsequent incubation on ice for 20 min for enzymatic lysis. To cleave DNA, 0.5 mg/ml DNase I and 5 mM MgCl$_2$ were added. Disruption of the cells was achieved by ultrasonication on ice in a 50 ml glas beaker with the ultrasonic homogenizer Sonopuls HD 2070 and KE76 probe from Bandelin electronic. Three short pulses (10 s each, 60 % intensity) and two to four long pulses (30 s each, 60 % intensity) were performed followed by 1 min breaks to reduce heat. Cell fragments were pelleted by centrifugation (3,900 x g, 1 h, 4 °C) and the supernatant was filtered (0.8 µm pore size). 10 µl samples of total lysate and filtered supernatant were taken and diluted with 20 µl PBS buffer for further analysis by SDS-PAGE. Lysis of *E. coli* Codon Plus DE3 (RIL) after expression of the Crm1$_{1062}$VLV430AAA mutant was performed likewise except for the resuspension buffer. Here, harvested bacteria were lysed in Ni-NTA binding buffer.

2.4.1.2 GST AFFINITY CHROMATOGRAPHY

The enzyme glutathione-S-transferase (GST) binds its substrate glutathione (GSH) and can therefore be used to isolate GST fusions via affinity chromatography (Smith and Johnson, 1988). In this work GSTrap™ 4B columns (5 ml) prepacked with Glutathione Sepharose™ as matrix from GE Healthcare were used. GST fusion proteins bind to the matrix and host cell proteins without tag are removed with the buffer flow.

First, the GSTrap 4B column was equilibrated with 15 ml Milli-Q H2O followed by 50 ml PBS buffer at a flow rate of 1–2 ml/min using the peristaltic pump P-1 from GE Healthcare. After equilibration, the filtered supernatant containing the recombinant GST fusion protein was loaded onto the column at a flow rate of approximately 0.5 ml/min. The flow through was collected and the column was subsequently washed with 35 ml PBS buffer at a flow rate of 1–1.5 ml/min. 10 µl sample of the flow through diluted with 20 µl PBS buffer and 30 µl samples of the washing step were taken for further analysis by SDS-PAGE. The elution of the protein of interest was either carried out with the ÄKTApurifier system in case of Survivin$_{120}$ (section 2.4.1.2.1) or manually for all other proteins (section 2.4.1.2.2). Afterwards, the column was regenerated by washing with 10 ml Milli-Q H$_2$O and 10 ml 6 M guanidine hydrochloride, which removes denatured proteins from the column. PBS (25 l) was used to restore the pH of 7.4 followed by another washing step with 20 ml Milli-Q H$_2$O. Last, 20 % ethanol was loaded onto the column for storage at 4 °C.

2.4.1.2.1 ELUTION WITH THE ÄKTAPURIFIER

Subsequent washing steps and the elution of GST-tagged Survivin$_{120}$ were performed with the ÄKTApurifier system controlled by the Unicorn^{TM} 7.0 control software from GE Healthcare. The column was washed with 100 ml PBS containing 500 mM sodium chloride to improve purity of the protein followed by 50 ml PBS buffer at a flow rate of 5 ml/min. Next, elution was conducted with 90 ml GSH-elution buffer while collecting 2 ml fractions. Fractions were analyzed by SDS-PAGE and united if no impurities were observed. For this purpose, 10 µl fraction sample were taken. After the optional addition of PreScission protease for tag cleavage (section 2.4.1.3.1), the protein solution was concentrated to obtain a volume less than 3 ml was reached as preparation for size exclusion chromatography (section 2.4.1.6).

2.4.1.2.2 MANUAL ELUTION

After loading onto the GSTrap column and washing with PBS, GST fusion proteins were eluted competitively with 50 ml GST-elution buffer or, in case of GST-tag cleavage, proteins were eluted by PreScission cleavage before proceeding with anion exchange chromatography (section 2.4.1.7). For this, a HiTrap^{TM} Q HP column was equilibrated and mounted downstream of the GSTrap column to enable binding of the target protein to its matrix.

2.4.1.3 PROTEOLYTIC CLEAVAGE BY PRESCISSION PROTEASE

GST fusion proteins expressed from the pET41-GST-PreSc vectors contain a PreScission cleavage site between the GST-tag and the protein of interest. The tag can be cleaved by

PreScission protease, which is a fusion protein of human rhinovirus 3C protease and GST (Leong, 1999).

2.4.1.3.1 OFF COLUMN CLEAVAGE

After Survivin$_{120}$ protein fractions were united, the protein concentration was determined with Bradford reagent and the required amount of PreScission protease was calculated. For 1 mg of GST fusion protein 1 µg PreScission protease was added. Cleavage was performed for at least 8 hours at 4 °C before SEC was started.

2.4.1.3.2 ON COLUMN CLEAVAGE

For other GST fusion proteins, cleavage was carried out on column. After loading the protein to the GSTrap column and subsequent washing with PCB, GST-tagged PreScission protease was loaded onto the column as well (200 µg/ml in PCB, 5 ml). During an incubation overnight, the tag was cleaved. Afterwards, proteins of interest were washed from the GSTrap column to a HiTrap Q HP anion exchange column with 50 ml PCB while the protease remained on the GSTrap column and was later eluted during their regeneration steps.

2.4.1.4 NI-NTA-AFFINITY CHROMATOGRAPHY

The Crm1$_{1062}$VLV430AAA mutant was expressed as fusion with a 6x polyhistidine (His)-tag for Nickel-Nitrilotriacetic acid (Ni-NTA)-affinity chromatography. A HisTrap^{TM} FF column was equilibrated with 15 ml Milli-Q H$_2$O followed by 25 ml binding buffer at a flow rate of 1–2 ml/min using a peristaltic pump P-1. After sonication and centrifugation, the lysate was immobilized on a HisTrap FF column and washed twice with 25 ml Ni-NTA binding buffer. Samples from flow through and wash fractions were taken as before (section 2.4.1.2). The protein was eluted in Ni-NTA elution buffer (25 ml). The HisTrap column was regenerated by washing with Milli-Q H$_2$O, stripping buffer, Ni-NTA binding buffer and Milli-Q H$_2$O (each 25 ml). Afterwards, the column was recharged with 3 ml Ni sulfate (0.1 M) and washed with Milli-Q H$_2$O, Ni-NTA binding buffer, again Milli-Q H$_2$O and 20 % ethanol (each 25 ml).

2.4.1.5 PROTEOLYTIC CLEAVAGE BY TEV PROTEASE

After elution, the His-tag was cleaved by TEV protease (Sigma Aldrich). For this, the concentration of the eluted protein was measured with Bradford and diluted to 1–2 mg/ml with TEV dialysis buffer. 0.1 mg TEV protease cleaves 10 mg target protein, thus the required amount was calculated and added to the protein solution. Afterwards, the protein mixture was transferred into a dialysis tube and dialyzed against TEV dialysis buffer overnight at 4 °C. Next,

the solution passed another equilibrated HisTrap FF column to remove the cleaved His-Tag and the TEV protease, which is also fused to a His-tag, and was then loaded onto a HiTrap Q HP column for ion exchange chromatography (section 2.4.1.7).

2.4.1.6 SIZE EXCLUSION CHROMATOGRAPHY (SEC)

Size exclusion chromatography was performed as additional purification step for Survivin$_{120}$. Thereby, the target protein is separated from proteins with other molecular weights due to their different mobility through the column matrix. The SEC column used in this work is a Sephadex 75 pg 26/600 from GE Healthcare and was operated with the ÄKTApurifier system. Since Survivin$_{120}$ migrates as a dimer through the column (Bäcker, 2018) and the GST-tagged PreScission protease has the same molecular weight, a GSTrap 4B column was installed downstream of the SEC column. The column was equilibrated with 100 ml Milli-Q H$_2$O and 330 ml SEC buffer at a flow rate of 1.5 ml/min and a pressure limit of 0.3 MPa. Afterwards, the protein sample was loaded onto the column and the elution was performed with 330 ml SEC buffer at a flow rate of 1.5 ml/min, while 3 ml fractions were collected. The fractions (10 µl) were analyzed by SDS-PAGE (2.4.6). The fractions containing pure Survivin$_{120}$ were pooled and concentrated to approximately 1.2 mM. A final sample for SDS-PAGE was taken (2.5 µl) and diluted with PBS buffer (27.5 µl). After determination of the protein concentration (section 2.5.3), protein aliquots were shock frozen in liquid nitrogen and stored at -80 °C. The SEC column was regenerated with 100 ml Milli-Q H$_2$O and 330 ml 20 % ethanol and then stored at 4 °C. The GSTrap 4B column was regenerated as described before (section 2.4.1.2).

2.4.1.7 ION EXCHANGE CHROMATOGRAPHY (IEC)

As additional purification step, target proteins were loaded onto a HiTrap Q HP column after GST or Ni-NTA affinity chromatography. The column was equilibrated with 15 ml Milli-Q H$_2$O and 20 ml IEC buffer A. Negatively charged proteins bind to the positively charged column matrix. After protein loading, all subsequent steps were conducted by the ÄKTApurifier system. First, the column was washed with 10 ml IEC buffer A. Afterwards, the protein was eluted with increasing sodium chloride concentrations. For this purpose, a salt gradient of 25–1000 mM sodium chloride with IEC buffers A and B was applied with a total volume of 75 ml. The flow rate was 1.5 ml/min and the pressure limit was 0.3 MPa. Fractions of 2 ml were collected and further processed according to SEC proceedings (section 2.4.1.6).

2.4.2 CONCENTRATION OF PROTEIN SOLUTIONS

To concentrate protein solutions, VivaSpin® centrifugal concentrators (0.5, 6 or 15 ml) from Sartorius with 10, 30 or 50 kDa cutoff were used depending on the molecular size of the protein. The concentrators were equilibrated with the respective protein buffer by centrifugation. Subsequently, the protein solution was concentrated by applying multiple centrifugation steps (4,000 x g or 14,000 x g for 0.5 ml concentrators, 5–20 min, 4 °C) until the desired volume was obtained.

2.4.3 DIALYSIS OF PROTEIN SOLUTIONS

Dialysis was performed to exchange buffer systems, for example before ITC experiments. For this, the protein solution was transferred to a Slide-A-Lyzer™ G2 cassette (0.5 or 3 ml) or MINI dialysis device (0.1 ml) from Thermo Fisher Scientific with 10 kDa molecular weight cutoff and dialyzed overnight at 4 °C against at least 2 l dialysis buffer.

2.4.4 DETERMINATION OF PROTEIN CONCENTRATION

The concentration of isolated proteins was measured with the NanoDrop™ 2000 c spectrophotometer, whereas protein concentration of cell lysates was determined with the Bradford assay.

2.4.4.1 *NANODROP™ 2000 C SPECTROPHOTOMETER*

Quantification of protein concentrations with the spectrophotometer is based on the absorbance at 280 nm, which results from aromatic amino acids. First, the extinction coefficient and corresponding molecular weight of the protein were entered in the software and a reference measurement with the respective buffer was performed before the protein solution was measured.

2.4.4.2 *BRADFORD ASSAY*

For concentration measurement of cell lysates, 1 µl of sample lysate was diluted in 800 µl PBS, mixed with 200 µl of 5x concentrated Bio-Rad Protein Assay Dye Reagent and incubated for 5 min at RT. The absorbance at 595 nm was measured using the "BRADFORD micro" program of the BioPhotometer® Plus from Eppendorf. The whole cell protein concentration was determined by the photometer using a standard calibration curve of bovine serum albumin (BSA) concentrations (1–25 µg/ml).

2.4.5 PULL-DOWN ASSAY

The pull-down assay was used to investigateeffects of the tweezers on the Survivin/Crm1 interaction. Pull-down assays were performed at RT in pull-down buffer. GST-tagged proteins were immobilized on 50 µl GSH-coated Sepharose 4B beads from GE Healthcare and used as bait to capture their binding partners. First, GSH-beads were washed twice with 500 µl pull-down buffer for 5 min under rotation with subsequent centrifugation (500 x g, 5 min).

For the investigation of the inhibitory tweezer concentration, 200 µg 293T cell lysates with overexpressed $Survivin_{142}$-HA were pre-incubated with tweezers in varing concentrations in pull-down buffer in a total of 500 µl for 1 h. In case of the peptide tweezers concentrations of 0.01 to 200 µM and for the oligomer tweezers concentrations of 0.01 to 50 µM were used. At the same time, GSH-beads were blocked with 500 µl pull-down blocking buffer (1 h) to prevent unspecific binding. After blocking and simultaneous pre-incubation, 2 mM dGTP, 35 µg GST-Crm1 and 55 µg RanQ68L were added to the lysates. A 30 µl input sample was taken for subsequent Western blot analysis (section 2.4.8) and mixed with 5 x SDS sample buffer. The rest of the protein mixture was then incubated with the beads for 2 h under rotation. Afterwards, the beads were washed three times with 500 µl pull-down buffer for 5 min under rotation and were subsequently centrifuged (5 min, 500 x g). Last, 30 µl pull-down buffer and 7,5 µl 5 x SDS sample buffer were added to the beads.

For the investigation of the K90/103T mutant, 40 µg $GST-Survivin_{120}$ or $GST-Survivin_{120}$-K90/103T mutant were prebound to equilibrated GSH-beads in 500 µl pull-down buffer containing either no ligand or 50 µM TW, TW-ELTL, TW-ELTLGEFL or peptides ELTL and ELTLGEFL, by incubation for 1 h under rotation. After subsequent washing and blocking of the beads, a protein mixture containing 2 mM dGTP, 50 µg CRM1 and 50 µg constitutively active RanQ69L (Klebe et al., 1995) was added and the beads were incubated for 2 h under rotation. 30 µl samples of the input were taken. After incubation, the beads were washed three times and the SDS samples were prepared as before. All SDS samples were denatured at 95 °C for 10 min.

2.4.6 SDS-POLYACRYLAMIDE GEL ELECTROPHORESIS

SDS-polyacrylamide gel electrophoresis (SDS-PAGE) separates proteins according to their electrophoretic mobility within an electric field (Laemmli, 1970). The mobility depends on the protein size and amount of negatively charged sodium dodecyl sulfate (SDS) molecules bound to the denatured polypeptide chain as well as the polyacrylamide concentration and thus pore

size of the gel. In this work, SDS-PAGE was used to analyze samples taken during protein purification and pull-down assays. Samples were mixed with 5x SDS sample buffer and denatured at 95 °C for 10 min before they were loaded onto the gel. Additionally, 5 µl Spectra Multicolor Broad Range protein ladder (Thermo Fisher Scientific) was used as size standard. Discontinuous SDS polyacrylamide gels with a thickness of 1 mm consisting of a 4 % stacking gel and a 12.5 % separation gel (Table 2-15) were used. Gels were prepared in a Mini-PROTEAN® Tetra Cell Casting Module from Bio-Rad Laboratories, Inc. First, the separation gel was cast. After polymerization, the stacking gel was poured on top and a comb was inserted to form wells. The gel was transferred to a Mini-PROTEAN® Tetra Vertical Electrophoresis Cell filled with SDS-PAGE running buffer. Samples were loaded onto the gel and the electrophoresis was performed at 200 V for 50–70 min. Afterwards, the gel was either stained with Coomassie (section 2.4.7) or used for Western blotting (section 2.4.8).

Table 2-15: Composition of SDS-polyacrylamide gels with a thickness of 1 mm.

Component	Separation gel (12.5 %)	Stacking gel (4 %)
Milli-Q H_2O	1.6 ml	2.5 ml
4x Separation gel buffer	1.3 ml	-
4x Stacking gel buffer	-	1.3 ml
30 % Acrylamide solution	2.1 ml	0.65 ml
10 % APS	0.05 ml	0.05 ml
TEMED	0.005 ml	0.005 ml

2.4.7 COOMASSIE-STAINING OF POLYACRYLAMIDE GELS

After electrophoresis, Coomassie brilliant blue G-250 was used to stain proteins as it binds to basic amino acids. The polyacrylamide gels were shortly boiled in Coomassie staining solution and then incubated for 45–60 min at RT under shaking. Afterwards, the gels were rinsed with Milli-Q H_2O and incubated in Coomassie destaining solution at RT until background staining was removed and distinct protein bands were visible. If necessary, the destaining solution was replaced.

2.4.8 WESTERN BLOTTING

Western blotting is a method used to transfer proteins from a polyacrylamide gel to a membrane in order to visualize them with specific antibodies. In an electric field, negatively

charged proteins migrate to the positively charged anode. Thus, the membrane is placed between the protein-loaded gel and the anode to enable immobilization of proteins. Afterwards, they can be detected on the membrane using antigen-antibody interactions. In this work, the tank blot technique was applied to transfer proteins to an Amersham™ Hybond™ P polyvinylidene difluoride (PVDF) membrane with 0.2 µm pore size (GE Healthcare). For activation, the PVDF membrane was incubated in 100 % methanol (1 min) and subsequently in transfer buffer (10 min). The polyacrylamide gel and four pieces of Rotilabo® blotting paper (Carl Roth) were equilibrated in transfer buffer as well (10 min). The blot was assembled from anode to cathode with two layers of blotting paper, the PVDF membrane, the gel and two additional layers of blotting paper. The blot cassette was inserted into the PerfectBlue™ tank electro blotter (PEQLAB) filled with transfer buffer. The transfer was performed at 350 mA for 150 min at 4 °C.

Afterwards, unspecific binding sites were blocked by incubating the membrane in WB blocking buffer for 30 min. Next, the membrane was incubated overnight at 4 °C in primary antibody solution. After washing 3x with TBST for 5 min each, the membrane was incubated in solution containing HRP-conjugated secondary antibody for 1 h at RT. Subsequently, the membrane was washed 3x with TBST and once with TBS for 5 min each. The proteins of interest were detected using Pierce™ ECL Plus Western Blotting Substrate or SuperSignal™ West Femto Maximum Sensitivity Substrate (both Thermo Fisher Scientific) and the ChemiDoc™ Imaging System (Bio-Rad).

2.4.9 ISOTHERMAL TITRATION CALORIMETRY

Isothermal titration calorimetry (ITC) experiments were performed with a MicroCal iTC200 from Malvern Panalytical. The measurements were conducted in PBS, pH 7.4 at 25 °C, the injection rate was set to 0.5 µl/s and the reference power was 5 µcal/s. The protein was dialyzed over night at 4 °C against buffer. Tweezers were dissolved in the respective dialysis buffer. 300 µM TW in the cell were titrated with a solution of 300 µM $Survivin_{120}$ WT or 321 µM K90/103T in the syringe. A solution of 100 µM TW-ELTL or TW-ELTLGEFL in the cell was titrated with 1.2 mM $Survivin_{120}$ WT or 2 mM $Survivin_{120}$ K90/103T in the syringe. 26 injections (1.5 µl) were applied with 120 s spacing time between injections. Data were fit to a *one set of sites* model with the software Origin provided with the ITC instrument.

In case of the oligomer double tweezers, a solution of 400 µM $Survivin_{120}$ was titrated to 200 µM oligomer dTW in the cell. 39 injections (1 µl) were applied with 120 s spacing time between injections. To assess binding of Survivin to gold nanoparticles, a solution of 1.2 mM

Survivin$_{120}$ WT was titrated to azide-terminated (c(Au) = 170 µg/ml) or tweezer-equipped nanoparticles (c(Au) = 170 µg/ml; c(TW) = 30 µM). 39 injections (1 µl) were applied with 150 s spacing time between injections. Data was fit with the simple model stoichiometric approach with AFFINImeter.

2.4.10 FLUORESCENCE ANISOTROPY EXPERIMENTS

Fluorescence anisotropy was measured with a Jasco Spectrofluorometer FP-8300 equipped with a Jasco CTU-100 circulating thermostat unit. Experiments were performed in PBS buffer, pH 7.4, at 25 °C. Data were fit with GraphPad Prism using the equations listed below.

2.4.10.1 COMPETITIVE BINDING ANALYSIS

To quantitatively assess the Survivin/Crm1 interaction, Survivin$_{120}$ was labeled with Atto 488 maleimide from Jenabioscience according to the manufacturer's instructions and mixed with the CRM1$_{1\text{-}1062}$VLV430AAA mutant in a ratio of 1:15. The protein complex was then titrated with the tweezers until a final concentration of approx. 180 µM tweezers was reached. Data were transformed to logarithmic scale and IC_{50} fit using the equation,

$$y = A_{min} + \frac{\left(A_{max} - A_{min}\right)}{1 + 10^{x - \log(IC_{50})}}$$

(Eq. 1)

where A$_{max}$ is the anisotropy in the absence of tweezer, A$_{min}$ is the anisotropy at the end of the titration and x is the concentration of tweezer. A$_{max}$ was constrained for every data set, whereas A$_{min}$ and IC$_{50}$ were fit.

2.4.10.2 TWEEZER BINDING STUDIES

Fam-labeled molecular tweezers (200 nM) were titrated with Survivin$_{120}$ WT or K90/103T mutant until final concentrations of approx. 180 µM (WT) and 350 µM (K90/103T), respectively, were reached. Data were then normalized to the measured anisotropy A_0 at the beginning of the experiment in the absence of protein. Using a single-site binding model, the fluorescence anisotropy data were fit using the equation,

$$y = A \cdot \frac{\left(L + x + K_D\right) - \sqrt{\left(L + x + K_D\right)^2 - 4 \cdot x \cdot L}}{2 \cdot L}$$

(Eq. 2)

where A is the anisotropy at saturation, L is the ligand concentration, x is the protein concentration and K$_D$ is the dissociation constant.

2.4.11 1D-¹H-NMR SPECTROSCOPY

Nuclear magnetic resonance (NMR) spectroscopy was used to evaluate proper folding of Survivin$_{120}$ mutants. For this, samples contained 100–500 µM Survivin mutants in 50 mM KPi pH 6.5, 90 mM KCl and 2 mM DTT with 10 % D_2O. One dimensional (1D) proton spectra with water suppression were recorded at 25 °C using a 700 MHz Ultrashield NMR spectrometer from Bruker with a 5 mm inverse TCI cryo probe. Spectra were compared to those of Survivin$_{120}$ WT and protein folding was assessed based on the dispersion of amide, aromatic and methyl signals. 1D-¹H-NMR spectroscopy was performed by Dr. Christine Beuck (Bayer group, University of Duisburg-Essen).

2.4.12 NMR TITRATIONS

NMR titration experiments were performed to map putative tweezer binding sites on Survivin$_{120}$. For this purpose, ¹⁵N-labeled GST-tagged Survivin$_{120}$ was expressed in *E. coli* SoluBL21 using M9 minimal medium supplemented with 0.6 g/l ¹⁵N-labeled ammonium chloride as nitrogen source or using LB medium with 6 g/l ¹⁵N-labeled ammonium chloride. The protein was purified by GSH affinity chromatography with subsequent cleavage of the GST-tag by PreScission protease and additional SEC as described before (section 2.4.1). NMR spectra were recorded at 25 °C with the 700 MHz Ultrashield NMR spectrometer. Samples contained 938 µM ¹⁵N-labeled Survivin$_{120}$ in 50 mM KPi pH 6.5, 90 mM KCl, 2 mM DTT and 10 % D_2O. Survivin120 assignments were transferred from the BMRB database entry # 6342. A stock solution containing 5 mM tweezers was titrated stepwise to the protein sample and ¹H-¹⁵N-BEST-TROSY-HSQC NMR spectra were recorded for each titration step. The chemical shift perturbation $\Delta\delta$ was calculated from the ¹H- and ¹⁵N-shifts according to the following equation by using the spectra with 0 and 500 µM, 750 µM or euimolar amounts of the tweezers, where $\Delta\delta_N$ and $\Delta\delta_H$ represent the chemical shift perturbation values of the amide nitrogen and proton:

$$\Delta\delta = \sqrt{\Delta\delta_H^2 + (0.154 \cdot \Delta\delta_N)^2}$$ (Eq. 3)

Relative signal intensities I/I_0 were obtained by dividing the intensities in the presence of 500 µM or 750 µM tweezers by the intensities in the absence of tweezers.

2.5 CELL BIOLOGICAL METHODS

2.5.1 CULTIVATION OF EUKARYOTIC CELL LINES

The adherent eukaryotic cell lines HEK 293T and HeLa Kyoto were cultivated in DMEM++ growth medium and incubated at 37 °C, 5 % CO_2 and 90 % relative humidity. Cells were split twice a week in a ratio of 1:20 to control cell density and to ensure supply with fresh growth medium. For this purpose, old growth medium was discarded and the cells were washed with 10 ml DPBS. Afterwards, 2 ml of TrypLE™ Express were added to the cell culture flask, which was then placed on a heating plate until all cells were enzymatically detached. Next, 8 ml of new growth medium were added, cells were resuspended and 0.5 ml of the suspension were transferred to a new T-75 flask together with 9.5 ml of fresh DMEM++. After approximately 40 passages cells were discarded.

2.5.2 FREEZING AND THAWING OF CELLS

For freezing, detached cells were centrifuged at 300 x g for 5 min at RT and resuspended at a concentration of approximately 2×10^6 cells/ml in FCS with 10% DMSO. Afterwards, 1 ml aliquots were transferred into cryo tubes and frozen in a Mr. Frosty™ freezing container (Thermo Fisher Scientific) at -80 °C. Cells were afterwards stored in a liquid nitrogen tank. Cells were thawed by warming up the cryo tube in a water bath at 37 °C. Cells were then carefully added to a tube containing 9 ml of pre-heated DMEM++. The suspension was centrifuged at 300 x g for 5 min at RT, cells were resuspended in 10 ml fresh growth medium and transferred into a T-75 flask. The next day, growth medium was replaced.

2.5.3 TRANSIENT TRANSFECTION OF EUKARYOTIC CELLS

Transient transfection temporally introduces exogenous DNA into eukaryotic cells. For pull-down assays, HEK 293T cells were transfected with calcium phosphate. Cells were seeded (1:10) in 10 cm cell culture dishes and incubated at 37 °C, 5 % CO_2. The next day, transfection was achieved with a calcium phosphate transfection solution containing 13.75 µg DNA according to Table 2-16. The mixture was incubated for 10 min, before 1 ml was added to the 10 cm dishes. The cells were then incubated for 24 h prior to cell lysis (section 2.5.4).

Table 2-16: Transfection mixture.

	Volume [µl]
Cell culture volume	10,000
10 mM Tris-HCl	495
2 M CaCl$_2$	55
2x HBS	550
Transfection volume	1000

2.5.4 PREPARATION OF WHOLE CELL LYSATES FROM EUKARYOTIC CELLS

Transfected HEK 293T cells were chemically lysed in RIPA buffer. Approximately 24 h after transfection, the cell culture dishes were placed on ice for 5 min prior to detachment of cells with a scraper and transfer to a 15 ml reaction tube. Cells were pelleted by centrifugation (500 x g, 4 °C, 5 min) and resuspended in 1 ml PBS. The cells were centrifuged (500 x g, 4 °C, 5 min), resuspended in 100–150 µl RIPA buffer and incubated on ice for 15 min. Afterwards, the cells were sonicated (15 s at 90 % intensity) with the Sonopuls mini20 device using the ultrasonic probe MS 1.5 (Bandelin). Cell debris was removed by centrifugation (20,000 x g, 4 °C, 20 min), the supernatant was transferred in a new reaction tube and the whole protein concentration was measured via Bradford Assay (section 2.4.4.2).

2.5.5 STAINING OF CELLS WITH FLUORESCENT DYES

For tweezer localization studies, HeLa Kyoto cells were incubated with fluorescently labeled tweezers (10 µM) overnight and then stained with CellTracker™ Deep Red Dye (Invitrogen™) and Hoechst33342. For this, a CellTracker™ stock solution of 1 mM was prepared in DMSO. The dye was then freshly diluted in Opti-MEM™ medium and preheated at 37 °C immediately before staining. Cells were incubated with 2.7 µM CellTracker™ Deep Red Dye in Opti-MEM™ medium for 30 min at 37 °C and 5 % CO$_2$. Afterwards, the staining solution was removed and DMEM++ containing 10 µg/ml Hoechst33342 was added for 15 min for DNA staining. Next, cells were washed 3x with preheated DMEM++ before FluoroBrite™ DMEM++ media was added for microscopy analysis.

2.5.6 CONFOCAL FLUORESCENCE MICROSCOPY

Fluorescence microscopy is a technique that uses light of a specific wavelength to excite a fluorophore, which then emits light at a higher wavelength and is detected using a fluorescence

microscope. For enhancement of resolution and contrast, a confocal laser scanning microscope can be used, which only excites a small layer of the sample through a spatial pinhole (Davidovits and Egger, 1969). In this work, confocal fluorescence microscopy images were acquired with a scanning microscope TCS SP8 (Leica Microsystems) equipped with four lasers (Argon: 458/476/488/496/514 nm; DPSS: 561 nm; Helium Neon: 633 nm; UV Diode: 405 nm), two PMT confocal imaging detectors and one sensitive imaging hybrid detector. A HCX PL APO CS 63.0 x / 1.20 water objective was used. The microscope was operated with the Leica Application Suite X (LAS X) software. For life cell imaging, cells were supplied with 5 % CO_2 at 37 °C during acquisition.

2.6 COMPUTATIONAL METHODS

Computational methods were used to assess the binding mode of the tweezers to Survivin's surface. All simulations were performed and analyzed by Dr. Yasser B. Ruiz-Blanco together with Dr. Joel Mieres-Perez (both Sánchez-García group, University of Duisburg-Essen).

2.6.1 MD SIMULATIONS

Molecular dynamic (MD) simulations were used to analyze the complexation of four different lysines (K23, K90, K91, K103) by TW-ELTL. The software NAMD (Phillips et al., 2005) was used to perform 80 ns (2x40 ns) MD simulations of 1:1 protein-tweezer complexes on the respective lysines. The simulations were performed in the NPT ensemble (constant pressure of 1 Atm and constant temperature of 300 K) using the CHARMM36m force field (Klauda et al., 2010; Vanommeslaeghe et al., 2010; Huang et al., 2017). The system was placed in a TIP3P water box (Mark and Nilsson, 2001), which was built with a padding of 20 Å and neutralized with sodium ions. For Van der Waals interactions, a cut-off of 12 Å was used and for the evaluation of long-range electrostatics the Particle Mesh Ewald method (Darden et al., 1993) was used. Geometries where initially minimized and equilibrated at 300 K by performing 150 ps each of NVT (constant temperature) and NPT simulations with time steps of 2 fs.

2.6.2 QM/MM SIMULATIONS

Quantum mechanics/ molecular mechanics (QM/MM) optimizations were performed to assess the stability of the different tweezer-lysine complexes using ChemShell (Sherwood et al., 2003) with the DL-FIND geometry optimizer (Kästner et al., 2009) and Turbomole (Ahlrichs et al.,

1989) for the QM region. The QM region contained the tweezer and the methylene groups in positions δ and ε of the sidechain of the respective lysine, while the MM region was formed by the rest of the protein atoms, solvent and ions. The MM region was calculated with the CHARMM36m force-field and the QM region with the density functional theory (B3LYP-D3)/ Def2SVP (Grimme, 2011). Five snapshots from the previosly performed MD simulations were used as initial geometries for QM/MM optimizations. The analysis was performed using the quality threshold algorithm as implemented for the software VMD, with a root-mean-square deviation cutoff of 3 Å.

2.6.3 GaMD SIMULATION

Gaussian accelerated molecular dynamics (GaMD) simulations (Pang et al., 2017) were performed with the software NAMD using an analogous setup as for the MD simulations. The statistics for the biasing potential were collected during 50 ns of equilibration ahead of the production run, which was extended to 100 ns. The threshold value for the biasing potential was fixed to the maximum potential energy during the equilibration step. The standard deviation of the biasing potential was controlled allowing a maximum value of 10 kT.

3 RESULTS

The protein Survivin is highly upregulated in almost all types of cancer cells, correlating with a resistance against radio- and chemotherapy and poor patient outcomes (Adida et al., 2000; Capalbo et al., 2007). Its cancer-relevant dual role as an apoptosis inhibitor and a regulator of mitosis is mediated via the interaction with the export receptor Crm1 (Knauer et al., 2007). Hence, this protein-protein interaction is a very attractive target for cancer research and drug development. However, no specific inhibitor for this important PPI exists so far. Supramolecular chemistry enables the rational development of ligands containing several molecular building blocks, e.g. artificial host molecules like amino acid binders and peptide fragments for specific protein surface areas. In this work, the combination of multiple tweezers, precision macromolecules, ultra-small gold nanoparticles, or peptides in order to target Survivin's NES should be explored and assessed with regard to their binding affinity for Survivin and inhibitory potential for the Survivin/Crm1 interaction.

3.1 CHARACTERIZATION OF PEPTIDE-MODIFIED TWEEZERS

Previously, first peptide-modified tweezers were generated in order to target Survivin's protein surface (Bäcker, 2018; Heid, 2018). A short (ELTL) and an elongated (ELTLGEFL) peptide sequence derived from Survivin's dimer interface [95]ELTLGEFL[102] were clicked to the molecular tweezer (Figure 3-1). Hence, these peptides mimic one of Survivin's natural binding sites and shall direct the tweezers to this particular surface region, which partly overlaps with Survivin's NES. First experimental and computational results indicated binding of TW and TW-ELTL to Survivin's NES and all tweezers showed inhibitory effects on the Survivin/Crm1 interaction (Bäcker, 2018). However, the assessment of regioselectivity and signal-specificity of the peptide-modified tweezers should be further elucidated, and TW-ELTLGEFL needed to be characterized more thoroughly.
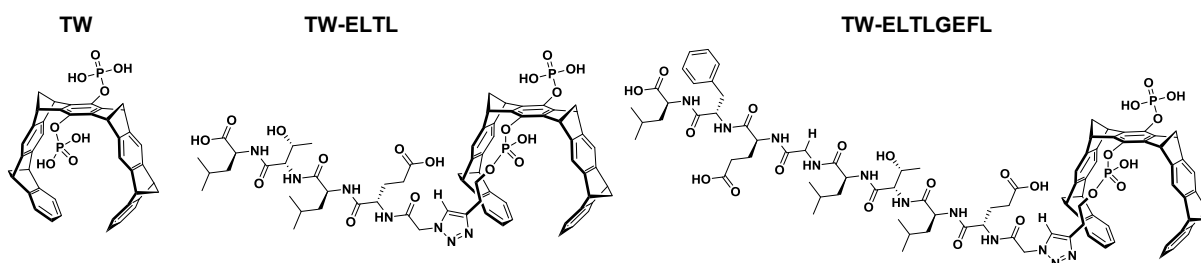
Figure 3-1: TW was modified with peptides derived from Survivin's dimer interface.

Peptide motifs (ELTL/ ELTLGEFL) were selected from Survivin's dimer interface (aa 89–102) for the conjugation to the tweezer. Images were provided by Inesa Hadrovic (Schrader group, University of Duisburg-Essen).

3.1.1 PEPTIDE-MODIFIED TWEEZERS BIND TO SURVIVIN'S NES WITH LOW MICROMOLAR AFFINITY

Binding of tweezers to Survivin was assessed by ITC experiments. Titrations of Survivin$_{120}$ WT to each of the tweezer molecules resulted in exothermic binding curves (Figure 3-2). The data were fit with the *one set of sites* model in the software Origin and revealed binding affinities in the low micromolar range. The dissociation constants K_D correspond to 38 ± 4 µM for TW, 24 ± 4 µM for TW-ELTL and 19 ± 3 µM for TW-ELTLGEFL. The tweezer with the longest peptide sequence (TW-ELTLGEFL) showed the lowest dissociation constant and, in turn, binds Survivin most strongly. Furthermore, big differences could be observed between the stoichiometries of the unmodified and the peptide-equipped tweezers. TW revealed a stoichiometry of approx. 20 tweezers per protein, while TW-ELTL and TW-ELTLGEFL produced a stoichiometry of approx. 2 tweezers per Survivin$_{120}$ molecule.

	A			B			C	
K_D	=	38 ± 4 µM	K_D	=	24 ± 4 µM	K_D	=	19 ± 3 µM
N	=	20.8 ± 0.4	N	=	2.03 ± 0.07	N	=	1.94 ± 0.07
ΔH	=	-1.33 ± 0.02 kcal/mol	ΔH	=	-2.53 ± 0.06 kcal/mol	ΔH	=	-1.92 ± 0.05 kcal/mol
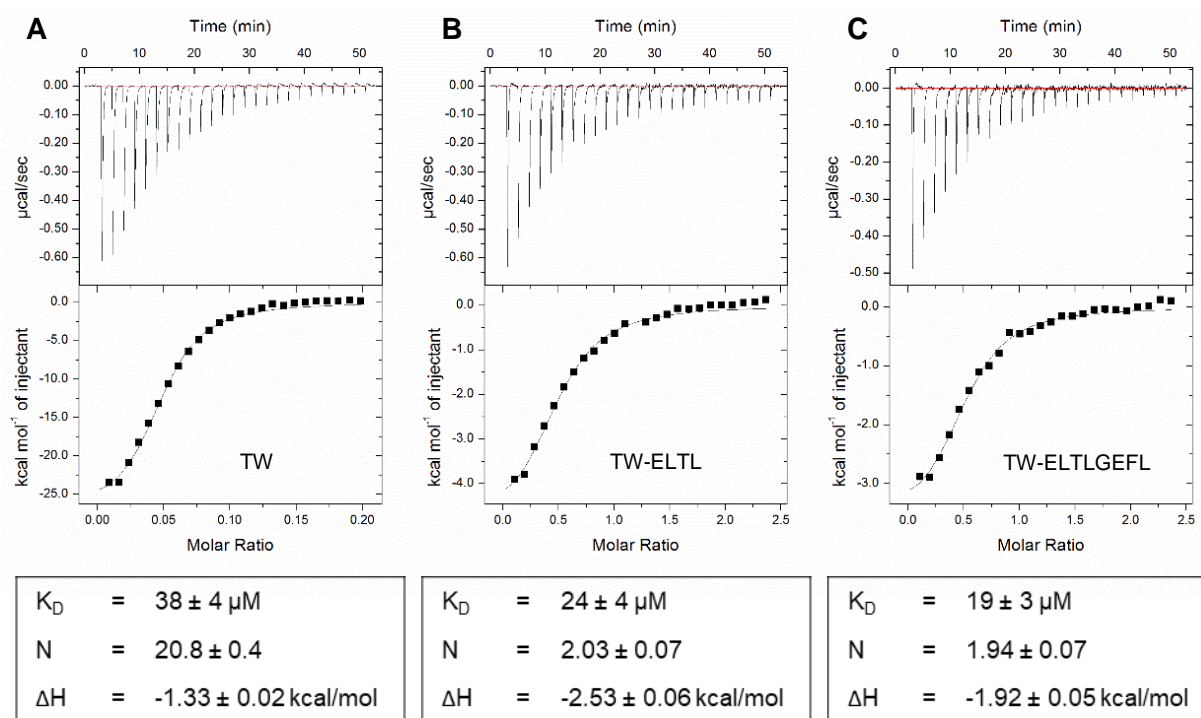
Figure 3-2: Survivin$_{120}$ binds to tweezers with low micromolar affinity as evidenced by ITC.
(A) Titration of 300 µM TW in the cell with 300 µM Survivin$_{120}$ WT in the syringe. Titration of 100 µM TW-ELTL (B) or TW-ELTLGEFL (C) in the cell with 1.2 mM Survivin$_{120}$ WT in the syringe. All titrations were performed in PBS, pH 7.4, at 25 °C. The heat of dilution was subtracted as constant, which was averaged from data points in the saturation region. Depicted is one representative ITC experiment per tweezer. The black lines in the bottom panels are the fit of the data to a *one set of sites* model. Values reported below are the mean ± s.e.m. of the fit. The depicted ITC experiments with TW-ELTL and TW-ELTLGEFL were performed by Dr. Sandra Bäcker. Experiments were performed in triplicates, however, only the curve with the lowest fitting error is shown. K_D, dissociation constant; N, stoichiometry of binding; H, enthalpy. Tweezers were provided by Dr. Christian Heid and Inesa Hadrovic (both Schrader group, University of Duisburg-Essen).

To map tweezer binding to distinct amino acid residues, NMR titration experiments adding up to equimolar amounts of TW-ELTLGEFL to ^{15}N-labeled Survivin$_{120}$ (Figure A1) were performed and the chemical shift perturbations as well as the relative signal intensities were compared to those of TW and TW-ELTL, which had been previously described (Bäcker, 2018). NMR titrations and subsequent analyses were performed by Dr. Christine Beuck (Bayer group, University of Duisburg-Essen).
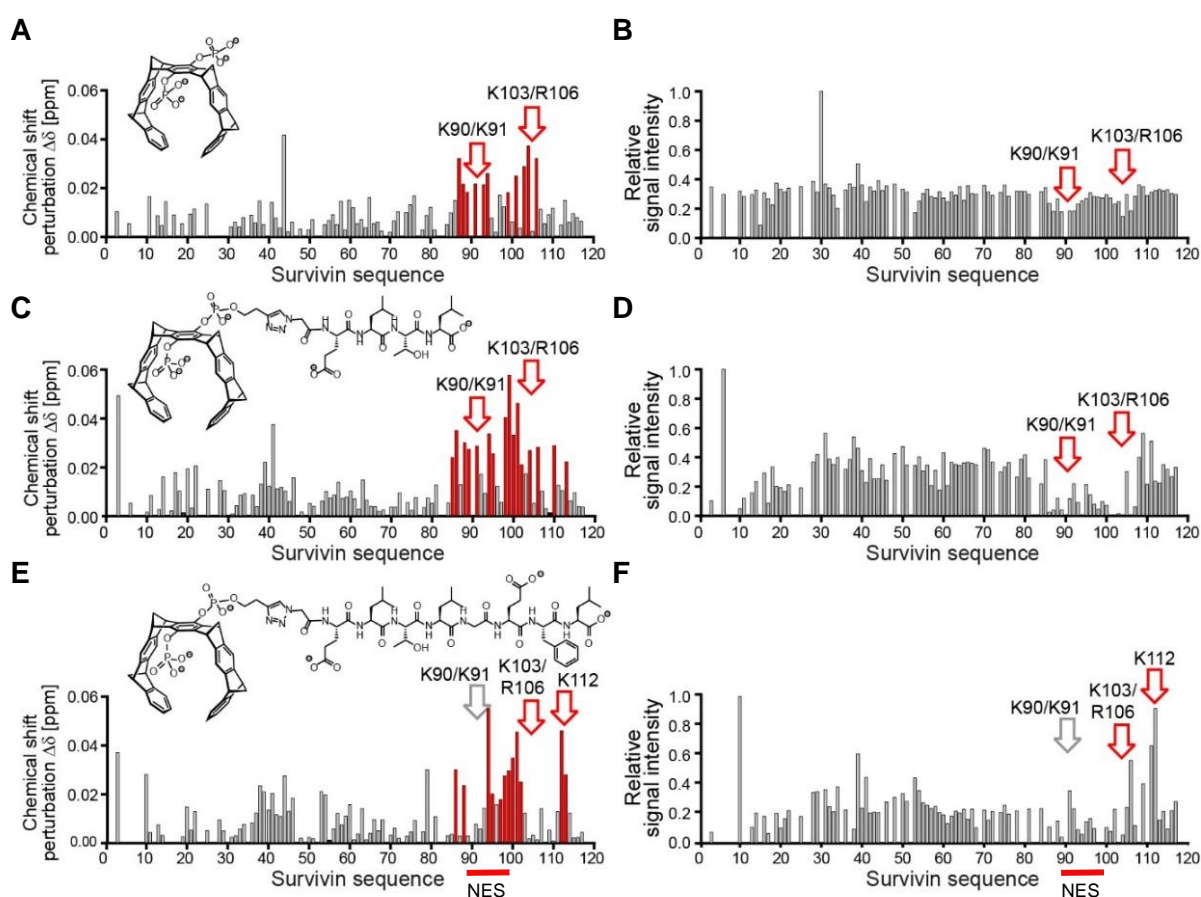

Figure 3-3: Peptide-modified tweezers bind to Survivin's NES as evidenced by NMR chemical shift perturbation and signal intensity analyses.

NMR signal shifts (A; C; E) and relative signals (B; D; F) of Survivin$_{120}$ in complex with one equivalent of tweezers compared to sole Survivin$_{120}$ were plotted against the amino acid sequence (aa 2–117). Signal shifts and normalized signal intensities for the unmodified TW (top), TW-ELTL (center) and TW-ELTLGEFL (bottom) were identified for each signal. Prominent shifts or reduced signal intensities mainly occurred for basic residues around Survivin's NES (red bar) and are marked with a red arrow. For TW-ELTL and TW-ELTLGEFL signal intensities collapsed around the NES region. NMR titrations and subsequent analyses were performed by Dr. Christine Beuck (Bayer group, University of Duisburg-Essen). This figure was partially published in Bäcker (2018).

Prominent shifts and decreased signal intensities for certain amino acids usually indicate binding of a ligand to that region and, thus, putative binding sites of the tweezers might be

mapped from this experiment (Williamson, 2013). Hence, chemical shift perturbations and signal intensities were plotted against the amino acid sequence of Survivin$_{120}$ (Figure 3-3). The previous titration of TW resulted in signal shifts around the basic amino acids K91, K103, and R106 (Figure 3-3 A) (Bäcker, 2018). Furthermore, signal intensities decreased in the same regions identifying the latter as potential tweezer binding sites (Figure 3-3 B). Titration of TW-ELTL, and now TW-ELTLGEFL, increased the signal shifts for the same basic residues and decreased the signal intensities even stronger (Figure 3-3 C-E). More importantly, the residues between lysines 90 and 103 showed significant signal shifts and reduced intensities upon titration of TW-ELTL and TW-ELTLGEFL as well. This confirmed that the peptides indeed contact the NES region.

In addition to the biochemical experiments, the interaction between the tweezers and Survivin$_{120}$ was assessed with MD and GaMD simulations as well as QM/MM calculations. These experiments were designed, performed and analyzed by Prof. Dr. Elsa Sánchez-García, Dr. Yasser B. Ruiz-Blanco and Dr. Joel Mieres-Perez (Sánchez-García group, University Duisburg-Essen). As the NES region overlaps with the dimer interface, the NES is rather hidden in the dimeric state. In the monomer, however, it is exposed. Therefore, a protomer derived from the dimeric structure (PDB ID: 1XOX; protomer A) was used to calculate the interactions between the tweezers and lysines on Survivin's surface. Four surface-exposed lysines (K23, K90, K91 and K103) were selected to assess their complexation with TW-ELTL.

The complexes between lysines K23 and K90 seemed to be unfavorable as relative energies of the QM regions are much higher than observed for K91 and K103 (Table 3-1). Intriguingly, a conserved interaction between the peptide ELTL and the homologous region on Survivin's surface (^{95}ELTL^{98}) only occurred when the tweezer cavity encapsulated K103 and thus allowed pairing of the peptide and the NES region of Survivin similar to the natural dimer structure (Figure 3-4 A). In addition, K103 produced the most stable complex as indicated by the lowest relative energy and, hence, seemed to be the most favorable binding site of the tweezer. Furthermore, binding of the tweezer to K103 seemed to be additionally stabilized by a salt-bridge with R106 (Figure A2).

Table 3-1: Relative energies of the QM regions identify K91 and K103 as the most stable tweezer-anchors.

Lysine	Relative energy QM region (kcal/mol)
K103	0 ± 11
K91	1 ± 14
K90	27 ± 6
K23	68 ± 3

As K103 was identified as ideal anchor residue for the tweezer with the short peptide-modification (ELTL), subsequent GaMD simulations with TW-ELTL and the elongated TW-ELTGEFL were performed with the tweezer cavity anchored at K103. TW-ELTLGEFL forms more non-covalent interactions with the ^{95}ELTL^{98} sequence and, thus, contacts the whole NES region more frequently compared to the truncated TW-ELTL (Figure 3-4 B).
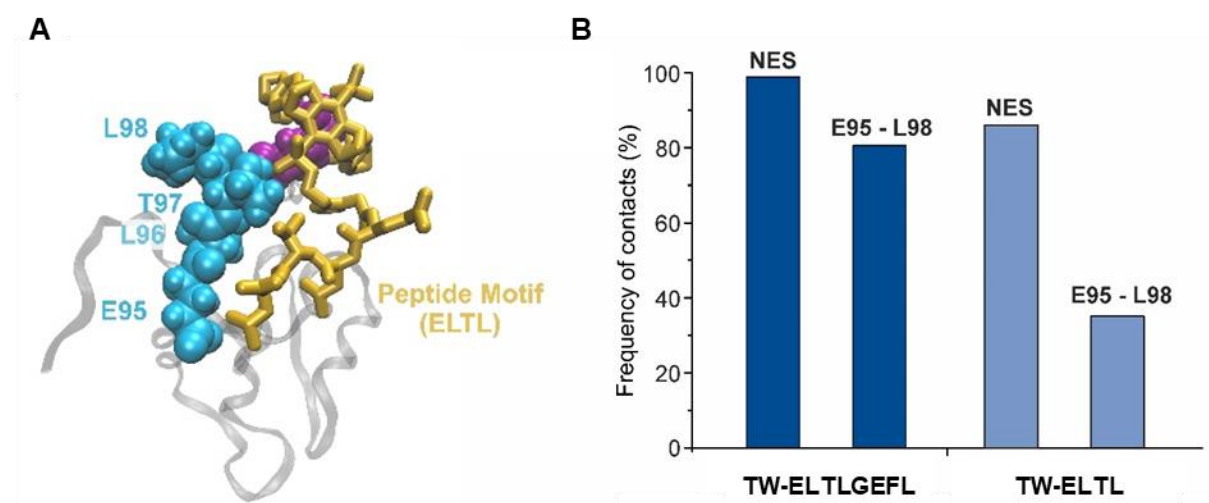
Figure 3-4: Both peptide-modified tweezers interact with the NES region on the Survivin$_{120}$ protomer when anchored to K103.
A) Representation of TW-ELTL (gold) bound to Survivin$_{120}$ (grey). The anchor lysine residue K103 (violet) is encapsulated by the tweezer cavity while the peptide motif ELTL (gold) interacts with the ^{95}ELTL^{98} region of the Survivin protomer (blue). The peptide ELTL of the tweezer and sequence ^{95}ELTL^{98} of the protomer show pairing similar to the natural dimer (PDB ID: 1XOX). B) Frequency of contacts between the tweezer's peptides ELTL or ELTLGEFL and the NES region or ^{95}ELTL^{98} sequence on the Survivin$_{120}$ protomer is depicted. TW-ELTLGEFL contacts both, the whole NES, as well as ^{95}ELTL^{98} more frequently compared to TW-ELTL. The simulations were done by Dr. Yasser B. Ruiz-Blanco, and the figure was prepared by Dr. Joel Mieres-Perez (both Sánchez-García group, University of Duisburg-Essen).

So far, all simulations were performed on a Survivin protomer. However, Survivin occurs as a homodimer in solution and the peptide used for modification of the tweezers mimics the dimer interface [95]ELTLGEFL[102]. Therefore the question arose whether or not the peptide-modified tweezers will disrupt the dimeric state or whether they will be able to bind to the NES region despite the existence of the dimer. GaMD simulations with the dimer in an explicit solvent box were performed to get insights into the dimer dynamics and flexibility. During the simulation, the frequency of hydrogen bond formation in the dimer interface was analyzed. Up to two hydrogen bonds can be formed within the analyzed sequence [95]ELTL[98] (Figure 3-5 A). Most frequently, no hydrogen bonds occurred during the simulation (Figure 3-5 B). The strongest interaction with two hydrogen bonds was the least prevalent state. This indicates that this part of the dimer interface is likely dynamic and flexible and potentially enables binding of a matching ligand between the protomers.

Dimer Interface (hydrogen bonds at the ELTL region)
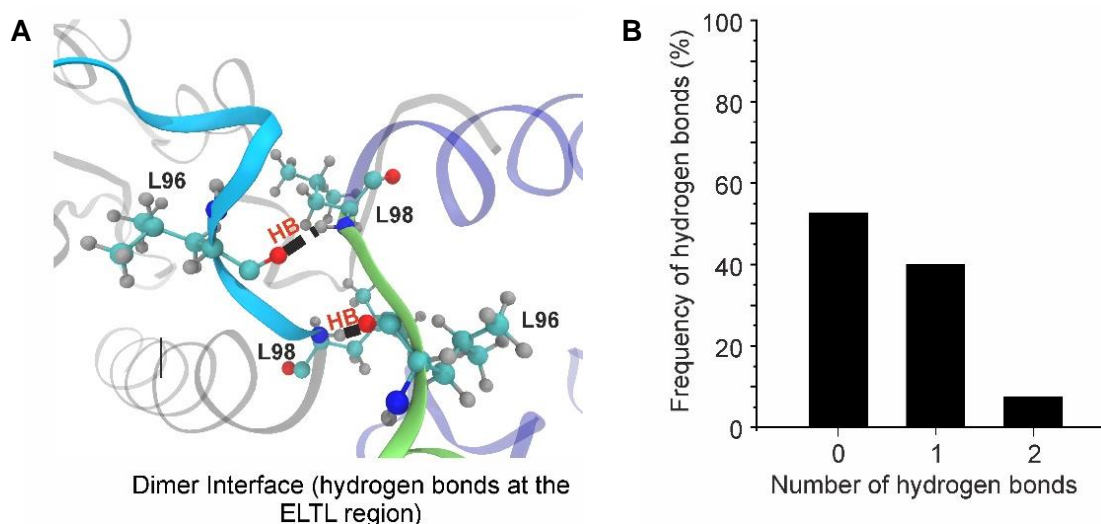
Figure 3-5: Hydrogen bonds are rarely formed between both [95]ELTL[98] fragments within Survivin's homodimerization interface.
A) The peptide fragments ([95]ELTL[98]) of the two protomers (PDB ID: 1XOX) can form two hydrogen bonds (HB) involving the leucines L96 and L98, respectively. The leucines are depicted as ball-and-stick models. The NESs of the two protomers are colored in blue and green. B) Frequency of the hydrogen bonds between the [95]ELTL[98] sequences within the dimer interface. The most stable interaction maintained by two hydrogen bonds at the same time is the least prevalent indicating a rather weak and, thus, likely dynamic dimer interface between [95]ELTL[98]. The simulations were done by Dr. Yasser B. Ruiz-Blanco, who analyzed the data together with Dr. Joel Mieres-Perez, who prepared the figure (both Sánchez-García group, University of Duisburg-Essen).

3.1.2 PEPTIDE-MODIFIED TWEEZERS INTERFERE WITH THE SURVIVIN/CRM1 INTERACTION *IN VITRO*

Previously, the peptide-modified tweezers had shown an inhibitory effect on the Survivin/Crm1 interaction in pull-down assays (Bäcker, 2018). However, TW-ELTLGEFL had not been tested in a concentration-dependent manner. For this purpose, recombinant GST-Crm1 was used as bait for heterologous expressed HA-tagged $Survivin_{142}$ in 293T cell lysates, which were pre-incubated with TW-ELTLGEFL in concentrations ranging between 10 nM and 200 µM. Just like the unmodified and short peptide tweezers, the elongated TW-ELTLGEFL revealed a concentration-dependent interference with the Survivin/Crm1 interaction (Figure 3-6).
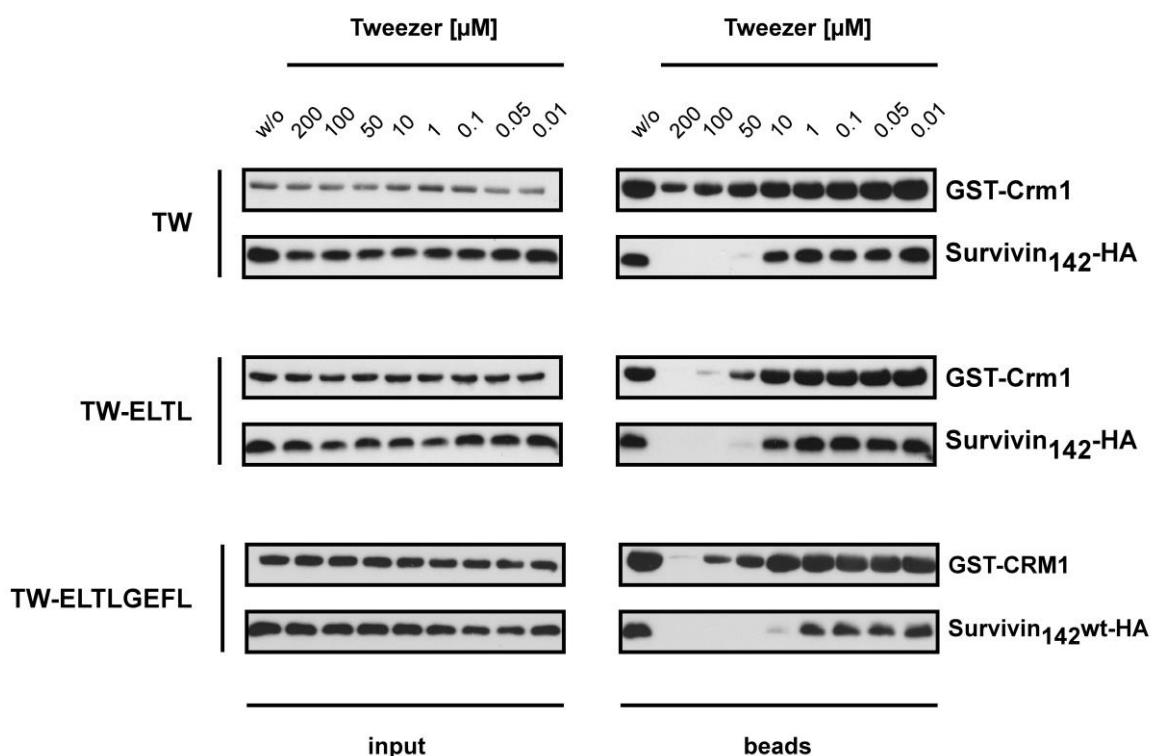
Figure 3-6: Peptide tweezers inhibit the Survivin/Crm1 interaction in a concentration-dependent manner.
293T cells were transfected with Survivin142-HA. Respective lysates were pre-incubated with unmodified TW (top), TW-ELTL (center), and TW-ELTLGEFL (bottom) at concentrations between 0.01 and 200 µM. GST-CRM1 bait protein was mixed with either non- or tweezer-incubated cell lysates, with recombinant RanQ6C9L and dGTP to enable complex assembly. Protein complexes were pulled by GSH-Sepharose beads. Proteins in input and beads samples were analyzed via immunoblotting with antibodies specific for GST and HA. Pull-downs and subsequent evaluations were conducted by Dr. Sandra Bäcker (Knauer group, University of Duisburg-Essen). Tweezers were provided by Dr. Christian Heid (Schrader group, University of Duisburg-Essen). This figure was partially published in Bäcker (2018).

Pull-down experiments showed an inhibitory concentration of 1–10 µM for TW-ELTLGEFL, while TW and TW-ELTL inhibited the Survivin/Cmr1 interaction only at higher concentrations between 10–50 µM. Therefore, the modification of the molecular tweezer with an elongated peptide (ELTLGEFL) seemed to enhance the inhibitory effect. Of note, an additional inhibition of GST binding to GSH-Sepharose beads could be observed at the highest concentrations, which might indicate tweezer binding to GST. Pull-down experiments were conducted by Dr. Sandra Bäcker (Knauer group) and tweezers were provided by Dr. Christian Heid (Schrader group, University of Duisburg-Essen).

Since pull-down experiments and subsequent Western Blot analyses give only semi-quantitative results, a fluorescence anisotropy dissociation assay was established. This assay is based on the complex formation between Survivin labeled with an Atto 488 fluorophore and a $Crm1_{1062}VLV430AAA$ mutant ($Crm1_{mut}$), which is able to bind Survivin irrespective of RanGTP (Figure 3-7 A). The protein complex gives a higher anisotropy signal in contrast to unbound $Survivin_{Atto}$ due to its higher mass. Thus, complex dissociation upon tweezer titration is indicated by decreasing anisotropy signals. Indeed, this could be observed for all tested tweezers (Figure 3-7 B). The data were fit with GraphPad Prism as described in section 2.4.10.1 and IC50 values of 53 µM for the unmodified TW, 39 µM for TW-ELTL and 12 µM for TW-ELTLGEFL were determined (Figure 3-7 C). Notably, the expression yield of the Crm1 mutant did not allow the calculation of a K_D for the $Survivin_{Atto}/Crm1_{mut}$ interaction as the small amount of pure $Crm1_{mut}$ was not enough to reach saturation in titration experiments of $Crm1_{mut}$ to $Survivin_{Atto}$. Therefore, the quantification of K_I values for the dissociation assay was not possible. Nevertheless, these fluorescence anisotropy dissociation experiments substantiated the findings from previous pull-down experiments and further confirmed the enhancement of the tweezers by peptide-modification.
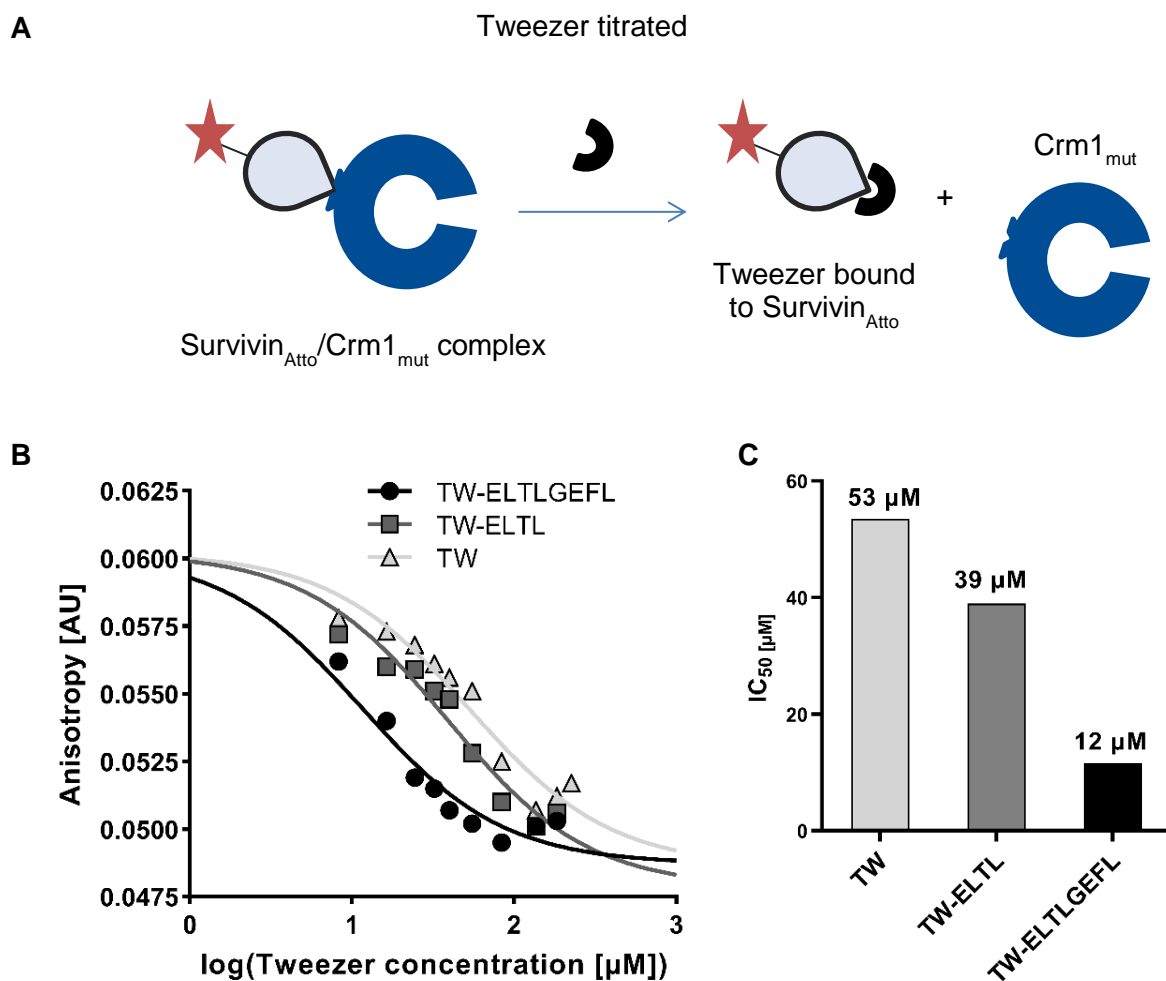
Figure 3-7: Peptide-modifications enhance the inhibitory potential of the tweezers.

A) Experimental set-up for the fluorescence anisotropy dissociation assay. B) Fluorescence anisotropy signal upon tweezer titration. Survivin$_{Atto}$ was mixed with Crm1$_{mut}$ and titrated with unmodified or peptide-conjugated tweezers. C) IC50 values determined from dissociation curves. TW-ELTLGEFL is the most potent inhibitor tested for the Survivin/Crm1 interaction. Tweezers were provided by Dr. Christian Heid (Schrader group, University of Duisburg-Essen).

3.1.3 PEPTIDE-MODIFIED TWEEZERS BIND REGIOSELECTIVE AND SIGNAL-SPECIFIC TO SURVIVIN

The peptide-modification enhanced the tweezer's affinity for Survivin and its ability to interfere with the Survivin/Crm1 interaction as indicated by ITC, pull-down and fluorescence anisotropy experiments. However, the question whether the observed effects are really caused by specific binding of the tweezers to Survivin's NES directed by the peptide-sequence remained unresolved. For this, several experiments with a Survivin mutant lacking the putative binding

sites of the tweezers, identified from NMR titrations, were performed subsequently. Furthermore, studies involving a tweezer with a scrambled peptide sequence were conducted in order to investigate the signal-specificity of the peptide-modified tweezer.

3.1.3.1 ANALYSIS OF SURVIVIN$_{120}$ MUTANTS LACKING PUTATIVE BINDING SITES

Survivin's nuclear export signal is flanked by lysines 90, 91 and 103 as well as arginine 106, which are putative binding sites for the molecular tweezers as indicated by NMR titrations (section 3.1.1). Survivin mutants, in which these relevant amino acids are substituted to non-basic amino acids, should not be targeted by the tweezers since their essential anchor residues are lacking. Therefore, different Survivin$_{120}$ mutants were generated by site-directed mutagenesis with subsequent 1D-^{1}H-NMR spectroscopy to ensure the correct folding of the protein. NMR spectra were compared to the spectrum of Survivin$_{120}$ WT (Figure 3-8). Correct folding was examined, especially with regard to the region of 6–10 ppm resulting from amides and aromatics, and below 1 ppm obtained from methyl groups (McDonald and Phillips, 1967; Page et al., 2005). Survivin$_{120}$ WT showed a wide signal dispersion in the amide/aromatic range and distinct methyl signals. While the 1D-spectrum of folded Survivin$_{120}$ WT revealed sharp and narrow signals, most mutants like K90/91/103S showed less but broadened peaks in the amide and aromatic region and reduced or no peaks in the far methyl region < 1 ppm. The NMR signals reflect the local environment of each amino acid, and in the folded state, they have different chemical environments due to the presence of secondary and tertiary structure elements. Thus, a large signal dispersion is observed for folded Survivin$_{120}$ WT. However, for most mutants the amide and methyl signals collapsed into the spectral regions typical for random coil conformation (amides ~7.8–8.6 ppm and methyl groups 1.0–1.5 ppm) and, thus, they seemed to be in an unfolded state, in which the protons are not in a distinct structural environment anymore.

Other mutants like K103S or K90/103S precipitated during the measurement, and hence are not suitable either. Survivin$_{120}$ K90/103T was stable and folded correctly as evidenced by a similar 1D-^{1}H-Spectrum to Survivin$_{120}$ WT. Therefore, this mutant was used as control in further assays to prove the necessity of lysines 90 and 103 for efficient tweezer binding and, thus, for the inhibitory effect of the tweezers.
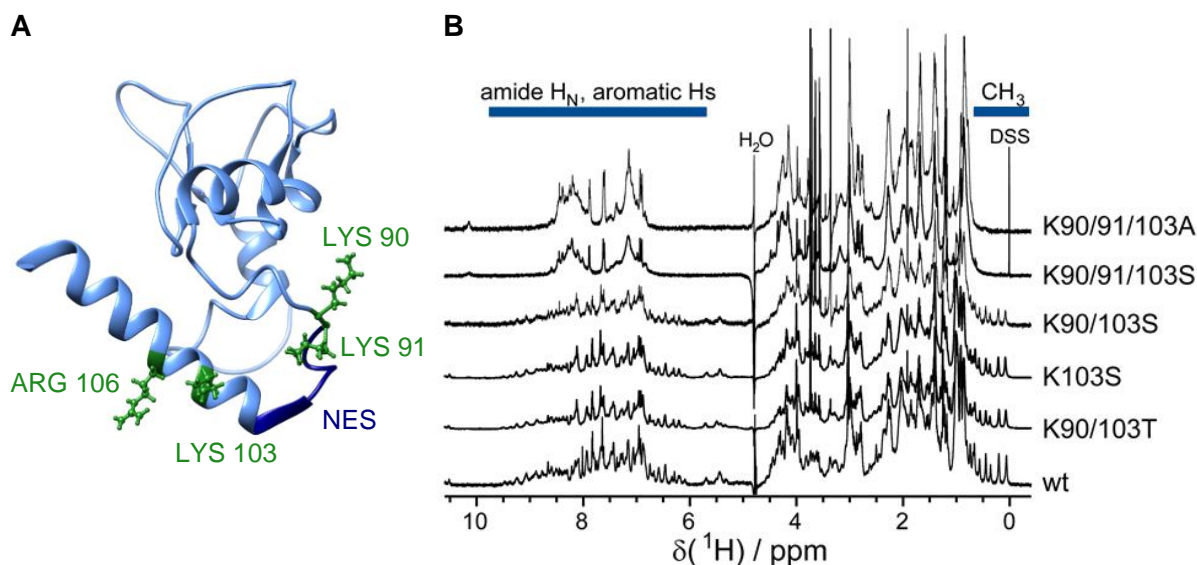
Figure 3-8: Survivin mutant K90/103T lacking amino acids essential for tweezer binding folds correctly.
A) The Survivin$_{120}$ protomer (PDB ID: 1XOX) has two basic patches around the NES (dark blue). K90, K91, K103, and R106 are depicted as stick models. The lysines were substituted to alanine, serine or threonine. B) The correct folding of Survivin$_{120}$ mutants was analyzed via 1D-^{1}H-NMR spectroscopy by Dr. Christine Beuck (Bayer group, University Duisburg-Essen). Spectra were compared to that of Survivin$_{120}$ WT. Correct folding was examined especially in the region of 6–10 ppm resulting from amides and aromatics, and below 1 ppm obtained from methyl groups (both highlighted in blue). Mutant K90/103T was stable, folded correctly, and was, hence, chosen for further analysis.

After having found a stable mutant lacking the putative binding sites for NES-targeting tweezers, binding of FAM-labeled tweezers to Survivin$_{120}$ WT as well as to the double threonine mutant (K90/103T) was analyzed in fluorescence anisotropy experiments. Since the molecular tweezers only target positively charged amino acids, a substitution of the surface-exposed lysines 90 and 103 to threonine should reduce the affinity of the tweezers to Survivin. Fluorescent tweezers were titrated with either Survivin120 WT or K90/103T mutant and the fluorescence anisotropy was measured (Figure 3-9). Afterwards, dissociation constants were determined with a one-to-one binding model. Peptide tweezers containing a FAM label were synthesized by Inesa Hadrovic (Schrader group, University of Duisburg-Essen).
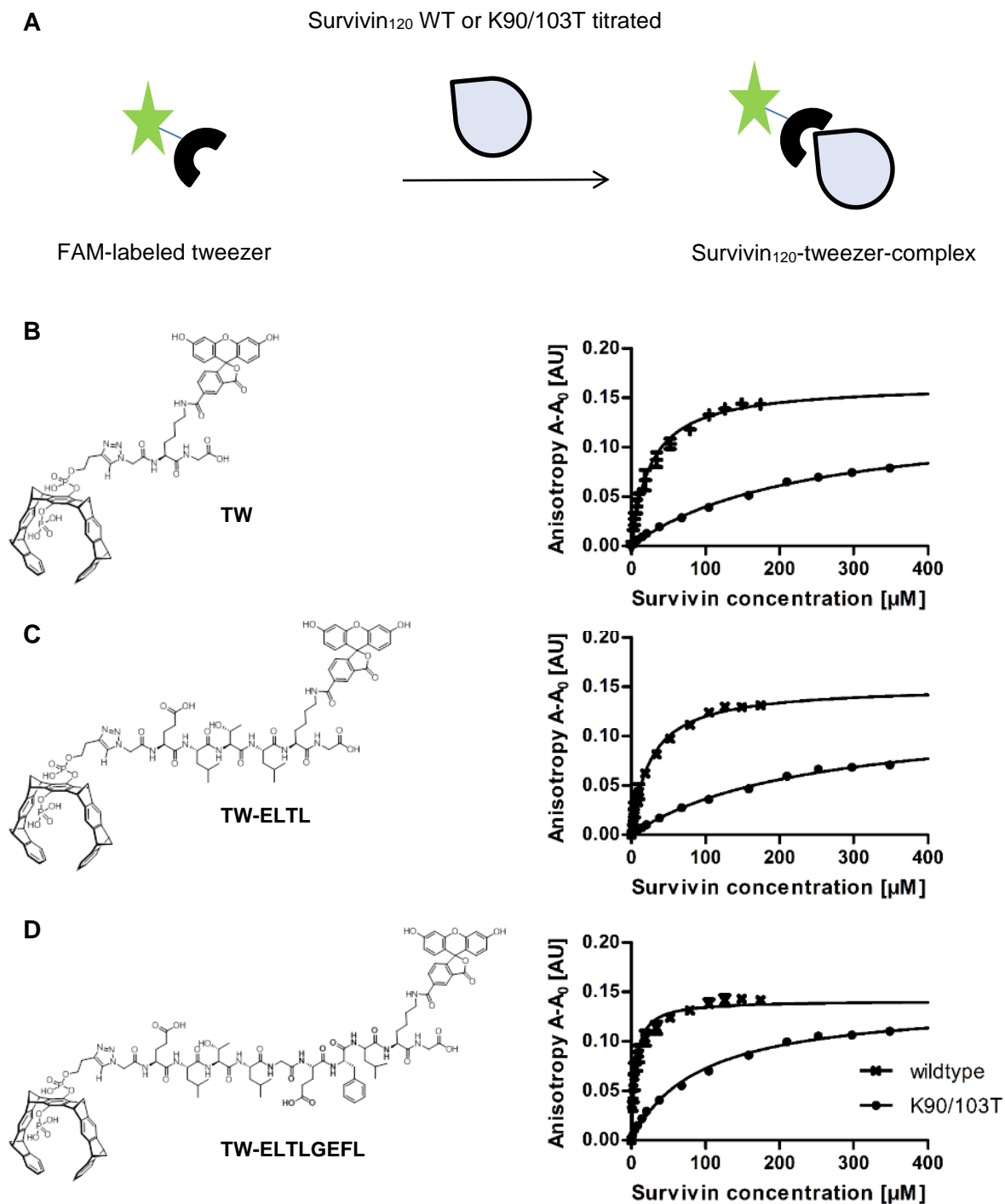
Figure 3-9: Fluorescence anisotropy experiments reveal reduced affinities of Survivin$_{120}$ K90/103T for the tweezers compared to Survivin$_{120}$ WT.

A) Functional principle of the fluorescence anisotropy assay. B-D) Structure of the FAM-labeled TW (B), TW-ELTL (C) and TW-ELTLGEFL (D). E-G) FAM-labeled tweezers were titrated with either Survivin$_{120}$ WT or K90/103T and the fluorescence anisotropy was measured (n=3). Upon assembly of the Survivin-tweezer-complex, the anisotropy increased. Binding of Survivin$_{120}$ WT to the unmodified tweezer as well as peptide-modified tweezers was much stronger compared to Survivin$_{120}$ K90/103T. Fluorescently labeled tweezers were provided by Inesa Hadrovic (Schrader group, University of Duisburg-Essen).

For the interaction with Survivin$_{120}$ WT, dissociation constants were determined to be approx. 27 ± 2 µM for the unmodified tweezer, 26 ± 2 µM for TW-ELTL and 5 ± 1 µM for the elongated TW-ELTLGEFL (Table 3-2) and correspond to the values obtained in ITC titrations, which were in the same order of magnitude and identified TW-ELTLGEFL as strongest binder as well. In contrast, Survivin$_{120}$ K90/103T revealed much lower affinities for the FAM-labeled tweezers with more than 10-fold higher dissociation constants. Titrations with the Survivin$_{120}$ mutant resulted in binding affinities of approx. 236 ±15 µM for TW, 241 ± 15 µM for TW-ELTL and 92 ± 5 µM for TW-ELTLGEFL.

Table 3-2: Binding affinities of tweezers to Survivin$_{120}$ WT and K90/103T mutant as determined via fluorescence anisotropy.

	TW	TW-ELTL	TW-ELTLGEFL
Survivin$_{120}$ WT	27 ± 2	26 ± 2	5 ± 1
Survivin$_{120}$ K90/103T	236 ± 15	241 ± 15	92 ± 5

Values reported are the mean ± standard deviation in micromolar (n=3).

The influence of the lysine substitutions in and near Survivin's NES on tweezer binding was additionally analyzed via ITC. Titration of Survivin$_{120}$ K90/1903T to each tweezer resulted in exothermic binding curves (Figure 3-10), comparable with Survivin$_{120}$ WT titrations. The data were fit with the *one set of sites* model in the software Origin and revealed binding affinities in the low micromolar range. The dissociation constants K_D were fit to 49 ± 5 µM for TW, 50 ± 10 µM for TW-ELTL and 36 ± 10 µM for TW-ELTLGEFL. Hence, the binding affinities lie in the same order of magnitude for the K90/103T mutant and wildtype. Nevertheless, the mutant revealed lower affinities compared to wildtype Survivin for all tweezers. The stoichiometry of Survivin$_{120}$ K90/103T and TW was approx. 34, while TW-ELTL and TW-ELTLGEFL produced stoichiometries of approx. one tweezer per protein. Concluding, the substitution of lysines 90 and 103 to threonine reduced the affinity of the tweezers, both, in fluorescence anisotropy as well as in ITC titration experiments. Thus, the binding sites mapped by NMR titrations were confirmed and a suitable Survivin mutant was obtained as control for further experiments.
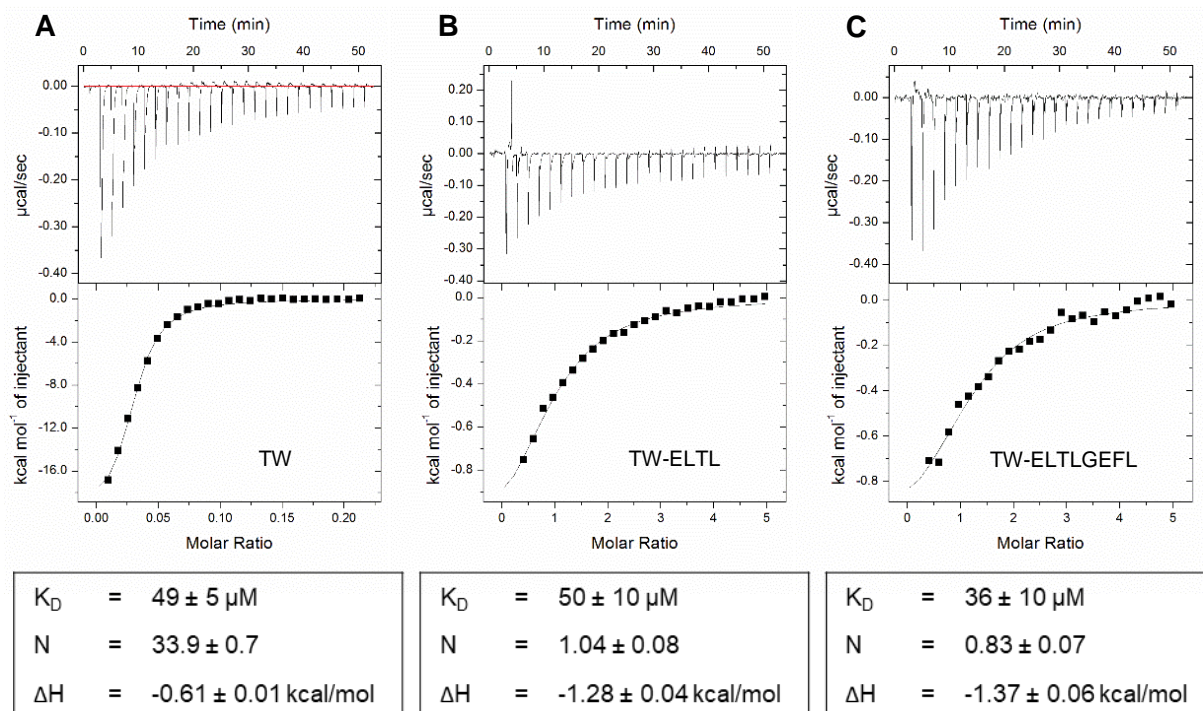
Figure 3-10: The Survivin$_{120}$ K90/103T mutant binds to the tweezers with lower affinity compared to wildtype Survivin$_{120}$ in ITC.

(A) Titration of 300 µM TW in the cell with 321 µM Survivin$_{120}$ K90/103T in the syringe. (B) Titration of 100 µM TW-ELTL in the cell with 2 mM Survivin$_{120}$ K90/103T in the syringe. (C) Titration of 100 µM TW-ELTLGEFL in the cell with 2 mM Survivin$_{120}$ K90/103T in the syringe. All titrations were performed in PBS, pH 7.4, at 25 °C. The heat of dilution was subtracted as constant, which was averaged from data points in the saturation region. Depicted is one representative ITC experiment per tweezer. The black lines in the bottom panels are the fit of the data to a one-site model. Values reported below are the mean ± s.e.m. of the fit. Experiments were performed in triplicates, however, only the curve with the lowest fitting error is depicted. K$_D$, dissociation constant; N, stoichiometry of binding; H enthalpy. Tweezers were provided by Inesa Hadrovic.

Next, pull-down assays were performed to test whether the substitution of lysines 90 and 103 reduce the tweezers' ability to interfere with the Survivin/Crm1 interaction, and thereby, whether binding of the tweezers is indeed regioselective for Survivin's NES. GST-Survivin$_{120}$ WT and K90/103T mutant were used as bait proteins for Crm1 and pre-incubated with tweezers or peptides. Afterwards, Crm1, the constitutively active RanQ69L mutant, which has a strongly reduced GTPase activity (Klebe et al., 1995), and dGTP were added to enable complex assembly. Input and bead samples were analyzed via immunoblotting (Figure 3-11 A). The Western Blot intensities were quantified (Figure 3-11 B).
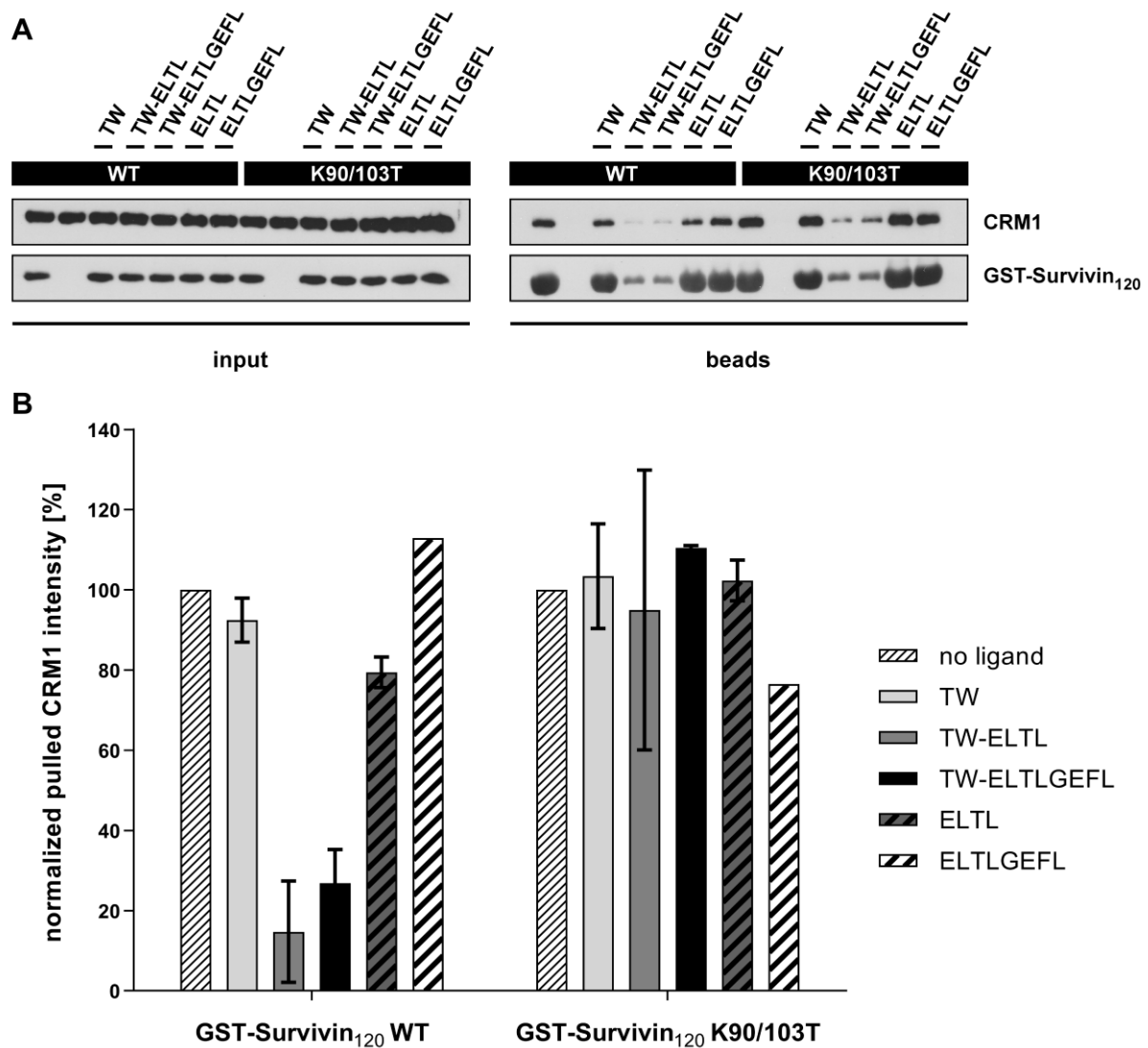
Figure 3-11: Lysine substitutions in and near Survivin's NES abolish the inhibitory effect of the Tweezers.
A) Western Blot results from one pull-down assay. GST-Survivin$_{120}$ WT or K90/103T were incubated with 50 μM respective tweezer or peptides. Beads were pre-incubated with GST-Survivin$_{120}$ proteins and then mixed with Crm1 and RanQ69L prey proteins as well as dGTP to enable complex assembly. Input and bead samples were analyzed via Western Blot with specific antibodies for Crm1 and GST. B) Quantification of two independent pull-down experiments (n=2). First, the Crm1 negative control was subtracted from the pulled Crm1 intensity. Afterwards, it is first normalized by the GST-Survivin$_{120}$ intensity and then additionally normalized by the Crm1 intensity without Tweezer incubation. The Survivin/Crm1 interaction is only inhibited in case of Survivin$_{120}$ WT, but not when the K90/103T mutant was used. Peptides without tweezer did not inhibit at all. Of note, peptide ELTLGEFL was only used in one comparable pull-down experiment and could not be quantified twice. Pull-downs and subsequent analysis were conducted by Dr. Sandra Bäcker (Knauer group, University of Duisburg-Essen). Tweezers and peptides were provided by Dr. Christian Heid (Schrader group, University of Duisburg-Essen).

In these pull-down experiments, both peptide tweezers strongly inhibited the interaction between Survivin$_{120}$ WT and Crm1, and reduced the intensities to less than 30 % compared to

the control without tweezer. The unmodified tweezer as well as the peptides without tweezers had only little to no influence on the protein complex formation. In contrast, for the double threonine mutant, neither tweezer nor peptide had a noticeable inhibitory effect on the interaction with Crm1. This indicates that the tweezer's inhibitory effect observed for Survivin$_{120}$ WT is indeed caused by regioselective binding of the peptide tweezers to lysines in and near its NES.

3.1.3.2 *ANALYSIS OF TWEEZERS EQUIPPED WITH A SCRAMBLED PEPTIDE SEQUENCE*

The signal-specificity of TW-ELTLGEFL was tested by scrambling the sequence of the peptide. This should reduce the binding affinity and the inhibitory potential of the tweezer as the peptide does not match Survivin's surface anymore and cannot direct the tweezer specifically to Survivin's NES. The FoldX program (Buß et al., 2018) was used by Dr. Yasser B. Ruiz-Blanco and Dr. Joel Mieres-Perez (both Sánchez-García group, University of Duisburg-Essen) to predict the least favorable sequences for the NES region. All possible permutations of the peptide ELTLGEFL were docked onto Survivin's NES region. The resulting scores based on the relative stability with respect to the original peptide were assorted. The scrambled sequence was then selected taking the most important component of the NES, the leucine spacing, into account, which is the essential part of the NES consensus sequence. It is important to disrupt this spacing in order to hinder unspecific binding of the peptide to Survivin. Hence, the sequence LFEEGLLT was chosen, clicked to the tweezers and tested in ITC, NMR titration and pull-down experiments.

To assess the effect of the scrambled peptide tweezer on the Survivin/Crm1 interaction, pull-down experiments were performed. For this purpose, recombinant GST-Crm1 was used as bait for heterologous expressed HA-tagged Survivin$_{142}$ in 293T cell lysates, which had been pre-incubated with TW-ELTLGEFL or scrambled peptide TW-LFEEGLLT in concentrations ranging between 10 nM and 200 µM. Subsequent western blot analysis revealed that the inhibitory concentration of TW-LFEEGLLT was between 10–50 µM; compared to 1–10 µM for TW-ELTLGEFL (Figure 3-12). Hence, the scrambled peptide tweezer only reached the inhibitory level of the unmodified tweezer (section 3.1).
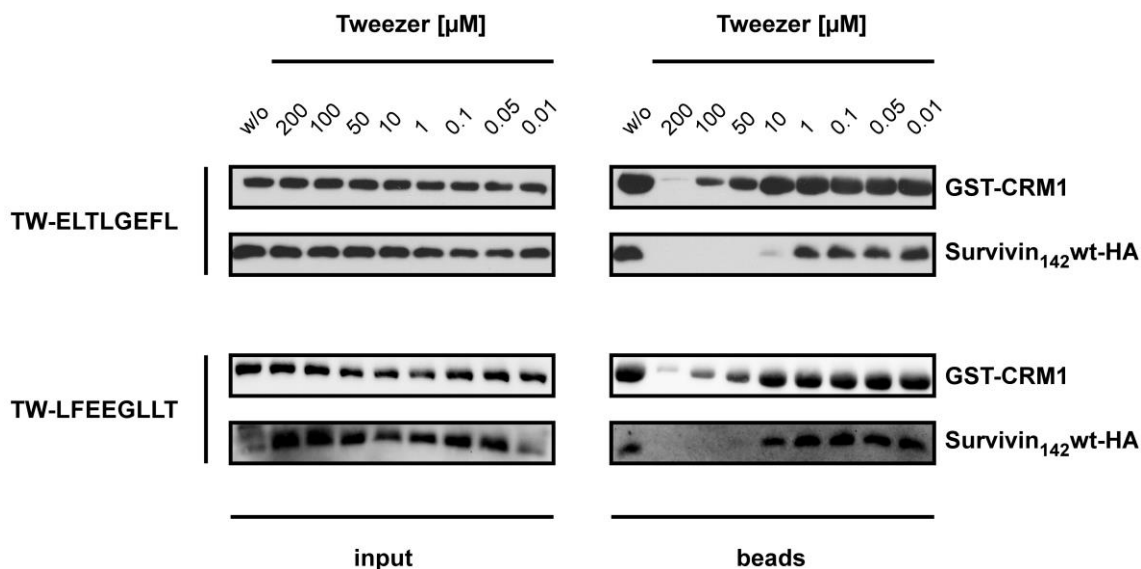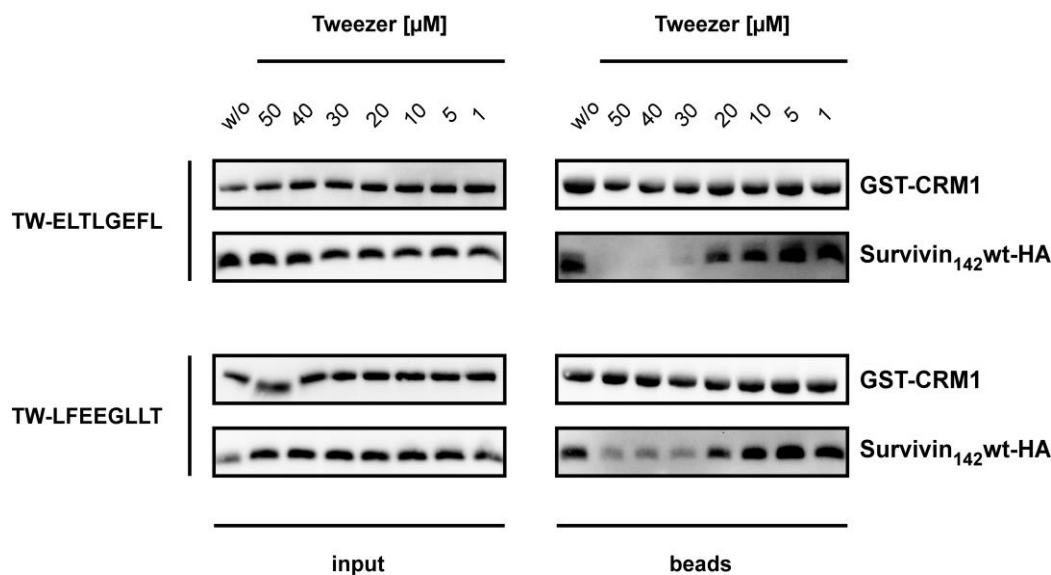
Figure 3-12: Scrambling of the peptide sequence reduces the inhibitory effect of the peptide tweezer.
293T cells were transfected with Survivin$_{142}$-HA. Respective lysates were pre-incubated with TW-ELTLGEFL (top) or scrambled peptide TW-LFEEGLLT at concentrations between 0.01 and 200 µM. GST-CRM1 bait protein was mixed with either non- or tweezer-incubated cell lysates, recombinant RanQ69L and dGTP to enable complex assembly. Protein complexes were pulled by GSH-Sepharose beads. Proteins in input and beads samples were analyzed via immunoblotting with antibodies specific for GST and HA. TW-ELTLGEFL was supplied by Dr. Christian Heid and TW-LFEEGLLT was synthesized by Inesa Hadrovic (both Schrader group, University of Duisburg-Essen). The pull-down experiment with TW-ELTLGEFL and subsequent western blotting was conducted by Dr. Sandra Bäcker (Knauer group, University of Duisburg-Essen).

To further pinpoint down the inhibitory concentrations of TW-ELTLGEFL and the scrambled peptide TW-LFEEGLLT, pull-downs with additional concentrations between 1 and 50 µM were performed simultaneously for both tweezers (Figure 3-13). While TW-ELTLGEFL inhibited the interaction between Survivin and Crm1 already at 20–30 µM, the protein complex was still detectable at 50 µM after incubation with the scrambled peptide tweezer. Therefore, the inhibitory effect of TW-ELTGEFL indeed seems to be based on the signal-specific recognition of the NES by the peptide sequence.

Figure 3-13: Scrambling of the peptide sequence deteriorated the inhibitory effect of the tweezer by half.
293T cells were transfected with Survivin$_{142}$-HA. Respective lysates were pre-incubated with TW-ELTLGEFL (top) or scrambled peptide TW-LFEEGLLT (bottom) at concentrations between 0.01 and 50 μM. GST-CRM1 bait protein was mixed with either non- or tweezer-incubated cell lysates, recombinant RanQ69L and dGTP to enable complex assembly. Protein complexes were pulled by GSH-Sepharose beads. Proteins in input and beads samples were analyzed via immunoblotting with antibodies specific for GST and HA. TW-ELTLGEFL inhibited the Survivin/Crm1 interaction efficiently at a concentration of 20-30 μM, whereas the scrambled peptide tweezer did not reach a comparable effect even at 50 μM. Tweezers were supplied by Inesa Hadrovic (Schrader group, University of Duisburg-Essen).

To quantitatively assess the interaction between Survivin$_{120}$ and the tweezer modified with the scrambled peptide sequence (LFEEGLLT), ITC experiments were performed. Titration of Survivin$_{120}$, both wildtype and K90/103T, to the scrambled peptide TW-LFEEGLLT revealed exothermic reactions (Figure 3-14). The data were fit to a single set of sites model with Origin and yielded binding affinities of 69 ± 23 μM for Survivin$_{120}$ WT and 55 ± 26 μM for Survivin$_{120}$ K90/103T. Both dissociation constants are lower than those of TW-ELTLGEFL binding to Survivin$_{120}$ WT (19 ± 3 μM) and Survivin$_{120}$ K90/103T (36 ± 10 μM). Therefore, scrambling the peptide sequence did indeed impair the binding affinity of the tweezer for Survivin$_{120}$.
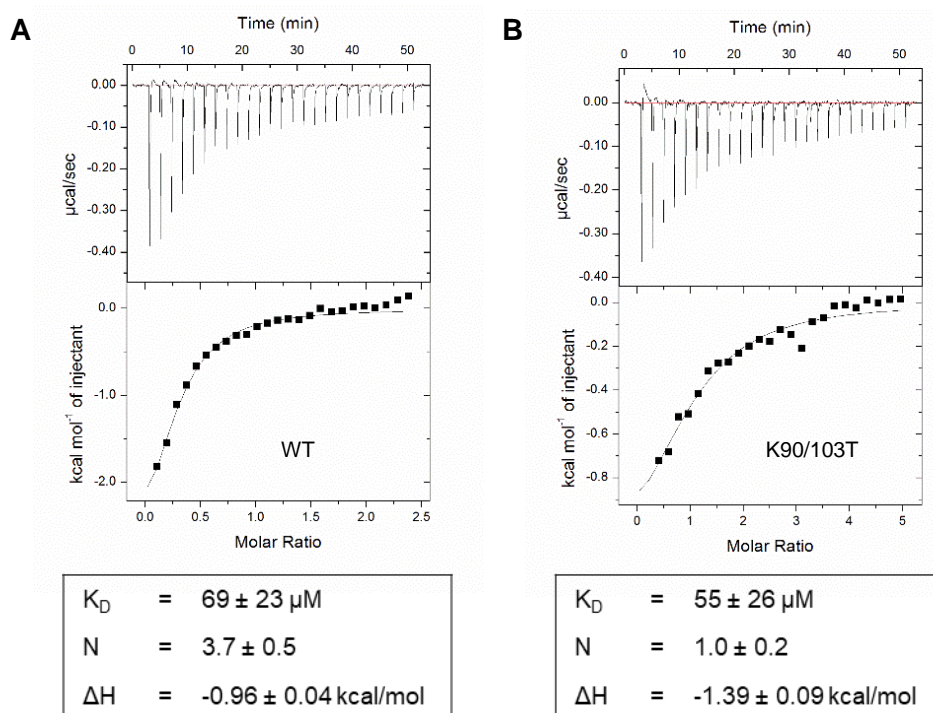
Figure 3-14: The scrambled peptide tweezer TW-LFEEGLLT binds to Survivin$_{120}$ WT and K90/103T with reduced affinity.

Titrations of 100 µM TW-LFEEGLLT in the cell with 1.2 mM Survivin$_{120}$ WT (A) or 2.5 mM Survivin$_{120}$ K90/103T (B) in the syringe. All titrations were performed in PBS, pH 7.4, at 25 °C. The heat of dilution was subtracted as constant, which was averaged from data points in the saturation region. Depicted is one representative ITC experiment per tweezer. The black lines in the bottom panels are the fit of the data to a *one set of sites* model. Values reported below are the mean ± s.e.m. of the fit. Experiments were performed in triplicates, however, only the curve with the lowest fitting error is depicted. K$_D$, dissociation constant; N, stoichiometry of binding; H, enthalpy. Tweezers were provided by Inesa Hadrovic (Schrader group, University of Duisburg-Essen).

Furthermore, binding of the scrambled peptide-tweezer (TW-LFEEGLLT) to Survivin$_{120}$ was assessed by NMR titrations (Figure A3). Chemical shift perturbations and relative signal intensities were plotted against the Survivin$_{120}$ amino acid sequence as before (Figure 3-15). The tweezer with the scrambled peptide sequence is still able to bind to the two basic patches K90/K91 and K103/R106 like the unmodified TW as indicated by the chemical shift perturbation and reduced intensities around the respective amino acids. However, strong chemical shift perturbations comparable to those revealed by TW-ELTL and TW-ELTLGEFL titrations were not observed inbetween the patches (aa 91–103) for TW-LFEEGLLT.
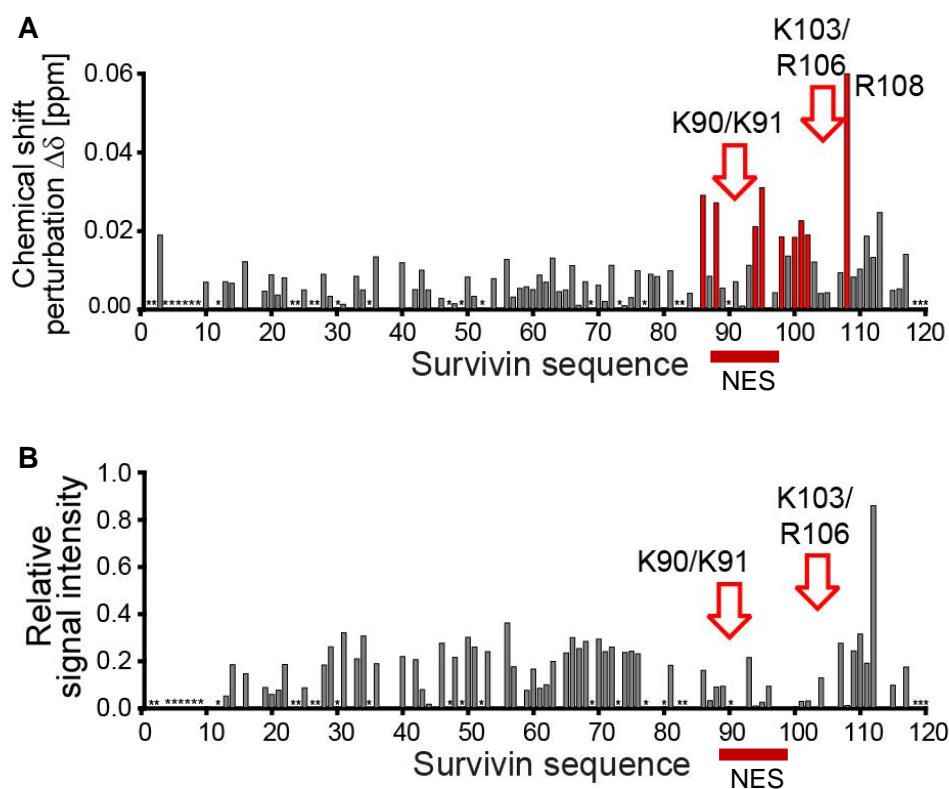
Figure 3-15: Few chemical shift perturbations indicate binding of TW-LFEEGLLT to Survivin.

NMR signal shift perturbations (A) and relative signals (B) of Survivin$_{120}$ in complex with one equivalent of TW-LFEEGLLT compared to free Survivin$_{120}$ were plotted against the amino acid sequence (residues 2–117). Signal shifts and normalized signals were identified for each signal. Prominent shift or reduced signal intensity mainly occurred for basic residues around Survivin's NES (red bar) and are marked with a red arrow. NMR titrations and subsequent analyses were performed by Dr. Christine Beuck (Bayer group, University of Duisburg-Essen).

3.1.4 ANALYSIS OF CELLULAR UPTAKE AND LOCALIZATION OF PEPTIDE TWEEZERS

To analyze the effects of the molecular tweezers on the Survivin/Crm1 interaction in a cellular environment, it is important to get insight into the exact localization of the tweezer molecules. The tweezers have to be able to enter cell nuclei in order to interfere with the nuclear export complex formation. To investigate the localization of the tweezers, HeLa Kyoto cells were incubated with FAM-labeled tweezers overnight and then stained with CellTracker DeepRed and Hoechst33342. Confocal laser scanning microscopy revealed the accumulation of FAM-labeled un-modified as well as the peptide-modified tweezers exclusively in vesicles in the cytoplasm (Figure 3-16).
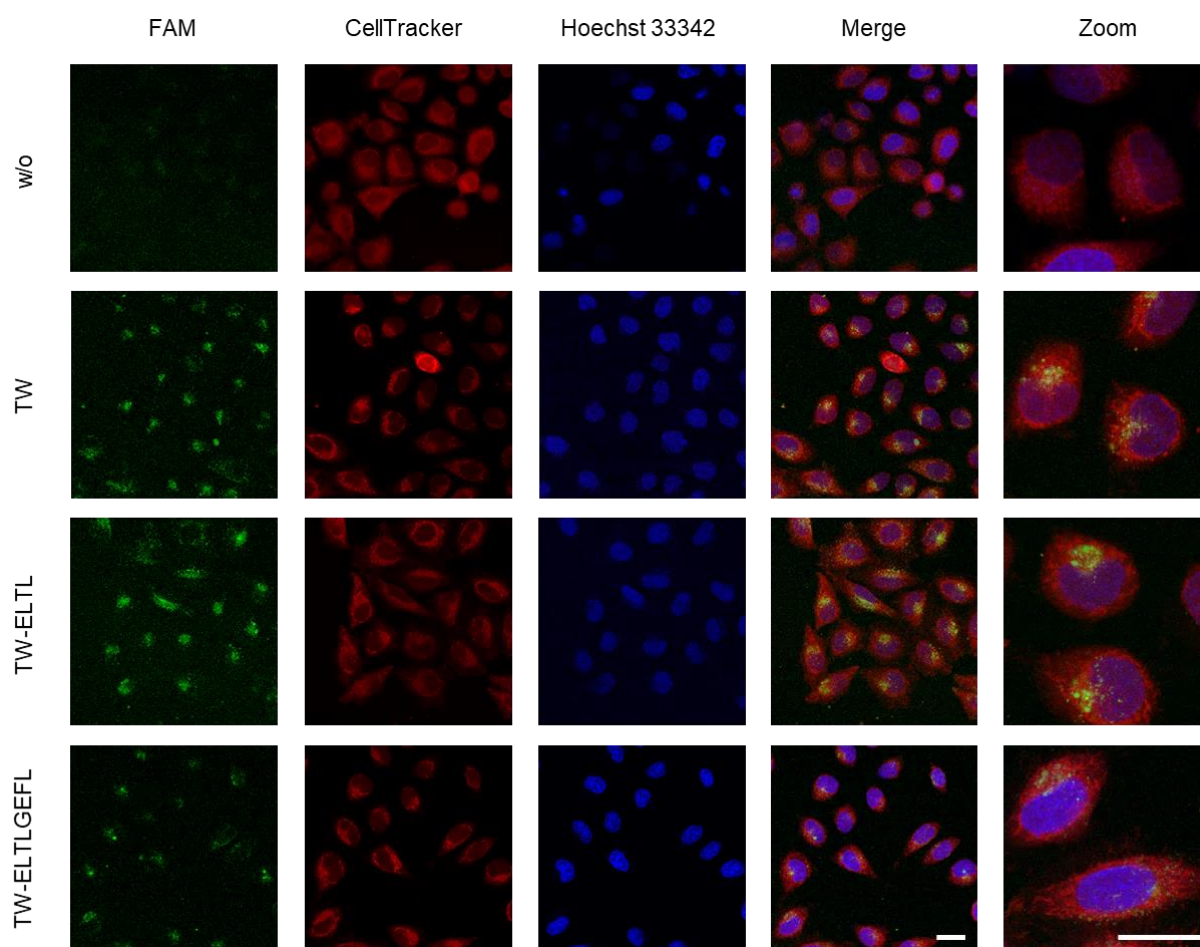
Figure 3-16: FAM-labeled tweezers localize in vesicles in HeLa Kyoto cells irrespective of peptide modification.

HeLa Kyoto cells were treated with 10 µM FAM-labeled tweezers for 20 h and then stained with 2.7 µM CellTracker™ Deep Red (red) and 10 µg/ml Hoechst33342 (blue). The images were taken with a Leica SP8 confocal laser scanning microscope (scale bar: 25 µm). Fluorescent tweezers were synthesized by Inesa Hadrovic (Schrader group, University of Duisburg-Essen).

To determine the localization of the molecules more precisely, further studies were performed with markers for the endosomal pathway. HeLa Kyoto cells were transfected with the early endosome antigen 1 (EEA1) fused to mCherry and 24 h later incubated with FAM-labeled peptide tweezers as well as with FAM-labeled sole peptide ELTL. After 30 min the fluorescent tweezers co-localized with EEA1 (Figure 3-17). The fluorescent peptide ELTL alone was not taken up by the cells and probably remained in the intracellular matrix. This suggests that the molecular tweezers enter the cell via the endosomal pathway, but do not seem to be able to enter the nucleus.
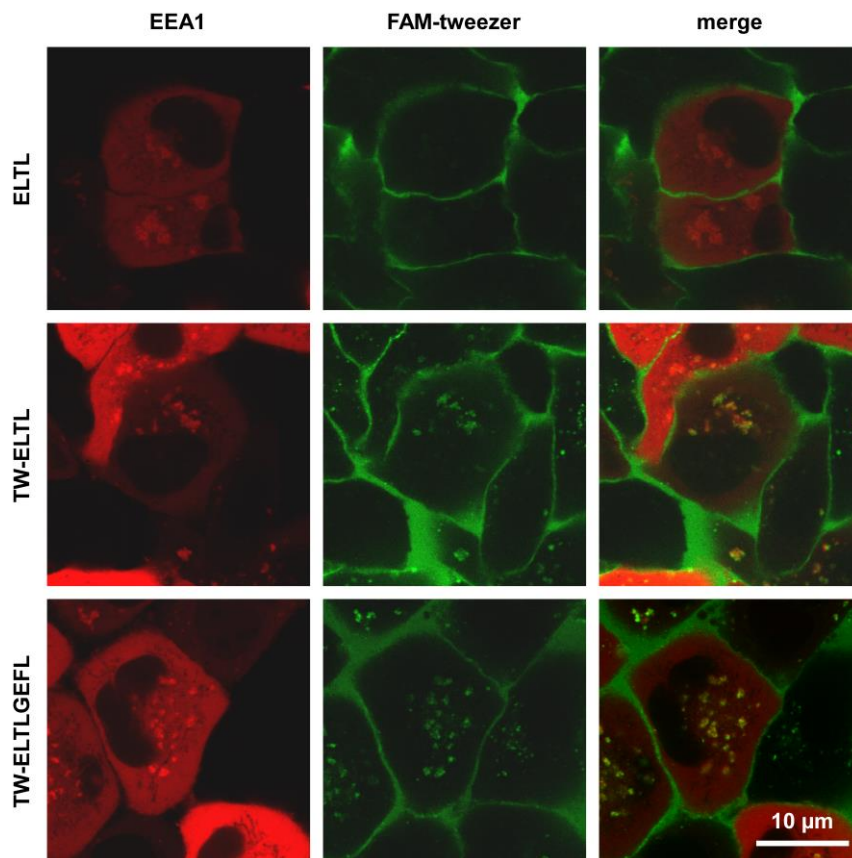
Figure 3-17: Fluorescent tweezers co-localize with early endosome antigen 1 after 30 min.

HeLa Kyoto cells were transfected with early endosome antigen 1 fused to mCherry (red). After 24 h, 10 µM FAM-labeled tweezers or peptide ELTL (both green) were added to the cells. Cells were imaged after 30 min with a Leica SP8 confocal laser scanning microscope. Fluorescent tweezers co-localized with the endosomal marker. Microscopy was performed by Dr. Cecilia Vallet (Knauer group, University of Duisburg-Essen) .

3.2 CHARACTERIZATION OF PRECISION OLIGOMER DOUBLE-TWEEZERS

Molecular tweezers have successfully been used to interfere with the Survivin/Crm1 interaction *in vitro* and the peptide modification via click chemistry has indeed increased their affinity as well as selectivity for the NES epitope. However, it might be even further enhanced for example by combining several tweezer units in specific distances in one macromolecule. This would enable to target several basic amino acids with the corresponding interspaces simultaneously and, thus, likely strengthen the interaction between the ligand and Survivin. For this purpose, three precision oligomers were developed together with the Hartmann group (Heinrich Heine University Düsseldorf) and the Schrader group (University of Duisburg-Essen). These macromolecules contain two tweezer units each, which are connected by oligomer linkers with different lengths. Hence, three different distances between the tweezer cavities are obtained. As Survivin possesses two basic patches (K90/91 and K103/R106) around its NES, it offers at least two anchor points for the tweezer-oligomer conjugates. Binding of the macromolecules to these patches simultaneously might shield Survivin's NES from interactions with the export receptor Crm1. Since the exact distance between the tweezer cavities in solution can hardly be predicted from the molecule structures, the three dTWs (Figure 3-18) were experimentally tested to identify the best oligomer length for targeting Survivin's NES. Binding of the macromolecules to Survivin was examined with ITC and NMR titrations and the ability to interfere with the Survivin/Crm1 interaction was assessed via pull-down assays.
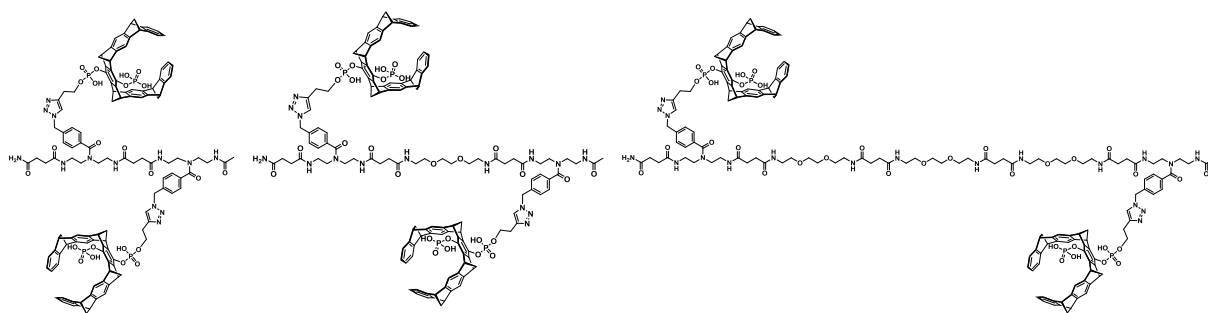
Figure 3-18: Oligomer dTW with different distances between the tweezer units were developed.

Three dTWs containing different amounts of oligomer block EDS as spacer, thus, creating different tweezer-tweezer distances, were developed. The images were provided by Inesa Hadrovic (Schrader group, University of Duisburg-Essen).

3.2.1 OLIGOMER DOUBLE-TWEEZERS BIND TO SURVIVIN

To investigate whether the oligomer dTWs are able to bind to Survivin, ITC was performed. The titration of Survivin$_{120}$ to the oligomer dTWs revealed exothermic reactions for each dTW (Figure 3-19). Furthermore, all oligomer dTWs showed a thermogram with at least two steps. Interestingly, these steps are more pronounced for the long and middle oligomer dTW than for the short oligomer dTW. The molar ratio required for saturation in each titration experiment (0.2–0.3 proteins per dTW) resembles the values observed in ITC titrations with the unmodified TW. Hence this indicates that several dTW molecules bind to the same protein. The oligomers were provided by Theresa Seiler (Hartmann group, Heinrich Heine University) and the tweezers were synthesized by Inesa Hadrovic (Schrader group, University of Duisburg-Essen).
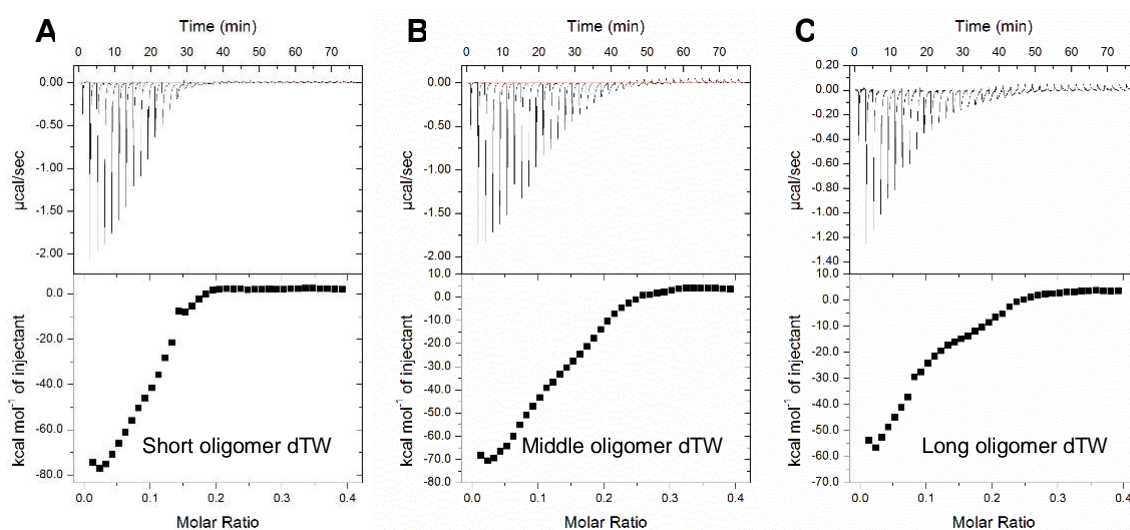
Figure 3-19: Oligomer dTWs bind to Survivin$_{120}$ with at least two binding events.
Titration of 400 µM Survivin$_{120}$ in the syringe to 200 µM of the short (A), middle (B) and long (C) oligomer dTW in the sample cell revealed exothermic binding reactions. The thermograms show at least two steps, which are more pronounced for the longer oligomer spacer. Unfortunately, no reasonable fit could be obtained with the available software. The oligomers were synthesized by Theresa Seiler (Hartmann group, Heinrich Heine University Düsseldorf) and clicked to the tweezers by Inesa Hadrovic (Schrader group, University of Duisburg-Essen).

Unfortunately, these ITC experiments could not be reasonably fit with the available software. Further, the interpretation is challenging, since there is no perfectly suitable binding model due to the complexity of the analyzed multivalent supramolecular system. The oligomer molecule consists of two tweezer units, which are able to bind one basic amino acid each. Additionally, Survivin contains several surface-exposed lysine and arginine residues that can be threaded into the tweezer's cavities. Besides, the protein occurs as a homodimer with a dimer interface overlapping with the NES. Hence, K90, K91, K103, and R106 of both protomers are lying in

close proximity, and not only the basic amino acids of one protomer can be targeted by the tweezer units, but also lysines or arginines of the complementary Survivin molecule might interact with the oligomer dTW. This makes it hard to fully understand the exact binding model of the dTWs to Survivin. Nevertheless, they revealed a biphasic thermogram, which is in accordance with a bivalent ligand such as the dTW.

3.2.2 OLIGOMER DOUBLE-TWEEZERS INFLUENCE THE SURVIVIN/CRM1 INTERACTION

Next, the influence of the oligomer dTWs on the Survivin/Crm1 interaction was investigated. Binding of the tweezers to K90/91 and K103 or R106 in and near Survivin's NES should impair the Crm1 interaction if the NES region is blocked by the dTWs. To test this, pull-down assays with 293T cell lysates containing HA-tagged $Survivin_{142}$ and increasing concentrations of oligomer dTWs between 10 nM and 50 µM were performed. $Survivin_{142}$-HA was pulled by GST-Crm1 using GSH-coated Sepharose 4B beads. Survivin and Crm1 were then detected via Western Blot in input and bead samples using specific antibodies against the HA- and GST-tags (Figure 3-20).

Indeed, the amount of detected $Survivin_{142}$-HA decreased with increasing tweezer concentrations for all oligomer dTWs. This indicates that the interaction between Survivin and Crm1 is inhibited in a concentration-dependent manner. For the short and middle oligomer dTWs the effective concentration was determined to be between 1–5 µM, while $Survivin_{142}$-HA was still detectable at concentrations of up to 25 µM. Thus, the longest oligomer dTW requires a 5–10 fold higher amount than the short and middle oligomer dTWs for comparable inhibition. Importantly, the inhibitory concentrations of the short and middle oligomer dTWs were much lower compared to the unmodified tweezer (10–50 µM; Figure 3-6).
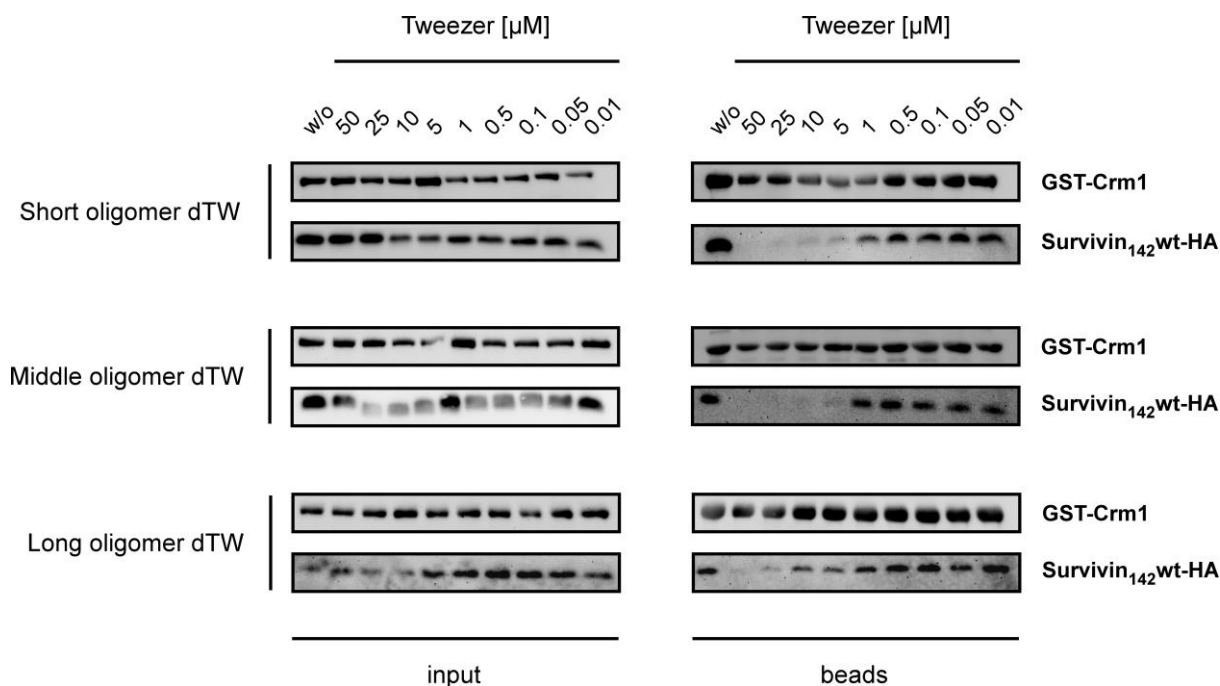
Figure 3-20: Oligomer dTWs influence the Survivin/Crm1 interaction in a concentration-dependent manner. 293T cells were transfected with Survivin$_{142}$-HA. Respective lysates were pre-incubated with short (top), middle (center) and long oligomer dTW (bottom) at concentrations between 0.01 and 50 µM. GST-Crm1 was mixed with either non- or tweezer-incubated cell lysates, with recombinant RanQ69L and dGTP to enable complex assembly. Protein complexes were pulled by GSH-Sepharose beads. Proteins in input and beads samples were analyzed via immunoblotting with antibodies specific for GST and HA. The Survivin/Crm1 interaction is impaired upon dTW concentrations between 1–25 µM. The oligomers were synthesized by Theresa Seiler (Hartmann group, Heinrich Heine University Düsseldorf) and clicked to the tweezers by Inesa Hadrovic (Schrader group, University of Duisburg-Essen).

3.2.3 ANALYSIS OF OLIGOMER DOUBLE-TWEEZER BINDING TO SURVIVIN$_{120}$ BY NMR TITRATION EXPERIMENTS

Binding of the oligomer dTWs to Survivin$_{120}$ has been observed in ITC experiments. However, NMR titrations of the short oligomer dTW to ^{15}N-labeled Survivin$_{120}$ WT and subsequent analysis were performed by Dr. Christine Beuck (Bayer group, University of Duisburg-Essen) to map tweezer binding to distinct amino acids as previously done for the peptide-modified tweezers (section 3.1.1), and therefore, to get more insights into the binding mode. For this, ^{1}H-^{15}N-BEST-TROSY-HSQC NMR spectra of 938 µM ^{15}N-labeled Survivin$_{120}$ were measured either without tweezer or with 500 µM and 750 µM short oligomer dTW (Figure A4). Afterwards, signal shifts and relative signal intensities were plotted against the Survivin$_{120}$ protein sequence. Since prominent shifts and reduced signal intensities for certain amino acids usually

indicate binding to that region, putative binding sites of the tweezer might be mapped from this experiment (Williamson, 2013). However, only marginal chemical shift perturbations could be observed after titration of the short oligomer dTW (Figure 3-21). For comparison, a dashed line representing the mean shift values after titration of the unmodified tweezer as shown previously (Bäcker, 2018) was added to the figure. Only shift perturbations above this line are considered as significant in this work. Unfortunately, only one amino acid (R108) showed a prominent shift perturbation upon titration of 500 µM short oligomer double-tweezer. It is important to note that in the 1H-15N-BEST-TROSY-HSQC spectrum (Figure A4) several signals around R108 are in very close proximity and could not be separated clearly, probably causing the only observed shift. Upon titration of 750 µM short oligomer dTW, neither of the amino acids showed a shift perturbation higher than the reference line obtained from titrations with TW.
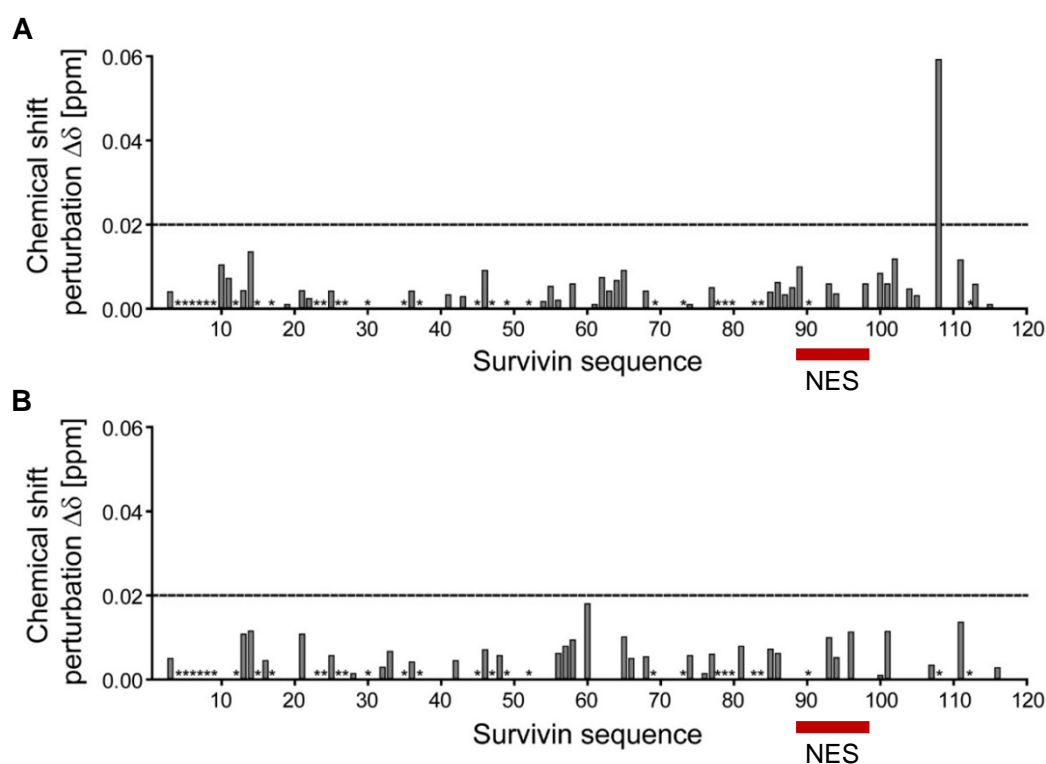
Figure 3-21: Chemical shift analysis does not identify a distinct binding site on Survivin$_{120}$.
NMR signal shift perturbations upon titration of 500 µM (A) and 750 µM (B) short oligomer dTW to ^{15}N-labeled Survivin$_{120}$ compared to Survivin$_{120}$ without tweezer were plotted against the amino acid sequence (aa 2-117). Amino acids labeled with a star could not be assigned. The NES region is highlighted by a red bar. The dashed line represents the mean shift value observed upon titration with the unmodified tweezer first shown in Bäcker (2018). Prominent shifts above the dashed line were not observed except for R108. The purification of ^{15}N-labeled Survivin$_{120}$, NMR measurements and subsequent analysis were conducted by Dr. Christine Beuck (Bayer group, University of Duisburg-Essen).

In addition to the signal shifts, relative intensities were plotted against the Survivin$_{120}$ WT sequence. Upon titration of 500 µM short oligomer dTW (Figure 3-22 A), lysines 91 and 103 as well as arginine 106 showed slightly reduced signal intensities, indicating tweezer binding to these amino acids. However, after the addition of 750 µM tweezer (Figure 3-22 B), all signal intensities for every assigned amino acid decreased strongly to approx. 20 % of the original intensity. Hence, reduced intensities in a distinct protein region as for the peptide tweezers (section 3.1.1) were not observed and an exact binding site could not be mapped. Furthermore, the overall reduction of the signal intensity indicated aggregation of Survivin$_{120}$.
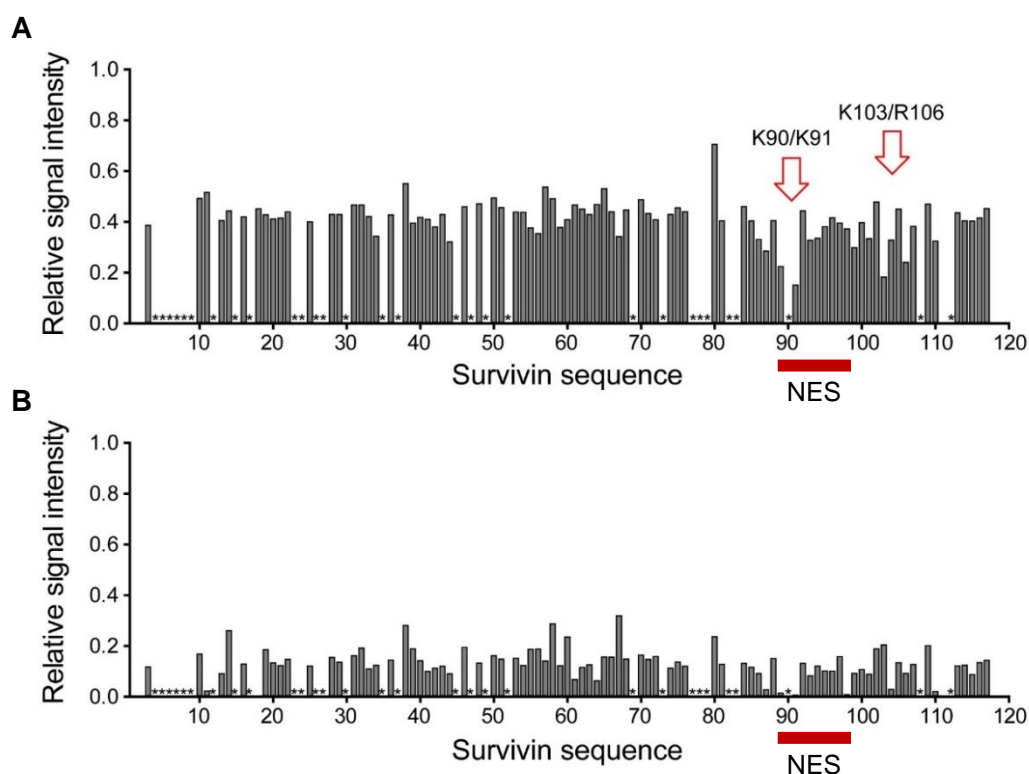
Figure 3-22: Reduced signal intensities indicate aggregation of Survivin$_{120}$ upon titration of the short oligomer dTW titration.

Relative NMR signal intensities of Survivin$_{120}$ upon titration of 500 µM (A) and 750 µM (B) short oligomer double-tweezer compared to Survivin without tweezer were plotted against the amino acid sequence (aa 2-117). Amino acids labeled with a star could not be assigned. The NES region is highlighted by a red bar. Titration of 500 µM tweezer slightly reduced the signal intensities of lysines 90, 103 and arginine 106. However, the addition of more tweezers resulted in a decrease in the overall signal intensity. The purification of ^{15}N-labeled Survivin$_{120}$, NMR measurements and subsequent analysis were conducted by Dr. Christine Beuck (Bayer group, University of Duisburg-Essen).

3.3 CHARACTERIZATION OF ULTRA-SMALL GOLD NANOPARTICLES EQUIPPED WITH TWEEZERS

Ultra-small gold nanoparticles with diameters of 1–2 nm are smaller than most proteins and can be covalently modified with recognition units, e.g. artificial receptors for single amino acids such as the molecular tweezer, via click chemistry (Kopp et al., 2017; van der Meer, 2020). As they are able to cross cell membranes and even enter the cell nuclei (van der Meer et al., 2019), they might facilitate cellular uptake of molecules that otherwise cannot escape the endosomal pathway like the molecular tweezer. The particle surface might serve as scaffold for the combination of several amino acid binders, thereby leading to a higher local concentration of binders due to the fixation on the nanoparticle surface (van der Meer et al., 2019). This increases the avidity to target a protein and, thus, might strengthen the binding.

Ultra-small gold nanoparticles were synthesized and covalently modified with molecular tweezers by Dr. Selina van der Meer (Epple group, University of Duisburg-Essen) (Figure 3-23 A). First of all, the integrity of the tweezers and their ability to bind to proteins was tested via ITC. The titration of Survivin$_{120}$ to tweezer-conjugated nanoparticles resulted in an exothermic reaction (Figure 3-23 C), which was fit with the simple model stoichiometric approach with the software AFFINImeter (Figure 3-23 D). A binding affinity of 8 ± 1 µM with a fixed 1:1 stoichiometry of protein to tweezer was determined. In contrast, the unmodified tweezer had produced an affinity of 38.3 ± 4.3 µM (section 3.1.1). A control experiment with azide-terminated nanoparticles, thus particles without recognition units for amino acid, did not produce comparable exothermic peaks (Figure 3-23 B) and only showed dilution effects. Therefore, an unspecific binding of the protein to the nanoparticles could be excluded.
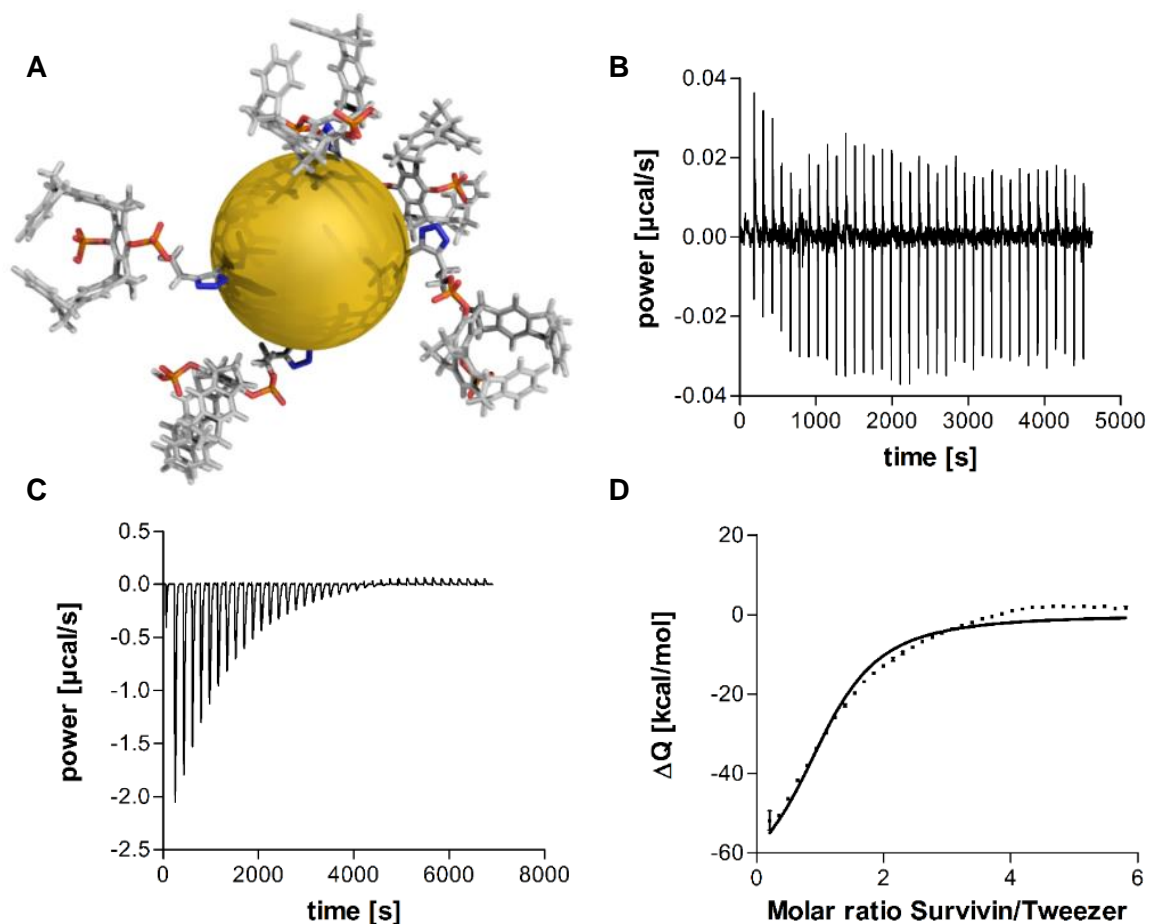
Figure 3-23: Tweezer-conjugated ultra-small gold nanoparticles bind to Survivin$_{120}$.

A) Schematic representation of the tweezer-modified gold nanoparticle. The image was provided by Dr. Selina van der Meer (Epple group, University of Duisburg-Essen). B) Processed heating power over time from ITC titration of 1.2 mM Survivin$_{120}$ to azide-terminated gold nanoparticles (Au-N3; control; c(Au) = 170 µg/ml). C) Processed heating power over time from Survivin$_{120}$ titration (1.2 mM) to tweezer-conjugated gold nanoparticles (c(Au) = 170 µg/ml; c(TW) = 30 µM). D) Integrated energy values over the molar ratio of protein and tweezer. The data were processed and fit using the simple model stoichiometric approach with the software AFFINImeter. Gold nanoparticles were synthesized and modified with tweezers by Dr. Selina van der Meer. The tweezers for the conjugation to the nanoparticles were provided by Inesa Hadrovic (Schrader group, University of Duisburg-Essen).

4 DISCUSSION

As Survivin is usually absent in normal resting tissues, but highly overexpressed in various tumor cells, it is a very cancer-specific protein (Ambrosini et al., 1997; Adida et al., 1998; Adida et al., 2000). Survivin's prevalence in cancer cells is associated with resistance against chemo- and radiotherapy and poor clinical prognosis (Adida et al., 2000; Capalbo et al., 2007). It fulfills a dual role as an inhibitor of apoptosis and mitotic effector, which is mediated via its NES interacting with the export receptor Crm1 (Knauer et al., 2007; Raetz et al., 2014). Unfortunately, Survivin is hard to target as it has no enzymatic activity nor deep pockets, which could be addressed by small molecules (Wheatley and Altieri, 2019). So far, therapeutic approaches mainly include antisense oligonucleotides or molecules that reduce the expression levels of Survivin as well as novel compounds, which target Survivin's dimerization, but none of these has yet reached the clinic (Wheatley and Altieri, 2019).

As part of the collaborative research center "Supramolecular Chemistry on Proteins" (CRC1093), this thesis focusses on developing and characterizing supramolecular ligands, which bind to Survivin's surface and thereby interfere with the cancer-relevant interaction with Crm1. In collaboration with the groups of Prof. Dr. Thomas Schrader, Prof. Dr. Matthias Epple (both University of Duisburg-Essen) and Prof. Dr. Laura Hartmann (Heinrich Heine University Düsseldorf), several supramolecular ligands were developed. All ligands contained the basic molecular tweezer, which is a selective binder for lysine and arginine residues and, hence, well suited to target protein epitopes and modulate their PPIs (Fokkens et al., 2005; Bier et al., 2013).

Survivin possesses two basic patches (K90/91 and K103/R106) in and near its NES, which can be addressed by the tweezers. Together with the Schrader group, molecules that contain a peptide sequence (ELTLGEFL) mimicking the dimer interface of Survivin (aa 95–102) were developed and assessed with regard to their binding properties and influence on the Survivin/Crm1 interaction (section 3.1). The peptide and linker that connects the tweezer with the peptide motif were chosen in order to anchor the tweezer at lysine 103 and enable binding of the peptide to the dimer interface of Survivin. Furthermore, precision macromolecules based on oligomeric structures containing two tweezer units were developed together with the Hartmann group. The ability of these ligands to target both basic patches surrounding Survivin's NES and to interfere with the Crm1 interaction was assessed (section 3.2). Last, ultra-small gold nanoparticles were equipped with tweezers. As they might facilitate cellular

uptake of tweezer ligands in the future, binding of the modified nanoparticles to Survivin was analyzed (section 3.3).

4.1 ASSESSMENT OF PEPTIDE-MODIFIED TWEEZERS

The peptide-modified tweezers TW-ELTL and TW-ELTLGEFL were designed to specifically target Survivin's NES sequence. For this purpose, the peptide sequences ELTL and ELTLGEFL were selected from Survivin's dimer interface (aa 95–98), which partly overlaps with the NES (aa 89–98). The interaction between Survivin and the export receptor Crm1 is pivotal for Survivin's mitotic as well as anti-apoptotic functions and mediated via its NES (Knauer et al., 2007). Shielding this important surface region with supramolecular tweezers would therefore interfere with the Crm1 interaction and thereby with Survivin's dual role. First evidence that these peptide-modified tweezers bind to Survivin's NES and inhibit the interaction with Crm1 was previously obtained (Bäcker, 2018; Heid, 2018). However, the question whether the peptide tweezers possess regioselectivity and signal-specificity for Survivin's NES remained unresolved and was addressed in this thesis.

4.1.1 PEPTIDE-MODIFICATION OF THE TWEEZER ENHANCES ITS AFFINITY AND INHIBITORY POTENTIAL FOR THE SURVIVIN/CRM1 INTERACTION

Binding of the unmodified TW, as well as peptide-modified TW-ELTL and TW-ELTLGEFL to Survivin was first analyzed via ITC titrations (section 3.1.1). Previously, ITC thermograms were fit to a one-to-one binding model with the software AFFINImeter (Bäcker, 2018). This model assumes that each tweezer binds to Survivin in a one to one ratio. In case of the peptide-modified tweezers this might be feasible but in case of the unmodified tweezer, which is certainly specific for lysine and arginine residues but other than that does not contain an additional protein-specific motif, the model seemed to be insufficient. Therefore, ITC thermograms were fit with a *one set of sites* model with the software Origin. This model assumes n-different binding sites, which all possess the same affinity. Thereby, the number of binding sites (n) is fit. Using this model, K_D values were determined to be approx. 38 µM for TW, 24 µM for TW-ELTL and 19 µM for TW-ELTLGEFL. Hence, the binding affinities for all tweezers and Survivin$_{120}$ WT are in the same order of magnitude, correlating well with the binding affinities observed for the phosphate tweezer binding to lysine of ~15 µM and ~34 µM for arginine (Dutt et al., 2013). Nevertheless, TW-ELTLGEFL showed the lowest dissociation constant and, in turn, appears to bind to Survivin most strongly. More strikingly, big differences

could be observed between the stoichiometries of the unmodified and the peptide-modified tweezers. TW revealed a stoichiometry of approx. 20 tweezers per protein, while TW-ELTL and TW-ELTLGEFL produced a stoichiometry of approx. 2 tweezers per Survivin$_{120}$ molecule. Therefore, the peptide-modification slightly enhanced the binding affinity and, moreover, had a strong influence on the selectivity of the tweezers as a multitude of former binding sites is not targeted by the peptide tweezers anymore.

To identify the binding site of the elongated TW-ELTLGEFL, an NMR titration was performed by adding up to equimolar amounts of TW-ELTLGEFL to ^{15}N-labeled Survivin$_{120}$. Binding of a ligand to a protein induces changes in the chemical environment of the residues close to the binding site, which cause chemical shift perturbations and intensity changes at the residues involved (Williamson, 2013). This method had been applied previously to map binding of TW and TW-ELTL to Survivin$_{120}$'s surface and suggested the basic amino acids K90, K91, K103, and R106 as putative binding sites for the molecular tweezers (Bäcker, 2018). Similar to the NMR titration experiment with TW-ELTL, titration of TW-ELTLGEFL to Survivin$_{120}$ led to signal shifts and reduced signal intensities around the same basic amino acids as TW and resulted in additional shifts and intensity loss in the region between the two basic patches K90/91 and K103/R106, which did not occur upon titration of TW. This indicates that the peptides ELTL as well as ELTLGEFL contact the whole NES region and, thereby, might have the potential to shield it against interactions with Crm1. In addition to that, these results correlate well with the initial design idea of the molecular tweezers, selecting the peptide sequence in order to mimic the dimer interface and, thus, facilitate binding of the tweezer to the NES.

Furthermore, the interaction between the peptide-modified tweezers and Survivin$_{120}$ was assessed with MD and QM/MM simulations. QM/MM calculations with four surface accessible lysines on the Survivin protomer identified K103 as an ideal anchor residue for TW-ELTL. Additional simulations with TW-ELTL and TW-ELTLGEFL on the Survivin$_{120}$ protomer revealed that the peptide-modified tweezers bind to Survivin's surface via several interactions. While the tweezer cavity encapsulates the anchor residue K103, the peptide interacts with the ^{95}ELTL^{98} sequence, or rather with the whole NES region on the protein. Additionally, a salt bridge between the phosphate tweezer and R106 stabilizes the peptide tweezer on the protein. Hence, additional interactions between the peptide and the Survivin protomer surface complement binding of the tweezer cavity to K103. These computational results are in very good agreement with the experimental results obtained in NMR titrations. Here, four basic amino acids showed prominent shifts and reduced intensities upon titration of TW-ELTL and TW-ELTLGEFL, namely K90, K91, K103, and R106. These findings can now be explained by

the binding mode suggested from the simulations. While the peptide interacts with the NES region, hence, resulting in shifts and intensity changes at the exact region, R106 stabilizes the tweezer and, thus, also causes changes in the NMR spectrum.

However, one big discrepancy between the NMR titrations and the computational work remains. In solution, e.g. for NMR experiments, Survivin$_{120}$ occurs as a homodimer (Chantalat et al., 2000; Verdecia et al., 2000). In contrast, a Survivin protomer derived from the dimeric structure (PDB ID: 1XOX) was used for the simulations. As previous gel filtration experiments did not necessarily indicate a disruption of the dimerization upon tweezer incubation (Bäcker, 2018) and, additionally, no evidence for such an effect was observed in NMR titrations, the question arose whether the peptide-modified tweezers may access the NES despite an intact dimer. Therefore, GaMD simulations with the dimer interface were performed to assess its flexibility. The frequency of hydrogen bond formation between the fragments ^{95}ELTL^{98} within the dimer interface of both protomers was analyzed. Indeed, this part of the dimer interface rather seems to be very flexible as most of the time no or only one hydrogen bond was formed. Regarding these simulations, one could conclude that the dimer interface might be flexible enough at this position (aa 95–98) to allow tweezer binding. However, the dimer interface consists of several additional amino acids. The PDBePISA (Proteins, Interfaces, Structures and Assemblies) tool (Krissinel and Henrick, 2007) predicts an involvement of 15 amino acids in the dimer interface of Survivin$_{120}$ (PDB ID: 1XOX). Hence, it seems to be unlikely that the interaction between the peptide-modified tweezer, even the elongated TW-ELTLGEFL, and the Survivin surface is sufficient to completely disrupt the dimerization. More likely, the tweezer, which is anchored to K103 right next to the NES, fits into the flexible dimer interface and the direct interaction between its peptide motif and Survivin's NES locks it at this position, where it remains even when Crm1 opens the interface and attempts to bind to the NES.

Since the peptide-modified tweezers were designed in order to shield Survivin's NES and NMR titration experiments as well as MD simulations substantiated this epitope as their binding site, the tweezers should be able to impair the Survivin/Crm1 interaction. To analyze the effect of the peptide-modified tweezers on this PPI, pull-down, and fluorescence anisotropy experiments were performed (section 3.1.2). Previously, the unmodified as well as both peptide-modified tweezers had already shown inhibitory potential for the Survivin/Crm1 interaction in pull-down assays (Bäcker, 2018). However, only TW and TW-ELTL were analyzed in a concentration-dependent manner. Recombinant GST-Crm1 was used as bait for heterologously expressed HA-tagged Survivin$_{142}$ in 293T cell lysates, which had been prior incubated with TW or TW-ELTL in concentrations ranging between 10 nM and 200 µM. For

both tweezers, a concentration-dependent inhibition was observed that revealed an inhibitory concentration of 10–50 µM, respectively (Bäcker, 2018). In this thesis, TW-ELTLGEFL showed a concentration-dependent interference with the Survivin/Crm1 interaction in pull-down experiments similar to the unmodified and short peptide tweezers. Importantly, a lower inhibitory concentration of 1–10 µM was required for TW-ELTLGEFL to achieve a similar inhibitory effect than the previously tested tweezers (Bäcker, 2018) and, therefore, the elongated peptide tweezer seemed to be the most potent inhibitor tested for the Survivin/Crm1 interaction.

In addition to the pull-down experiments, a more quantitative fluorescence anisotropy assay was established to assess the effects of tweezers on the Survivin/Crm1 interaction. To efficiently bind to Survivin's NES, Crm1 requires binding of RanGTP, which opens the NES cleft of Crm1 (Koyama and Matsuura, 2010). As the tripartite complex of Survivin, Crm1 and RanGTP, makes an evaluation of the measured signal rather complicated, a Ran-independent Crm1 mutant ($Crm1_{1062}VLV430AAA$/ $Crm1_{mut}$) with high affinity for NESs was used in this assay (Fox et al., 2011). This mutant enables binding to Survivin irrespective of RanGTP. To investigate the effects of the peptide-modified tweezers on the $Survivin/Crm1_{mut}$ interaction, the two proteins were pre-incubated and then titrated with increasing amounts of the respective tweezer. The unmodified as well as both peptide-modified tweezers resulted in decreasing anisotropy signals, which indicates that the protein complex is impaired and dissociates due to the tweezers. IC50 values were determined to be approx. 53 µM for TW, 39 µM for Tw-ELTL and 12 µM for TW-ELTLGEFL, respectively. Thus, less TW-ELTLGEFL is required to inhibit the $Survivin/Crm1_{mut}$ interaction. Of note, the fluorescence anisotropy assay could be performed only once due to the extremely low expression yield of $Crm1_{mut}$, which needs to be further improved.

To sum, pull-down and anisotropy assays both show that the modification of the molecular tweezer with an elongated peptide indeed enhanced the inhibitory effect of the tweezer for the Survivin/Crm1 interaction.

4.1.2 PEPTIDE-MODIFIED TWEEZERS BIND REGIOSELECTIVE AND SIGNAL-SPECIFIC TO SURVIVIN

The binding site of the peptide-modified tweezers (TW-ELTL/ TW-ELTLGEFL) was mapped to Survivin's NES region by NMR titration experiments, and was narrowed down to K90, K91, K103 and R106 in particular (Figure 3-3). These findings were supported by several QM/MM and GaMD simulations. To further experimentally confirm this binding site, $Survivin_{120}$ double and triple mutants with substitutions of the respective amino acids to alanine, serine or threonine were generated (section 3.1.3.1). If the peptide-modified tweezers indeed bind to these lysines or arginines flanking the NES, their mutation should abolish the previously observed effects and prove the regioselectivity of the tweezers. The binding affinity should be reduced for these mutants and inhibitory effects of the tweezers on the Survivin/Crm1 interaction should be impaired. To get reliable results in binding studies and experiments assessing the interaction between the Survivin mutants and Crm1, the correct folding of the mutants should be confirmed. ^{1}D ^{1}H NMR spectroscopy can be used as a preselective screening method to verify the folded state of proteins (Page et al., 2005). The correct folding was examined in the region of 6–10 ppm, resulting from amides and aromatics, and below 1 ppm obtained from methyl groups (McDonald and Phillips, 1967). While the spectrum of $Survivin_{120}$ WT exhibited a wide signal dispersion in the amide/aromatic range and distinct methyl signals with sharp and narrow signals, most mutants showed less but broadened peaks. The NMR signals reflect the local environment of each amino acid, and in the folded state, they have different environments because of secondary and tertiary structure elements (McDonald and Phillips, 1967). In the unfolded state, however, all amino acids have similar environments and, thus, show less and broad peaks in the ^{1}D ^{1}H NMR spectrum. Unfortunately, most mutants turned out to be unfolded, but mutant K90/103T was folded correctly, and used for further binding studies with the tweezers.

First, fluorescence anisotropy titrations revealed much lower binding affinities of the $Survivin_{120}$ K90/103T mutant to fluorescent unmodified or peptide-conjugated tweezers compared to wildtype with up to 18-fold higher dissociation constants. However, the exact K_D values for the tweezers determined by fluorescence anisotropy, especially for the unmodified tweezer, need to be treated with caution since the binding model used to fit the data assumes a one to one stoichiometry. For the peptide-modified tweezers (TW-ELTL and TW-ELTLGEFL), this stoichiometry seems to be in the right order of magnitude, which was also evidenced by NMR titrations, as only one surface area (K90-R106) showed decreased intensities as well as prominent shifts, and, further supported by ITC titrations with $Survivin_{120}$ wildtype, which revealed stoichiometries of approx. 2. However, for the unmodified tweezer the stoichiometry

was much higher in ITC titrations (~21) and, thus, the used binding model to fit the fluorescence anisotropy data does not reflect the real system.

To further strengthen the findings from fluorescence anisotropy experiments, ITC titrations were performed with Survivin$_{120}$ K90/103T. Titrations of the mutant to the tweezers resulted in higher dissociation constants compared to Survivin$_{120}$ WT for all tweezers. Thus, binding of the tweezers to the mutant appears to be weaker than to wildtype Survivin, which is in good agreement with the fluorescence anisotropy experiments as well as with the idea that depletion of the anchor residues for the tweezer will weaken the interaction. However, all tweezers, even the peptide-modified ones, were still able to bind to Survivin$_{120}$, which can be explained with the additional basic amino acids around Survivin's NES which could not be substituted, K91 and R106. Thus, these amino acids potentially are still able to anchor the tweezer to Survivin's surface. Unfortunately, all triple mutants generated so far, were either not stable or folded correctly and, thus, a mutant lacking all possible anchor residues in and near Survivin's NES could not be obtained. The stoichiometry of the peptide-modified tweezers and Survivin$_{120}$ WT was approx. 2 tweezers per protein, while the K90/103T mutant produced a stoichiometry of approx. one. Indeed, two orientations of the peptide-tweezer are conceivable, if the tweezer occupies K90/K91 and K103. In fact, K91 was identified as the second best anchor residue from QM/MM calculations. Therefore, it might be possible that the peptide-tweezer binds in two orientations to Survivin$_{120}$ WT and only in one direction to Survivin$_{120}$ K90/103T as suggested by the stoichiometries obtained from ITC experiments. Taken together, fluorescence anisotropy and ITC experiments both showed that the affinity of the tweezers to Survivin is indeed reduced upon substitutions of the anchor lysines. This strongly supports the binding site identified by NMR titrations and, thus, the regioselectivity of the peptide-modified tweezers.

Next, pull-down experiments with the unmodified and peptide-conjugated tweezers and Survivin$_{120}$ WT as well as K90/103T were performed to further emphasize the importance of the lysines for effective tweezer binding and, therefore, for the inhibition of the Survivin/Crm1 interaction. As expected, all tweezers had an inhibitory effect on the interaction between Crm1 and wildtype Survivin. By contrast, the tweezers had only little impact on the Crm1/Survivin K90/103T interaction. Hence, the inhibition of the complex formation between Survivin and Crm1 is compromised upon mutation of the lysines. Interestingly, unconjugated peptides did not inhibit the Survivin/ Crm1 interaction for neither wildtype nor mutant. Taken together, this also means that the inhibition, observed in previous pull-down and fluorescence anisotropy assays, was indeed due to regioselective binding of the peptide-modified tweezer to anchor

lysines near Survivin's NES, enabling the contact of the tweezer's peptide with the NES region and, thus, blocking Crm1. Notably, the same experiment was previously performed with the Survivin$_{120}$ K90/91/103S mutant and revealed the same effect (Bäcker, 2018), however, since the triple mutant was not folded correctly, those results remained arguable until now.

Regarding the specificity of the peptide-modified tweezers, the question arose whether the peptide binds signal-specific to the tweezer or if the stronger inhibition observed in fluorescence anisotropy and pull-down assays is caused due to simple unspecific, sterical blocking of the NES by the peptide. First evidence that the peptide ELTLGEFL is essentially involved in tweezer binding and shielding of the NES was obtained by ITC experiments. Indeed, higher affinities were revealed for the peptide-modified tweezers indicating an involvement of the peptide, which was supported by the MD simulations that showed frequent contacts between the attached peptides and the protein surface. Nevertheless, to experimentally prove the signal-specificity, the peptide was scrambled and clicked to the tweezer. This should reduce the binding affinity and the inhibitory potential of the tweezer as the peptide does not match Survivin's surface anymore and cannot shield the NES. The FoldX program (Buß et al., 2018) was used to predict the least favorable sequences for the NES region. All possible permutations of the peptide ELTLGEFL were docked onto Survivin's NES region and the scores were assorted according to the relative stability with respect to the original peptide sequence. Afterwards, sequences that contained the leucine spacing from the NES consensus sequence were excluded. As a result, the sequence LFEEGLLT was chosen, clicked to the tweezers and tested in ITC, NMR titration and pull-down experiments (section 3.1.3.2).

In pull-down experiments, higher concentrations of the scrambled peptide tweezer TW-LFEEGLLT were required in order to achieve comparable inhibition to TW-ELTLGEFL. Using a concentration range with high concentrations and big intervals (0.01–200 µM), a difference between the tweezers of approx. one order of magnitude was observed. TW-ELTGLEFL impaired the Survivin/Crm1 interaction already at 1–10 µM, while 10–50 µM of TW-LFEEGLLT were necessary for the same inhibition. In pull-down experiments with additional concentrations between 1–50 µM, the observed effect was not as strong, however, the scrambled peptide tweezer again revealed a higher inhibitory concentration compared to TW-ELTLGEFL. Furthermore, ITC titrations revealed lower binding affinities of TW-LFEEGLLT to Survivin$_{120}$ WT and K90/103T than TW-ELTLGEFL.

Binding of TW-LFEEGLLT to Survivin$_{120}$ was additionally assessed by NMR titrations. The tweezer with the scrambled peptide sequence was still able to bind to the two basic patches

K90/K91 and K103/R106 similar to the unmodified TW as indicated by small chemical shift perturbations and reduced intensities around the respective amino acids. Unspecific binding can also cause minor local conformational changes and, thus, usually leads to small shift changes in the NMR (Williamson, 2013). Indeed, small shift perturbations were observed between amino acids 91 and 103, which might be explained by the spatial proximity of the peptide LFEEGLLT to the anchor lysines for the tweezer and the resulting probability of the peptide to interact with the protein surface. However, the perturbations were not as strong as those observed during TW-ELTL and TW-ELTLGEFL titrations. This indicates that the peptide LFEEGLLT does not form the same contacts with the Survivin surface as the original peptide sequence (ELTLGEFL). Therefore, scrambling of the peptide sequence did indeed impair binding of the peptide tweezer to Survivin's NES as evidenced by fluorescence anisotropy, ITC, and NMR experiments.

At this point, it is important to emphasize that the 8-mer peptide sequence consists of only five different amino acids (E, L, T, G, and F). Therefore, it does not permit a large scope for complete and randomized scrambling of the peptide. The weak binding to $Survivin_{120}$ and, albeit lower, inhibition observed in pull-down experiments might still occur for TW-LFEEGLLT because of the similarity of the scrambled peptide sequence with the original ELTLGEFL sequence, and thus, the dimer interface. Nevertheless, binding of the peptide tweezer was indeed weakened upon scrambling and, therefore, seems to be specific.

Taken together, the results obtained with the $Survivin_{120}$ double mutant K90/103T and the scrambled peptide-tweezer confirm that binding of the tweezers to Survivin's NES epitope occurs regioselective and likely signal-specific and, due to this, impairs the Survivin/Crm1 interaction.

4.1.3 ASSESSMENT OF CELLULAR UPTAKE OF THE PEPTIDE TWEEZERS

To analyze potential effects of the tweezers on the Survivin/Crm1 interaction in the cell, it is important to get insights into the exact localization and mechanism of uptake of the tweezer molecules as the tweezers have to be able to enter cell nuclei in order to inhibit the Survivin/Crm1 interaction. To investigate the localization of the tweezers, HeLa Kyoto cells were incubated with FAM-labeled tweezers overnight. Confocal laser scanning microscopy revealed the accumulation of both peptide-modified and the unmodified tweezers exclusively in vesicles in the cytoplasm (section 3.1.4 and Figure 3-16). Further experiments with the FAM-

labeled tweezers showed a co-localization with the early endosome marker EEA1 after 30 min (Figure 3-17).

Both experiments indicate that the molecular tweezers enter the cell via the endosomal pathway. Even after 20 h, the tweezer is still captured in vesicle-like structures (Figure 3-16). This suggests that the tweezers will not be functional in the cellular environment since they do not reach the nucleus to impair the Survivin/Crm1 interaction. However, further co-localization experiments with other organelle markers and different time points are required to follow the route of the tweezer in the cell more thoroughly. Once molecules have entered the endocytic pathway, they can either end up in the lysosome, where they are enzymatically degraded, or they might escape from the endosomes (Varkouhi et al., 2011).

Strategies to prevent entrance into the endosomal pathway or ways to facilitate escape from it should be investigated in the future. Chemicals like chloroquine, which induces endosomal escape (Mellman et al., 1986; Heath et al., 2019), nanoparticle carrier (Patra et al., 2018) that might transport the tweezer through the membranes into the nucleus or the attachment of cell-penetrating peptides (Borrelli et al., 2018) to the tweezers are possibilities that need to be further explored.

4.2 ASSESSMENT OF OLIGOMER DOUBLE-TWEEZERS

The molecular tweezers have successfully been used to interfere with the Survivin/Crm1 interaction *in vitro* and their peptide modification via click chemistry has the potential to be further expanded by different types of macromolecules to create even stronger binders for Survivin's NES. As Survivin possesses several basic amino acids around its NES (K90, K91, K103, and R106), a ligand containing multiple tweezer units might have a higher affinity and specificity. For this purpose, three precision oligomers were developed together with the Hartmann group (Heinrich Heine University Düsseldorf) and the Schrader group (University of Duisburg-Essen). These macromolecules contain two tweezer units each, which are connected by oligomer linkers with different lengths. Binding of both tweezer units to the two basic patches simultaneously might shield Survivin's NES from interactions with the export receptor Crm1. Three dTWs were experimentally tested to identify the best oligomer tweezer candidate to target Survivin's NES (section 3.2). Binding of dTWs to Survivin was examined with ITC and NMR titrations and the ability to interfere with the Survivin/Crm1 interaction was assessed via pull-down assays.

For a quantitative analysis of oligomer dTW binding to Survivin, ITC titrations were performed (section 3.2.1). First, titrations of Survivin$_{120}$ to the different oligomer dTWs revealed at least two different binding sites, as indicated by the two-step thermograms. Interestingly, the two steps became more pronounced for the longer oligomer spacers. For the short oligomer dTW, the two steps were only hardly visible, while the long oligomer dTW distinctly exhibited two steps. This might indicate that the binding events, and thus the binding affinities of the two tweezer units differ more in case of the long oligomer dTW, while they seem to be similar for the short oligomer dTW as no distinct change of the slope was visible. However, data analysis of such a complex system involving a bivalent ligand, which binds to a protein with several potential binding sites and, thus, possesses different binding constants, remains difficult. Due to the lack of a good conventional model, the ITC titrations were not fit.

The influence of the oligomer dTWs on the Survivin/Crm1 interaction was investigated with pull-down experiments (section 3.2.2). Binding of the two tweezer units to K90/ K91 and K103/ R106 in and near Survivin's NES should impair binding of Crm1, assuming the oligomer blocks the competitor. Survivin$_{142}$-HA was pulled from 293T cell lysates incubated with different tweezer concentrations by GST-Crm1 using GSH-coated beads. Survivin and Crm1 were then detected via Western Blot in input and bead samples. Indeed, the amount of detected Survivin$_{142}$-HA decreased with increasing tweezer concentrations for each oligomer dTW. Hence, the interaction between Survivin and Crm1 is inhibited in a concentration-dependent manner. For the short and middle oligomer dTWs, the effective concentration was determined to be between 1–5 µM, while it was 10–25 µM for the long oligomer dTW. Thus, the longest oligomer dTW requires a much higher amount for comparable inhibition than the short and intermediate oligomer dTW. Importantly, the shorter oligomer dTWs showed much lower inhibitory concentrations than the unmodified TW (10–50 µM), while the long oligomer dTW seems to be in the same concentration range. In conclusion, the short and middle oligomers seem to have a suitable length to bind to the lysines around Survivin's NES and, thus, block Crm1, while the long oligomer dTW seems to be too long. It might be the case that the tweezer units of the long oligomer dTW still bind to Survivin, but the oligomer might be too long and forms a loop without making contact with the NES region. In contrast, the short and intermediate oligomers might be able to span across the NES epitope, while the tweezer cavities encapsulate the lysines nearby. However, these hypotheses need to be further tested e.g. with computational methods.

To map binding of the short oligomer dTWs to distinct amino acids, NMR titrations were performed (section 3.2.3). At a lower concentration of the oligomer dTW (500 µM), reduced intensities were observed for K90/91 and K103, which indicates that the tweezer has bound to these lysines. However, the protein seemed to aggregate during the measurement already at concentrations below the equimolar amount as an overall loss of the NMR signal intensities could be observed. Unfortunately, the binding site could not be identified with certainty due to the overall reduced signals. It is conceivable that the bivalent ligand does not only target lysines on the same protein molecule but also binds to lysines on different proteins, thereby cross-linking them. Especially because the two tweezer units are connected by an oligomer, rather than a peptide, which could direct the tweezer molecules to the protein surface. In case of TW-ELTLGEFL, three hydrogen bonds are formed between the peptide motif and the protein surface (Heid, 2018). Hence, the peptide enforces binding of the tweezer-molecule to the NES of Survivin. This effect does not exist in case of the oligomer dTWs and unspecific binding of the dTW to a pair of lysines with a matching distance seems to be likely.

Even though binding could not be mapped to a distinct region on the protein, the interaction between Survivin and Crm1 was strongly impaired, even stronger than with the peptide-modified tweezers. Therefore, the oligomer dTW approach seems to be valuable and should be further explored in combination with a peptide motif.

4.3 ASSESSMENT OF SURFACE-FUNCTIONALIZED GOLD NANOPARTICLES

As ultra-small gold nanoparticles with diameters of 1–2 nm are usually smaller than a protein, they might be used to specifically interact with epitopes on the protein surface after suitable modification with recognition units, e.g. amino acid selective binders like the tweezer (Kopp et al., 2017). As they are able to cross cell membranes and even enter the cell nuclei (van der Meer et al., 2019), they might facilitate cellular uptake of molecules like the tweezer. Recently, a synthesis protocol to obtain azide-terminated nanoparticles, which can be subsequently conjugated to alkyne-carrying ligands was developed (van der Meer et al., 2019). In this work, ultra-small gold nanoparticles were conjugated with tweezers via click chemistry. Aftwerwards, binding to Survivin was examined (section 3.3).

For a quantitative assessment of binding, an ITC titration of Survivin$_{120}$ to tweezer-conjugated nanoparticles was performed. However, analysis of such a complex system involving a protein with multiple binding sites and possibly different binding constants, and a multiavid ligand, such

as the tweezer-conjugated nanoparticles, is challenging. Due to the lack of a model describing this complex system and the resulting binding equilibria, the ITC titrations were fit with the simplest model, which provided a good fit of the data (stoichiometric equilibria approach/simple model with AFFINImeter). This model assumes that protein and tweezer form a 1:1 complex. The concentration of the tweezer units rather than the concentration of the gold nanoparticles was used to fit the data because this yielded good binding curves. A binding affinity of 8 ± 1 µM was calculated for the interaction between Survivin$_{120}$ and the tweezer-conjugated nanoparticles, which lies in the same order of magnitude as observed for interactions between the free, unmodified tweezer and lysine (15 µM) or even whole proteins like p97 (6 µM) (Dutt et al., 2013; Trusch et al., 2016). The affinity seems to be enhanced compared to free tweezer and Survivin$_{120}$ (38 ± 4 µM; section 3.1.1).

However, this model implies that ~11 tweezers on each gold nanoparticle bind to one protein independently. This also assumes that all tweezers can reach a lysine or arginine on the protein surface at the same time, which likely does not reflect the reality because the tweezers are attached in a spherical geometry. Since the size of the nanoparticle and the protein is comparable (low nanometer), it seems to be unlikely that each tweezer on the nanoparticle can dock onto the protein simultaneously. Binding of multiple proteins to one nanoparticle, each using one tweezer unit on the particle's surface is unlikely too, because of steric hindrance. In Figure 4-1 the binding mode of a tweezer-conjugated nanoparticle to the small protein hPin1 WW domain (~4.6 kDa) is depicted. Already for this protein, which is much smaller than Survivin (~16.4 kDa), it seems unlikely that each tweezer on the nanoparticle surface can be occupied by a protein at the same time. Therefore, the determined K_D might reflect the right order of magnitude, but the absolute value has to be treated with caution and the exact stoichiometries remain unclear.

Even though the exact values need to be taken with a grain of salt, the attachment of the tweezers on the nanoparticle surface seems to slightly increase the affinity of the tweezers for Survivin$_{120}$. Furthermore, the conjugation of the tweezers to the particles might also be advantageous in other areas. First, the nanoparticle is much bigger than the free tweezer and might cover a larger area on the protein surface and, hence, might interfere with protein-protein interactions such as the Survivin/Crm1 interaction more efficiently. Second, the nanoparticle enables the conjugation of more than one type of ligand on each particle, thereby creating multiavidity (Kopp et al., 2017; van der Meer et al., 2019). Different recognition units e.g. peptides, tweezers, or other ligands might be combined on the particle's surface to improve affinity and selectivity for a protein epitope of interest. Third, the nanoparticles might facilitate

the cellular uptake of the tweezers, which are otherwise captured in endosomes (section 3.1.4). This would enable the investigation of the tweezer's effects in cell-based assays such as the biosensor assay or proximity ligation assay (PLA) that are already established for the Survivin/Crm1 interaction (Bäcker, 2018; Oelschläger, 2018; Vallet, 2019). Indeed, comparable nanoparticles conjugated with fluorophores have already successfully entered the nuclei of HeLa cells (van der Meer et al., 2019; van der Meer, 2020), which would direct the tweezer to the right cell compartment for the inhibition of the Survivin/Crm1 interaction and, thus, for the interference with Survivin's dual function in carcinogenesis.
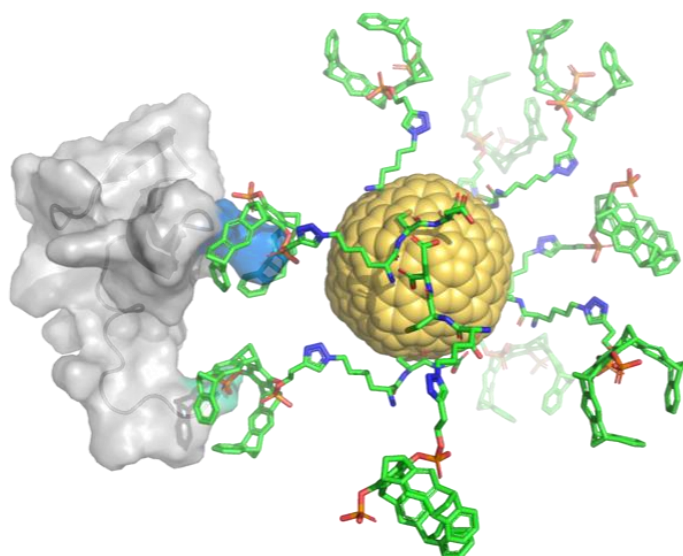
Figure 4-1: Schematic model of tweezer-conjugated nanoparticles binding to the hPin1 WW domain.

The gold nanoparticle (gold) was equipped with tweezers (green) and docked to one lysine (blue) on the surface of the hPin1 WW domain (grey; PDB ID: 2M8I). At least one other tweezer unit is able to bind to another lysine on the surface of the WW domain. The rest of the nanoparticle remains accessible for other proteins. Hence, a mixture of multiple proteins binding to one nanoparticle and multiple nanoparticles binding to the same protein seems to be likely and an exact model describing this system does not exist. The image was provided by Inesa Hadrovic (Schrader group, University of Duisburg-Essen).

4.4 CONCLUSION AND OUTLOOK

This work aimed to inhibit the cancer-relevant Survivin/Crm1 interaction by targeting Survivin's NES on the protein surface with supramolecular tweezers. Survivin's NES [89]VKKQFEELTL[98] is framed by two basic patches (K90/91 and K103/R106) and offers two anchor regions for tweezer units. Targeting the Survivin/Crm1 interaction might interfere with Survivin's mitotic as well as anti-apoptotic functions as both are essentially mediated via the NES. In cooperation with the groups of Prof. Dr. Thomas Schrader, Prof. Dr. Matthias Epple and Prof. Dr. Laura Hartmann, several supramolecular tweezer ligands – mono- or multiavid – were developed to specifically target Survivin's NES. Binding of those ligands to Survivin and their ability to interfere with the Survivin/Crm1 interaction was analyzed in this thesis. Tweezer-ELTLGEFL that features a peptide sequence derived from Survivin's natural binding site, the dimer interface, binds to Survivin's NES with micromolar affinity and interferes with the interaction with Crm1. The conjugation with the peptide that is specific for Survivin's NES increased the inhibitory potential and affinity of the tweezer compared to unmodified tweezers. However, the molecules still seemed to bind to other proteins like GST at high concentrations as indicated by pull-down assays, and their low micromolar affinity for Survivin might not be strong enough to exclusively interfere with the latter while other proteins are abundant. To circumvent these obstacles, the peptide-modified tweezers should be further enhanced by an additional recognition unit. One possibility is to attach a second tweezer unit to the opposed end of the peptide to create a peptide double-tweezer, which targets K90 and K103 at both ends of Survivin's NES similar to the already existing oligomer double-tweezers. This has the advantage that the peptide sequence can direct the tweezer to the protein surface and binding is strengthened by two tweezer units. The ideal length of the peptide and suitable linker were already determined by molecular dynamic studies performed by Inesa Hadrovic (Schrader group, University of Duisburg-Essen). Reducing the peptide sequence ELTLGEFL to ELTLG seems to enable an ideal distance between the two tweezer units to reach the respective lysines (Figure 4-2).

In this thesis, molecules with two tweezer units based on scaffolds made of oligomeric structures were already able to inhibit the Survivin/Crm1 interaction efficiently (section 3.2.2). However, their exact binding mode could not be solved, and NMR results point to several binding sites and mixed modes (section 3.2.1 and 3.2.3). Furthermore, ultra-small gold nanoparticles were equipped with tweezers and were shown to bind to Survivin with an enhanced affinity compared to free tweezers (section 3.3). After conjugation to the gold nanoparticles and oligomer scaffolds, the tweezers maintained their binding ability, which might enable further applications, e.g. in the cellular environment in the future.
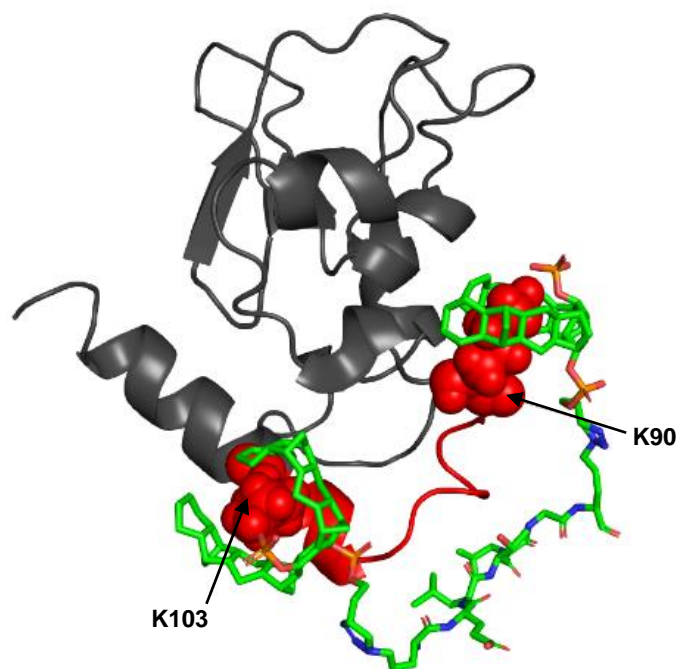
Figure 4-2: Model of the peptide double-tweezer binding to Survivin's NES.
The Survivin protomer (derived from PDB ID: 1XOX) is depicted in grey and the dTW in green. Two tweezer units were linked with a peptide sequence derived from Survivin's dimer interface (ELTLG). The length of this peptide potentially enables binding of the tweezer's cavities to K90 and K103 (red) simultaneously. The model was generated by Inesa Hadrovic (Schrader group, University of Duisburg-Essen).

Future challenges comprise improving the selectivity and affinity of the tweezer ligands as well as enabling cellular uptake. For this, multivalency will be further explored and precision macromolecules or ultra-small gold nanoparticles will continue to serve as scaffolds to combine supramolecular binding motifs (Figure 4-3). However, the attached motifs need to be strong binders for Survivin's surface and, thus, the existing precision macromolecules or nanoparticles will be supplemented with sequence-specific peptides e.g. the peptide ELTLGEFL, which produced promising results in this work. Additionally, the tweezer needs to enter the cell in an intact form. Therefore, the use of nanoparticles that cross the cell and even the nuclear membrane or the addition of cell-penetrating peptides to the tweezer ligands need to be further explored.
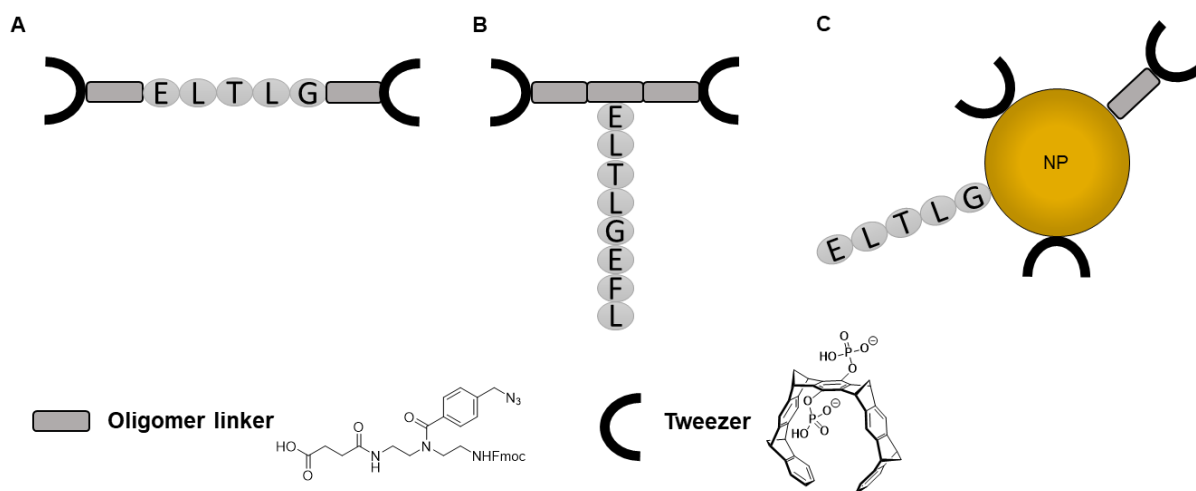
Figure 4-3: Further improvement of multivalent tweezer ligands based on scaffolds consisting of oligomers and nanoparticles.

Multivalent tweezer ligands are going to be further improved concerning their specificity and affinity. Approaches that will be used include combinations of oligomers and peptides, either with the peptide in line with the oligomer (A) or attached to the side chain (B), or different combinations of ligands conjugated to ultra-small gold nanoparticles (NP; C).

Overall, this thesis provides several promising approaches for the enhancement of the tweezers' affinity and specificity by the development of multivalent tweezer ligands containing additional recognition units for a protein surface. These results further substantiated the concept to specifically target functionally-relevant PPIs of Survivin by addressing its surface with supramolecular ligands, which might serve as a strategy in cancer therapies in the future.

5 References

Adida, C., Berrebi, D., Peuchmaur, M., Reyes-Mugica, M., and Altieri, D.C. (1998). Anti-apoptosis gene, survivin, and prognosis of neuroblastoma. The Lancet *351*, 882-883.

Adida, C., Haioun, C., Gaulard, P., Lepage, E., Morel, P., Briere, J., Dombret, H., Reyes, F., Diebold, J., and Gisselbrecht, C., et al. (2000). Prognostic significance of survivin expression in diffuse large B-cell lymphomas. Blood *96*, 1921-1925.

Ahlrichs, R., Bär, M., Häser, M., Horn, H., and Kölmel, C. (1989). Electronic structure calculations on workstation computers: The program system turbomole. Chemical Physics Letters *162*, 165-169.

Alber, F., Dokudovskaya, S., Veenhoff, L.M., Zhang, W., Kipper, J., Devos, D., Suprapto, A., Karni-Schmidt, O., Williams, R., and Chait, B.T., et al. (2007). The molecular architecture of the nuclear pore complex. Nature *450*, 695-701.

Alberts, B., Johnson, A., Lewis, J., Morgan, D., Raff, M., Roberts, K., and Walter, P. (2017). Molekularbiologie der Zelle (Weinheim: Wiley-VCH).

Albrecht, M. (2007). Supramolecular chemistry-general principles and selected examples from anion recognition and metallosupramolecular chemistry. Die Naturwissenschaften *94*, 951-966.

Altieri, D.C. (2010). Survivin and IAP proteins in cell-death mechanisms. The Biochemical journal *430*, 199-205.

Ambrosini, G., Adida, C., and Altieri, D.C. (1997). A novel anti-apoptosis gene, survivin, expressed in cancer and lymphoma. Nature medicine *3*, 917-921.

Andrade, M.A., and Bork, P. (1995). HEAT repeats in the Huntington's disease protein. Nature genetics *11*, 115-116.

Arnaoutov, A., Azuma, Y., Ribbeck, K., Joseph, J., Boyarchuk, Y., Karpova, T., McNally, J., and Dasso, M. (2005). Crm1 is a mitotic effector of Ran-GTP in somatic cells. Nature cell biology *7*, 626-632.

Ashkenazi, A. (2008). Directing cancer cells to self-destruct with pro-apoptotic receptor agonists. Nature reviews. Drug discovery *7*, 1001-1012.

Bäcker, S. (2018). Dissection and modulation of (patho)biological Survivin functions by supramolecular ligands. Dissertation (Essen).

Baier, M., Giesler, M., and Hartmann, L. (2018). Split-and-Combine Approach Towards Branched Precision Glycomacromolecules and Their Lectin Binding Behavior. Chemistry (Weinheim an der Bergstrasse, Germany) *24*, 1619-1630.

Beck, M., and Hurt, E. (2017). The nuclear pore complex: understanding its function through structural insight. Nature reviews. Molecular cell biology *18*, 73-89.

Bier, D., Rose, R., Bravo-Rodriguez, K., Bartel, M., Ramirez-Anguita, J.M., Dutt, S., Wilch, C., Klärner, F.-G., Sanchez-Garcia, E., and Schrader, T., et al. (2013). Molecular tweezers modulate 14-3-3 protein-protein interactions. Nature chemistry *5*, 234-239.

Bischoff, F.R., Klebe, C., Kretschmer, J., Wittinghofer, A., and Ponstingl, H. (1994). RanGAP1 induces GTPase activity of nuclear Ras-related Ran. Proceedings of the National Academy of Sciences of the United States of America *91*, 2587-2591.

Bischoff, F.R., Krebber, H., Smirnova, E., Dong, W., and Ponstingl, H. (1995). Co-activation of RanGTPase and inhibition of GTP dissociation by Ran-GTP binding protein RanBP1. The EMBO Journal *14*, 705-715.

Bischoff, F.R., and Ponstingl, H. (1991). Catalysis of guanine nucleotide exchange on Ran by the mitotic regulator RCC1. Nature *354*, 80-82.

Borrelli, A., Tornesello, A.L., Tornesello, M.L., and Buonaguro, F.M. (2018). Cell Penetrating Peptides as Molecular Carriers for Anti-Cancer Agents. Molecules (Basel, Switzerland) *23*.

Bourne, H.R., Sanders, D.A., and McCormick, F. (1991). The GTPase superfamily: conserved structure and molecular mechanism. Nature *349*, 117-127.

Buß, O., Rudat, J., and Ochsenreither, K. (2018). FoldX as Protein Engineering Tool: Better Than Random Based Approaches? Computational and structural biotechnology journal *16*, 25-33.

C. W. Chen and H. W. Whitlock Jr. Molecular tweezers: a simple model of bifunctional intercalation.

Capalbo, G., Rödel, C., Stauber, R.H., Knauer, S.K., Bache, M., Kappler, M., and Rödel, F. (2007). The role of survivin for radiation therapy. Prognostic and predictive factor and therapeutic target. Strahlentherapie und Onkologie : Organ der Deutschen Rontgengesellschaft … [et al] *183*, 593-599.

Carmena, M., Wheelock, M., Funabiki, H., and Earnshaw, W.C. (2012). The chromosomal passenger complex (CPC): from easy rider to the godfather of mitosis. Nature reviews. Molecular cell biology *13*, 789-803.

Carvalho, A., Carmena, M., Sambade, C., Earnshaw, W.C., and Wheatley, S.P. (2003). Survivin is required for stable checkpoint activation in taxol-treated HeLa cells. Journal of cell science *116*, 2987-2998.

Castedo, M., Perfettini, J.-L., Roumier, T., Andreau, K., Medema, R., and Kroemer, G. (2004). Cell death by mitotic catastrophe: a molecular definition. Oncogene *23*, 2825-2837.

Chantalat, L., Skoufias, D.A., Kleman, J.P., Jung, B., Dideberg, O., and Margolis, R.L. (2000). Crystal structure of human survivin reveals a bow tie-shaped dimer with two unusual alpha-helical extensions. Molecular cell *6*, 183-189.

Chari, A., Vogl, D.T., Gavriatopoulou, M., Nooka, A.K., Yee, A.J., Huff, C.A., Moreau, P., Dingli, D., Cole, C., and Lonial, S., et al. (2019). Oral Selinexor-Dexamethasone for Triple-Class Refractory Multiple Myeloma. The New England journal of medicine *381*, 727-738.

Chen, P., Zhu, J., Liu, D.-Y., Li, H.-Y., Xu, N., and Hou, M. (2014). Over-expression of survivin and VEGF in small-cell lung cancer may predict the poorer prognosis. Medical oncology (Northwood, London, England) *31*, 775.

Ciesielski, M.J., Ahluwalia, M.S., Munich, S.A., Orton, M., Barone, T., Chanan-Khan, A., and Fenstermaker, R.A. (2010). Antitumor cytotoxic T-cell response induced by a survivin peptide mimic. Cancer immunology, immunotherapy : CII *59*, 1211-1221.

Cohen, G.M. (1997). Caspases: the executioners of apoptosis. The Biochemical journal *326 (Pt 1)*, 1-16.

Cotter, T.G. (2009). Apoptosis and cancer: the genesis of a research field. Nature reviews. Cancer *9*, 501-507.

Dahlberg, J.E., and Lund, E. (1998). Functions of the GTPase Ran in RNA export from the nucleus. Current Opinion in Cell Biology *10*, 400-408.

Darden, T., York, D., and Pedersen, L. (1993). Particle mesh Ewald: An N ·log(N) method for Ewald sums in large systems. The Journal of Chemical Physics *98*, 10089-10092.

Davidovits, P., and Egger, M.D. (1969). Scanning laser microscope. Nature *223*, 831.

Denning, D.P., Patel, S.S., Uversky, V., Fink, A.L., and Rexach, M. (2003). Disorder in the nuclear pore complex: the FG repeat regions of nucleoporins are natively unfolded. Proceedings of the National Academy of Sciences of the United States of America *100*, 2450-2455.

Dickmanns, A., Monecke, T., and Ficner, R. (2015). Structural Basis of Targeting the Exportin CRM1 in Cancer. Cells *4*, 538-568.

Dingwall, C., Robbins, J., Dilworth, S.M., Roberts, B., and Richardson, W.D. (1988). The nucleoplasmin nuclear location sequence is larger and more complex than that of SV-40 large T antigen. The Journal of cell biology *107*, 841-849.

Dohi, T., Okada, K., Xia, F., Wilford, C.E., Samuel, T., Welsh, K., Marusawa, H., Zou, H., Armstrong, R., and Matsuzawa, S.-i., et al. (2004). An IAP-IAP complex inhibits apoptosis. The Journal of biological chemistry *279*, 34087-34090.

Dölker, N., Blanchet, C.E., Voß, B., Haselbach, D., Kappel, C., Monecke, T., Svergun, D.I., Stark, H., Ficner, R., and Zachariae, U., et al. (2013). Structural determinants and mechanism of mammalian CRM1 allostery. Structure (London, England : 1993) *21*, 1350-1360.

Dong, X., Biswas, A., and Chook, Y.M. (2009a). Structural basis for assembly and disassembly of the CRM1 nuclear export complex. Nature structural & molecular biology *16*, 558-560.

Dong, X., Biswas, A., Süel, K.E., Jackson, L.K., Martinez, R., Gu, H., and Chook, Y.M. (2009b). Structural basis for leucine-rich nuclear export signal recognition by CRM1. Nature *458*, 1136-1141.

Du, C., Fang, M., Li, Y., Li, L., and Wang, X. (2000). Smac, a Mitochondrial Protein that Promotes Cytochrome c–Dependent Caspase Activation by Eliminating IAP Inhibition. Cell *102*, 33-42.

Dutt, S., Wilch, C., Gersthagen, T., Talbiersky, P., Bravo-Rodriguez, K., Hanni, M., Sánchez-García, E., Ochsenfeld, C., Klärner, F.-G., and Schrader, T. (2013). Molecular tweezers with varying anions: a comparative study. The Journal of organic chemistry *78*, 6721-6734.

Ebbesen, M.F., Gerke, C., Hartwig, P., and Hartmann, L. (2016). Biodegradable poly(amidoamine)s with uniform degradation fragments via sequence-controlled macromonomers. Polym. Chem. *7*, 7086-7093.

Eckelman, B.P., Salvesen, G.S., and Scott, F.L. (2006). Human inhibitor of apoptosis proteins: why XIAP is the black sheep of the family. EMBO reports *7*, 988-994.

Elmore, S. (2007). Apoptosis: a review of programmed cell death. Toxicologic pathology *35*, 495-516.

Engelsma, D., Rodriguez, J.A., Fish, A., Giaccone, G., and Fornerod, M. (2007). Homodimerization antagonizes nuclear export of survivin. Traffic (Copenhagen, Denmark) *8*, 1495-1502.

Englmeier, L., Fornerod, M., Bischoff, F.R., Petosa, C., Mattaj, I.W., and Kutay, U. (2001). RanBP3 influences interactions between CRM1 and its nuclear protein export substrates. EMBO reports *2*, 926-932.

Erba, H.P., Sayar, H., Juckett, M., Lahn, M., Andre, V., Callies, S., Schmidt, S., Kadam, S., Brandt, J.T., and van Bockstaele, D., et al. (2013). Safety and pharmacokinetics of the antisense oligonucleotide (ASO) LY2181308 as a single-agent or in combination with idarubicin and cytarabine in patients with refractory or relapsed acute myeloid leukemia (AML). Investigational new drugs *31*, 1023-1034.

Fenstermaker, R.A., Ciesielski, M.J., Qiu, J., Yang, N., Frank, C.L., Lee, K.P., Mechtler, L.R., Belal, A., Ahluwalia, M.S., and Hutson, A.D. (2016). Clinical study of a survivin long peptide vaccine (SurVaxM) in patients with recurrent malignant glioma. Cancer immunology, immunotherapy : CII *65*, 1339-1352.

Ferreira, B.I., Cautain, B., Grenho, I., and Link, W. (2020). Small Molecule Inhibitors of CRM1. Front. Pharmacol. *11*.

Fischer, U., Huber, J., Boelens, W.C., Mattaj, L.W., and Lührmann, R. (1995). The HIV-1 Rev Activation Domain is a nuclear export signal that accesses an export pathway used by specific cellular RNAs. Cell *82*, 475-483.

Fokkens, M., Schrader, T., and Klärner, F.-G. (2005). A molecular tweezer for lysine and arginine. J. Am. Chem. Soc. *127*, 14415-14421.

Fornerod, M., Ohno, M., Yoshida, M., and Mattaj, I.W. (1997). CRM1 Is an Export Receptor for Leucine-Rich Nuclear Export Signals. Cell, 90(6), 1051-1060.

Fox, A.M., Ciziene, D., McLaughlin, S.H., and Stewart, M. (2011). Electrostatic interactions involving the extreme C terminus of nuclear export factor CRM1 modulate its affinity for cargo. The Journal of biological chemistry *286*, 29325-29335.

Frey, S., and Görlich, D. (2007). A saturated FG-repeat hydrogel can reproduce the permeability properties of nuclear pore complexes. Cell *130*, 512-523.

Frey, S., Richter, R.P., and Görlich, D. (2006). FG-rich repeats of nuclear pore proteins form a three-dimensional meshwork with hydrogel-like properties. Science (New York, N.Y.) *314*, 815-817.

Fuchigami, T., Ishikawa, N., Nozaki, I., Miyanari, Y., Yoshida, S., Yamauchi, M., Soejima, A., Haratake, M., and Nakayama, M. (2020). Discovery of inner centromere protein-derived small peptides for cancer imaging and treatment targeting survivin. Cancer science *111*, 1357-1366.

Fung, H.Y.J., Fu, S.-C., Brautigam, C.A., and Chook, Y.M. (2015). Structural determinants of nuclear export signal orientation in binding to exportin CRM1. eLife *4*.

Giaccone, G., Zatloukal, P., Roubec, J., Floor, K., Musil, J., Kuta, M., van Klaveren, R.J., Chaudhary, S., Gunther, A., and Shamsili, S. (2009). Multicenter phase II trial of YM155, a small-molecule suppressor of survivin, in patients with advanced, refractory, non-small-cell lung cancer. Journal of clinical oncology : official journal of the American Society of Clinical Oncology *27*, 4481-4486.

Görlich, D., and Kutay, U. (1999). Transport between the cell nucleus and the cytoplasm. Annual review of cell and developmental biology *15*, 607-660.

Görlich, D., Panté, N., Kutay, U., Aebi, U., and Bischoff, F.R. (1996). Identification of different roles for RanGDP and RanGTP in nuclear protein import. The EMBO Journal *15*, 5584-5594.

Grimme, S. (2011). Density functional theory with London dispersion corrections. WIREs Comput Mol Sci *1*, 211-228.

Grossman, E., Medalia, O., and Zwerger, M. (2012a). Functional architecture of the nuclear pore complex. Annual review of biophysics *41*, 557-584.

Grossman, S.A., Ye, X., Peereboom, D., Rosenfeld, M.R., Mikkelsen, T., Supko, J.G., and Desideri, S. (2012b). Phase I study of terameprocol in patients with recurrent high-grade glioma. Neuro-oncology *14*, 511-517.

Güttler, T., Madl, T., Neumann, P., Deichsel, D., Corsini, L., Monecke, T., Ficner, R., Sattler, M., and Görlich, D. (2010). NES consensus redefined by structures of PKI-type and Rev-type nuclear export signals bound to CRM1. Nature structural & molecular biology *17*, 1367-1376.

Hadrovic, I., Rebmann, P., Klärner, F.-G., Bitan, G., and Schrader, T. (2019). Molecular Lysine Tweezers Counteract Aberrant Protein Aggregation. Frontiers in chemistry *7*, 657.

Hamamoto, T., Gunji, S., Tsuji, H., and Beppu, T. (1983). Leptomycins A and B, new antifungal antibiotics. I. Taxonomy of the producing strain and their fermentation, purification and characterization. The Journal of antibiotics *36*, 639-645.

Heath, N., Osteikoetxea, X., Oliveria, T.M. de, Lázaro-Ibáñez, E., Shatnyeva, O., Schindler, C., Tigue, N., Mayr, L.M., Dekker, N., and Overman, R., et al. (2019). Endosomal escape enhancing compounds facilitate functional delivery of extracellular vesicle cargo. Nanomedicine (London, England) *14*, 2799-2814.

Heid, C. (2018). Molekulare Pinzetten zur Proteinoberflächenerkennung. Dissertation (Essen).

Hengartner, M.O. (2000). The biochemistry of apoptosis. Nature *407*, 770-776.

Hirohashi, Y., Torigoe, T., Maeda, A., Nabeta, Y., Kamiguchi, K., Sato, T., Yoda, J., Ikeda, H., Hirata, K., and Yamanaka, N., et al. (2002). An HLA-A24-restricted cytotoxic T lymphocyte epitope of a tumor-associated protein, survivin. Clinical cancer research : an official journal of the American Association for Cancer Research *8*, 1731-1739.

Huang, J., Rauscher, S., Nawrocki, G., Ran, T., Feig, M., Groot, B.L. de, Grubmüller, H., and MacKerell, A.D. (2017). CHARMM36m: an improved force field for folded and intrinsically disordered proteins. Nature methods *14*, 71-73.

Humphry, N.J., and Wheatley, S.P. (2018). Survivin inhibits excessive autophagy in cancer cells but does so independently of its interaction with LC3. Biology open *7*.

Izaurralde, E., Kutay, U., Kobbe, C. von, Mattaj, I.W., and Görlich, D. (1997). The asymmetric distribution of the constituents of the Ran system is essential for transport into and out of the nucleus. The EMBO Journal *16*, 6535-6547.

Jeyaprakash, A.A., Klein, U.R., Lindner, D., Ebert, J., Nigg, E.A., and Conti, E. (2007). Structure of a Survivin-Borealin-INCENP core complex reveals how chromosomal passengers travel together. Cell *131*, 271-285.

Kabachinski, G., and Schwartz, T.U. (2015). The nuclear pore complex--structure and function at a glance. Journal of cell science *128*, 423-429.

Kalderon, D., Roberts, B.L., Richardson, W.D., and Smith, A.E. (1984). A short amino acid sequence able to specify nuclear location. Cell, 39(3), 499-509.

Kapinos, L.E., Huang, B., Rencurel, C., and Lim, R.Y.H. (2017). Karyopherins regulate nuclear pore complex barrier and transport function. The Journal of cell biology *216*, 3609-3624.

Kapinos, L.E., Schoch, R.L., Wagner, R.S., Schleicher, K.D., and Lim, R.Y.H. (2014). Karyopherin-centric control of nuclear pores based on molecular occupancy and kinetic analysis of multivalent binding with FG nucleoporins. Biophysical journal *106*, 1751-1762.

Kar, G., Gursoy, A., and Keskin, O. (2009). Human cancer protein-protein interaction network: a structural perspective. PLoS computational biology *5*, e1000601.

Kästner, J., Carr, J.M., Keal, T.W., Thiel, W., Wander, A., and Sherwood, P. (2009). DL-FIND: an open-source geometry optimizer for atomistic simulations. J. Phys. Chem. A *113*, 11856-11865.

Kehlenbach, R.H., Dickmanns, A., Kehlenbach, A., Guan, T., and Gerace, L. (1999). A role for RanBP1 in the release of CRM1 from the nuclear pore complex in a terminal step of nuclear export. The Journal of cell biology *145*, 645-657.

Kerr, J.F., Wyllie, A.H., and Currie, A.R. (1972). Apoptosis: a basic biological phenomenon with wide-ranging implications in tissue kinetics. British journal of cancer *26*, 239-257.

Keskin, O., Gursoy, A., Ma, B., and Nussinov, R. (2008). Principles of protein-protein interactions: what are the preferred ways for proteins to interact? Chemical reviews *108*, 1225-1244.

Khanna, N., Dalby, R., Tan, M., Arnold, S., Stern, J., and Frazer, N. (2007). Phase I/II clinical safety studies of terameprocol vaginal ointment. Gynecologic oncology *107*, 554-562.

Kim, Y.H., Han, M.-E., and Oh, S.-O. (2017). The molecular mechanism for nuclear transport and its application. Anatomy & Cell Biology *50*, 77-85.

Klärner, F.-G., Benkhoff, J., Boese, R., Burkert, U., Kamieth, M., and Naatz, U. (1996). Molecular Tweezers as Synthetic Receptors in Host—Guest Chemistry: Inclusion of Cyclohexane and Self-Assembly of Aliphatic Side Chains. Angew. Chem. Int. Ed. Engl. *35*, 1130-1133.

Klauda, J.B., Venable, R.M., Freites, J.A., O'Connor, J.W., Tobias, D.J., Mondragon-Ramirez, C., Vorobyov, I., MacKerell, A.D., and Pastor, R.W. (2010). Update of the CHARMM all-atom additive force field for lipids: validation on six lipid types. The journal of physical chemistry. B *114*, 7830-7843.

Klebe, C., Bischoff, F.R., Ponstingl, H., and Wittinghofer, A. (1995). Interaction of the nuclear GTP-binding protein Ran with its regulatory proteins RCC1 and RanGAP1. Biochemistry *34*, 639-647.

Knauer, S.K., Bier, C., Habtemichael, N., and Stauber, R.H. (2006). The Survivin-Crm1 interaction is essential for chromosomal passenger complex localization and function. EMBO reports *7*, 1259-1265.

Knauer, S.K., Krämer, O.H., Knösel, T., Engels, K., Rödel, F., Kovács, A.F., Dietmaier, W., Klein-Hitpass, L., Habtemichael, N., and Schweitzer, A., et al. (2007). Nuclear export is essential for the tumor-promoting activity of survivin. FASEB journal : official publication of the Federation of American Societies for Experimental Biology *21*, 207-216.

Kopp, M., Kollenda, S., and Epple, M. (2017). Nanoparticle–Protein Interactions: Therapeutic Approaches and Supramolecular Chemistry. Acc. Chem. Res. *50*, 1383-1390.

Kosugi, S., Hasebe, M., Tomita, M., and Yanagawa, H. (2008). Nuclear export signal consensus sequences defined using a localization-based yeast selection system. Traffic (Copenhagen, Denmark) *9*, 2053-2062.

Koyama, M., and Matsuura, Y. (2010). An allosteric mechanism to displace nuclear export cargo from CRM1 and RanGTP by RanBP1. The EMBO Journal *29*, 2002-2013.

Krissinel, E., and Henrick, K. (2007). Inference of macromolecular assemblies from crystalline state. Journal of molecular biology *372*, 774-797.

Kubota, R., and Hamachi, I. (2015). Protein recognition using synthetic small-molecular binders toward optical protein sensing in vitro and in live cells. Chemical Society reviews *44*, 4454-4471.

Kudo, N., Matsumori, N., Taoka, H., Fujiwara, D., Schreiner, E.P., Wolff, B., Yoshida, M., and Horinouchi, S. (1999). Leptomycin B inactivates CRM1/exportin 1 by covalent modification at a cysteine residue in the central conserved region. Proceedings of the National Academy of Sciences of the United States of America *96*, 9112-9117.

Laemmli, U.K. (1970). Cleavage of structural proteins during the assembly of the head of bacteriophage T4. Nature *227*, 680-685.

Lapalombella, R., Sun, Q., Williams, K., Tangeman, L., Jha, S., Zhong, Y., Goettl, V., Mahoney, E., Berglund, C., and Gupta, S., et al. (2012). Selective inhibitors of nuclear export show that CRM1/XPO1 is a target in chronic lymphocytic leukemia. Blood *120*, 4621-4634.

Lehn, J.M. (1988). Supramolecular Chemistry-Scope and Perspectives Molecules, Supermolecules, and Molecular Devices (Nobel Lecture). Angew. Chem. Int. Ed. Engl. *27*, 89-112.

Lehn, J.-M. (2002). Toward complex matter: supramolecular chemistry and self-organization. Proceedings of the National Academy of Sciences of the United States of America *99*, 4763-4768.

Lens, S.M.A., Wolthuis, R.M.F., Klompmaker, R., Kauw, J., Agami, R., Brummelkamp, T., Kops, G., and Medema, R.H. (2003). Survivin is required for a sustained spindle checkpoint arrest in response to lack of tension. The EMBO Journal *22*, 2934-2947.

Leong, L.E.C. (1999). The use of recombinant fusion proteases in the affinity purification of recombinant proteins. Molecular biotechnology *12.3*, 269-274.

Li, F., Aljahdali, I., and Ling, X. (2019). Cancer therapeutics using survivin BIRC5 as a target: what can we do after over two decades of study? Journal of experimental & clinical cancer research : CR *38*, 368.

Li, F., and Altieri, D.C. (1999). Transcriptional analysis of human survivin gene expression. The Biochemical journal *344 Pt 2*, 305-311.

Li, F., Ambrosini, G., Chu, E.Y., Plescia, J., Tognin, S., Marchisio, P.C., and Altieri, D.C. (1998). Control of apoptosis and mitotic spindle checkpoint by survivin. Nature *396*, 580-584.

Li, Z., Ren, W., Zeng, Q., Chen, S., Zhang, M., Zhao, Y., Cheng, J., and Wang, X. (2016). Effects of survivin on angiogenesis in vivo and in vitro. American journal of translational research *8*, 270-283.

Lim, R.Y.H., Huang, N.-P., Köser, J., Deng, J., Lau, K.H.A., Schwarz-Herion, K., Fahrenkrog, B., and Aebi, U. (2006). Flexible phenylalanine-glycine nucleoporins as entropic barriers to nucleocytoplasmic transport. Proceedings of the National Academy of Sciences of the United States of America *103*, 9512-9517.

Lindsay, M.E., Holaska, J.M., Welch, K., Paschal, B.M., and Macara, I.G. (2001). Ran-binding protein 3 is a cofactor for Crm1-mediated nuclear protein export. The Journal of cell biology *153*, 1391-1402.

Mahajan, R., Delphin, C., Guan, T., Gerace, L., and Melchior, F. (1997). A Small Ubiquitin-Related Polypeptide Involved in Targeting RanGAP1 to Nuclear Pore Complex Protein RanBP2. Cell *88*, 97-107.

Mark, P., and Nilsson, L. (2001). Structure and Dynamics of the TIP3P, SPC, and SPC/E Water Models at 298 K. J. Phys. Chem. A *105*, 9954-9960.

Marusawa, H., Matsuzawa, S.-i., Welsh, K., Zou, H., Armstrong, R., Tamm, I., and Reed, J.C. (2003). HBXIP functions as a cofactor of survivin in apoptosis suppression. The EMBO Journal *22*, 2729-2740.

Mattaj, I.W., and Englmeier, L. (1998). Nucleocytoplasmic transport: the soluble phase. Annual review of biochemistry *67*, 265-306.

McDonald, C.C., and Phillips, W.D. (1967). Manifestations of the tertiary structures of proteins in high-frequency nuclear magnetic resonance. J. Am. Chem. Soc. *89*, 6332-6341.

Melchior, F., Paschal, B., Evans, J., and Gerace, L. (1993). Inhibition of nuclear protein import by nonhydrolyzable analogues of GTP and identification of the small GTPase Ran/TC4 as an essential transport factor. The Journal of cell biology *123*, 1649-1659.

Mellman, I., Fuchs, R., and Helenius, A. (1986). Acidification of the endocytic and exocytic pathways. Annual review of biochemistry *55*, 663-700.

Monecke, T., Dickmanns, A., and Ficner, R. (2014). Allosteric control of the exportin CRM1 unraveled by crystal structure analysis. The FEBS journal *281*, 4179-4194.

Monecke, T., Güttler, T., Neumann, P., Dickmanns, A., Görlich, D., and Ficner, R. (2009). Crystal structure of the nuclear export receptor CRM1 in complex with Snurportin1 and RanGTP. Science (New York, N.Y.) *324*, 1087-1091.

Monecke, T., Haselbach, D., Voß, B., Russek, A., Neumann, P., Thomson, E., Hurt, E., Zachariae, U., Stark, H., and Grubmüller, H., et al. (2013). Structural basis for cooperativity of CRM1 export complex formation. Proceedings of the National Academy of Sciences of the United States of America *110*, 960-965.

Mullis, K.B., and Faloona, F.A. (1989). Specific Synthesis of DNA in Vitro via a Polymerase-Catalyzed Chain Reaction. In Recombinant DNA Methodology (Elsevier), pp. 189–204.

Nakahara, T., Kita, A., Yamanaka, K., Mori, M., Amino, N., Takeuchi, M., Tominaga, F., Hatakeyama, S., Kinoyama, I., and Matsuhisa, A., et al. (2007). YM155, a novel small-molecule survivin suppressant, induces regression of established human hormone-refractory prostate tumor xenografts. Cancer research *67*, 8014-8021.

Newlands, E.S., Rustin, G.J., and Brampton, M.H. (1996). Phase I trial of elactocin. British journal of cancer *74*, 648-649.

Niedzialkowska, E., Wang, F., Porebski, P.J., Minor, W., Higgins, J.M.G., and Stukenberg, P.T. (2012). Molecular basis for phosphospecific recognition of histone H3 tails by Survivin paralogues at inner centromeres. Molecular biology of the cell *23*, 1457-1466.

Oelschläger, L. (2018). Analyse der Effekte supramolekularer Liganden auf die Funktion onkologisch relevanter Proteine (Essen).

Page, R., Peti, W., Wilson, I.A., Stevens, R.C., and Wüthrich, K. (2005). NMR screening and crystal quality of bacterially expressed prokaryotic and eukaryotic proteins in a structural genomics pipeline. Proceedings of the National Academy of Sciences of the United States of America *102*, 1901-1905.

Pang, Y.T., Miao, Y., Wang, Y., and McCammon, J.A. (2017). Gaussian Accelerated Molecular Dynamics in NAMD. Journal of chemical theory and computation *13*, 9-19.

Patra, J.K., Das, G., Fraceto, L.F., Campos, E.V.R., Rodriguez-Torres, M.D.P., Acosta-Torres, L.S., Diaz-Torres, L.A., Grillo, R., Swamy, M.K., and Sharma, S., et al. (2018). Nano based drug delivery systems: recent developments and future prospects. Journal of nanobiotechnology *16*, 71.

Pavlyukov, M.S., Antipova, N.V., Balashova, M.V., Vinogradova, T.V., Kopantzev, E.P., and Shakhparonov, M.I. (2011). Survivin monomer plays an essential role in apoptosis regulation. The Journal of biological chemistry *286*, 23296-23307.

Peczuh, M.W., and Hamilton, A.D. (2000). Peptide and Protein Recognition by Designed Molecules. Chem. Rev. *100*, 2479-2494.

Peery, R.C., Liu, J.-Y., and Zhang, J.-T. (2017). Targeting survivin for therapeutic discovery: past, present, and future promises. Drug discovery today *22*, 1466-1477.

Phillips, J.C., Braun, R., Wang, W., Gumbart, J., Tajkhorshid, E., Villa, E., Chipot, C., Skeel, R.D., Kalé, L., and Schulten, K. (2005). Scalable molecular dynamics with NAMD. Journal of computational chemistry *26*, 1781-1802.

Prabhudesai, S., Sinha, S., Attar, A., Kotagiri, A., Fitzmaurice, A.G., Lakshmanan, R., Ivanova, M.I., Loo, J.A., Klärner, F.-G., and Schrader, T., et al. (2012). Erratum to: A Novel "Molecular Tweezer" Inhibitor of α-Synuclein Neurotoxicity In Vitro and In Vivo. Neurotherapeutics *9*, 486.

Qi, J., Dong, Z., Liu, J., Peery, R.C., Zhang, S., Liu, J.-Y., and Zhang, J.-T. (2016). Effective Targeting of the Survivin Dimerization Interface with Small-Molecule Inhibitors. Cancer research *76*, 453-462.

Raetz, E.A., Morrison, D., Romanos-Sirakis, E., Gaynon, P., Sposto, R., Bhojwani, D., Bostrom, B.C., Brown, P., Eckroth, E., and Cassar, J., et al. (2014). A phase I study of EZN-3042, a novel survivin messenger ribonucleic acid (mRNA) antagonist, administered in combination with chemotherapy in children with relapsed acute lymphoblastic leukemia (ALL): a report from the therapeutic advances in childhood leukemia and lymphoma (TACL) consortium. Journal of pediatric hematology/oncology *36*, 458-463.

Reichelt, R., Holzenburg, A., Buhle, E.L., Jarnik, M., Engel, A., and Aebi, U. (1990). Correlation between structure and mass distribution of the nuclear pore complex and of distinct pore complex components. The Journal of cell biology *110*, 883-894.

Rexach, M., and Blobel, G. (1995). Protein import into nuclei: association and dissociation reactions involving transport substrate, transport factors, and nucleoporins. Cell *83*, 683-692.

Ribbeck, K., and Görlich, D. (2001). Kinetic analysis of translocation through nuclear pore complexes. The EMBO Journal *20*, 1320-1330.

Ribbeck, K., and Görlich, D. (2002). The permeability barrier of nuclear pore complexes appears to operate via hydrophobic exclusion. The EMBO Journal *21*, 2664-2671.

Richards, S.A., Carey, K.L., and Macara, I.G. (1997). Requirement of guanosine triphosphate-bound ran for signal-mediated nuclear protein export. Science (New York, N.Y.) *276*, 1842-1844.

Riedl, S.J., Renatus, M., Schwarzenbacher, R., Zhou, Q., Sun, C., Fesik, S.W., Liddington, R.C., and Salvesen, G.S. (2001). Structural Basis for the Inhibition of Caspase-3 by XIAP. Cell *104*, 791-800.

Röcker, A.E., Müller, J.A., Dietzel, E., Harms, M., Krüger, F., Heid, C., Sowislok, A., Riber, C.F., Kupke, A., and Lippold, S., et al. (2018). The molecular tweezer CLR01 inhibits Ebola and Zika virus infection. Antiviral research *152*, 26-35.

Rodríguez, J.A., Span, S.W., Ferreira, C.G.M., Kruyt, F.A.E., and Giaccone, G. (2002). CRM1-mediated nuclear export determines the cytoplasmic localization of the antiapoptotic protein Survivin. Experimental cell research *275*, 44-53.

Rout, M.P., Aitchison, J.D., Magnasco, M.O., and Chait, B.T. (2003). Virtual gating and nuclear transport: the hole picture. Trends in cell biology *13*, 622-628.

Rout, M.P., Aitchison, J.D., Suprapto, A., Hjertaas, K., Zhao, Y., and Chait, B.T. (2000). The yeast nuclear pore complex: composition, architecture, and transport mechanism. The Journal of cell biology *148*, 635-651.

Ruchaud, S., Carmena, M., and Earnshaw, W.C. (2007a). Chromosomal passengers: conducting cell division. Nature reviews. Molecular cell biology *8*, 798-812.

Ruchaud, S., Carmena, M., and Earnshaw, W.C. (2007b). The chromosomal passenger complex: one for all and all for one. Cell *131*, 230-231.

Sakiyama, Y., Panatala, R., and Lim, R.Y.H. (2017). Structural dynamics of the nuclear pore complex. Seminars in cell & developmental biology *68*, 27-33.

Sanhueza, C., Wehinger, S., Castillo Bennett, J., Valenzuela, M., Owen, G.I., and Quest, A.F.G. (2015). The twisted survivin connection to angiogenesis. Molecular cancer *14*, 198.

Sendino, M., Omaetxebarria, M.J., and Rodríguez, J.A. (2018). Hitting a moving target: inhibition of the nuclear export receptor XPO1/CRM1 as a therapeutic approach in cancer. CDR.

Sherwood, P., Vries, A.H. de, Guest, M.F., Schreckenbach, G., Catlow, C.R.A., French, S.A., Sokol, A.A., Bromley, S.T., Thiel, W., and Turner, A.J., et al. (2003). QUASI: A general purpose implementation of the QM/MM approach and its application to problems in catalysis. Journal of Molecular Structure: THEOCHEM *632*, 1-28.

Sinha, S., Lopes, D.H.J., Du, Z., Pang, E.S., Shanmugam, A., Lomakin, A., Talbiersky, P., Tennstaedt, A., McDaniel, K., and Bakshi, R., et al. (2011). Lysine-specific molecular tweezers are broad-spectrum inhibitors of assembly and toxicity of amyloid proteins. Journal of the American Chemical Society *133*, 16958-16969.

Smith, D.B., and Johnson, K.S. (1988). Single-step purification of polypeptides expressed in Escherichia coli as fusions with glutathione S-transferase. Gene *67*, 31-40.

Song, Z., Yao, X., and Wu, M. (2003). Direct interaction between survivin and Smac/DIABLO is essential for the anti-apoptotic activity of survivin during taxol-induced apoptosis. The Journal of biological chemistry *278*, 23130-23140.

Srinivasula, S.M., and Ashwell, J.D. (2008). IAPs: what's in a name? Molecular cell *30*, 123-135.

Stauber, R.H., Mann, W., and Knauer, S.K. (2007). Nuclear and cytoplasmic survivin: molecular mechanism, prognostic, and therapeutic potential. Cancer research *67*, 5999-6002.

Stauber, R.H., Rabenhorst, U., Rekik, A., Engels, K., Bier, C., and Knauer, S.K. (2006). Nucleocytoplasmic shuttling and the biological activity of mouse survivin are regulated by an active nuclear export signal. Traffic (Copenhagen, Denmark) *7*, 1461-1472.

Steed, J.W., Turner, D.R., and Wallace, K.J. (2007). Core concepts in supramolecular chemistry and nanochemistry (Chichester, England, Hoboken, NJ: John Wiley).

Stewart, M. (2007). Molecular mechanism of the nuclear protein import cycle. Nature reviews. Molecular cell biology *8*, 195-208.

Sun, Q., Carrasco, Y.P., Hu, Y., Guo, X., Mirzaei, H., Macmillan, J., and Chook, Y.M. (2013). Nuclear export inhibition through covalent conjugation and hydrolysis of Leptomycin B by CRM1. Proceedings of the National Academy of Sciences of the United States of America *110*, 1303-1308.

Sun, Q., Chen, X., Zhou, Q., Burstein, E., Yang, S., and Jia, D. (2016). Inhibiting cancer cell hallmark features through nuclear export inhibition. Signal transduction and targeted therapy *1*, 16010.

Trusch, F., Kowski, K., Bravo-Rodriguez, K., Beuck, C., Sowislok, A., Wettig, B., Matena, A., Sanchez-Garcia, E., Meyer, H., and Schrader, T., et al. (2016). Molecular tweezers target a protein-protein interface and thereby modulate complex formation. Chemical communications (Cambridge, England) *52*, 14141-14144.

U.S. Food and Drug Administration (2019). FDA approves new treatment for refractory multiple myeloma. https://www.fda.gov/news-events/press-announcements/fda-approves-new-treatment-refractory-multiple-myeloma.

Vallet, C. (2019). Modulation of Survivin's cancer-promoting functions with supramolecular ligands. Dissertation (Essen).

Vallet, C., Aschmann, D., Beuck, C., Killa, M., Meiners, A., Mertel, M., Ehlers, M., Bayer, P., Schmuck, C., and Giese, M., et al. (2020). Functional Disruption of the Cancer-Relevant Interaction between Survivin and Histone H3 with a Guanidiniocarbonyl Pyrrole Ligand. Angewandte Chemie (International ed. in English) *59*, 5567-5571.

van der Meer, S. (2020). Oberflächenfunktionalisierung von ultrakleinen Goldnanopartikeln für die selektive Proteinadressierung. Dissertation (Essen).

van der Meer, S.B., Loza, K., Wey, K., Heggen, M., Beuck, C., Bayer, P., and Epple, M. (2019). Click Chemistry on the Surface of Ultrasmall Gold Nanoparticles (2 nm) for Covalent Ligand Attachment Followed by NMR Spectroscopy. Langmuir : the ACS journal of surfaces and colloids *35*, 7191-7204.

van Dun, S., Ottmann, C., Milroy, L.-G., and Brunsveld, L. (2017). Supramolecular Chemistry Targeting Proteins. Journal of the American Chemical Society *139*, 13960-13968.

Vanommeslaeghe, K., Hatcher, E., Acharya, C., Kundu, S., Zhong, S., Shim, J., Darian, E., Guvench, O., Lopes, P., and Vorobyov, I., et al. (2010). CHARMM general force field: A force field for drug-like molecules compatible with the CHARMM all-atom additive biological force fields. Journal of computational chemistry *31*, 671-690.

Varkouhi, A.K., Scholte, M., Storm, G., and Haisma, H.J. (2011). Endosomal escape pathways for delivery of biologicals. Journal of controlled release : official journal of the Controlled Release Society *151*, 220-228.

Verdecia, M.A., Huang, H., Dutil, E., Kaiser, D.A., Hunter, T., and Noel, J.P. (2000). Structure of the human anti-apoptotic protein survivin reveals a dimeric arrangement. Nature structural biology *7*, 602-608.

Vetter, I.R., Arndt, A., Kutay, U., Görlich, D., and Wittinghofer, A. (1999). Structural View of the Ran–Importin β Interaction at 2.3 Å Resolution. Cell *97*, 635-646.

Vong, Q.P., Cao, K., Li, H.Y., Iglesias, P.A., and Zheng, Y. (2005). Chromosome alignment and segregation regulated by ubiquitination of survivin. Science (New York, N.Y.) *310*, 1499-1504.

Wang, F., Dai, J., Daum, J.R., Niedzialkowska, E., Banerjee, B., Stukenberg, P.T., Gorbsky, G.J., and Higgins, J.M.G. (2010). Histone H3 Thr-3 phosphorylation by Haspin positions Aurora B at centromeres in mitosis. Science (New York, N.Y.) *330*, 231-235.

Wang, J., and Li, W. (2014). Discovery of novel second mitochondria-derived activator of caspase mimetics as selective inhibitor of apoptosis protein inhibitors. The Journal of pharmacology and experimental therapeutics *349*, 319-329.

Wang, Q., Arnst, K.E., Xue, Y., Lei, Z.-N., Ma, D., Chen, Z.-S., Miller, D.D., and Li, W. (2018). Synthesis and biological evaluation of indole-based UC-112 analogs as potent and selective survivin inhibitors. European journal of medicinal chemistry *149*, 211-224.

Weis, K. (2007). The nuclear pore complex: oily spaghetti or gummy bear? Cell *130*, 405-407.

Wen, W., Meinkotht, J.L., Tsien, R.Y., and Taylor, S.S. (1995). Identification of a signal for rapid export of proteins from the nucleus. Cell *82*, 463-473.

Wendt, M.D., Sun, C., Kunzer, A., Sauer, D., Sarris, K., Hoff, E., Yu, L., Nettesheim, D.G., Chen, J., and Jin, S., et al. (2007). Discovery of a novel small molecule binding site of human survivin. Bioorganic & medicinal chemistry letters *17*, 3122-3129.

Wheatley, S.P., and Altieri, D.C. (2019). Survivin at a glance. Journal of cell science *132*.

Wheatley, S.P., Henzing, A.J., Dodson, H., Khaled, W., and Earnshaw, W.C. (2004). Aurora-B phosphorylation in vitro identifies a residue of survivin that is essential for its localization and binding to inner centromere protein (INCENP) in vivo. The Journal of biological chemistry *279*, 5655-5660.

Wiechno, P., Somer, B.G., Mellado, B., Chłosta, P.L., Cervera Grau, J.M., Castellano, D., Reuter, C., Stöckle, M., Kamradt, J., and Pikiel, J., et al. (2014). A randomised phase 2 study combining LY2181308 sodium (survivin antisense oligonucleotide) with first-line docetaxel/prednisone in patients with castration-resistant prostate cancer. European urology *65*, 516-520.

Williamson, M.P. (2013). Using chemical shift perturbation to characterise ligand binding. Progress in nuclear magnetic resonance spectroscopy *73*, 1-16.

Xiao, M., Wang, J., Lin, Z., Lu, Y., Li, Z., White, S.W., Miller, D.D., and Li, W. (2015). Design, Synthesis and Structure-Activity Relationship Studies of Novel Survivin Inhibitors with Potent Anti-Proliferative Properties. PloS one *10*, e0129807.

Xu, D., Farmer, A., Collett, G., Grishin, N.V., and Chook, Y.M. (2012). Sequence and structural analyses of nuclear export signals in the NESdb database. Molecular biology of the cell *23*, 3677-3693.

Zadmard, R., and Alavijeh, N.S. (2014). Protein surface recognition by calixarenes. RSC Adv *4*, 41529-41542.

Zimmerman, S.C. (2016). A journey in bioinspired supramolecular chemistry: from molecular tweezers to small molecules that target myotonic dystrophy. Beilstein journal of organic chemistry *12*, 125-138.

Zimmerman, S.C., and VanZyl, C.M. (1987). Rigid molecular tweezers: synthesis, characterization, and complexation chemistry of a diacridine.

6 APPENDIX

6.1 SUPPORTING INFORMATION

NMR TITRATIONS OF ^{15}N-LABELED SURVIVIN$_{120}$ WT WITH TW-ELTLGEFL
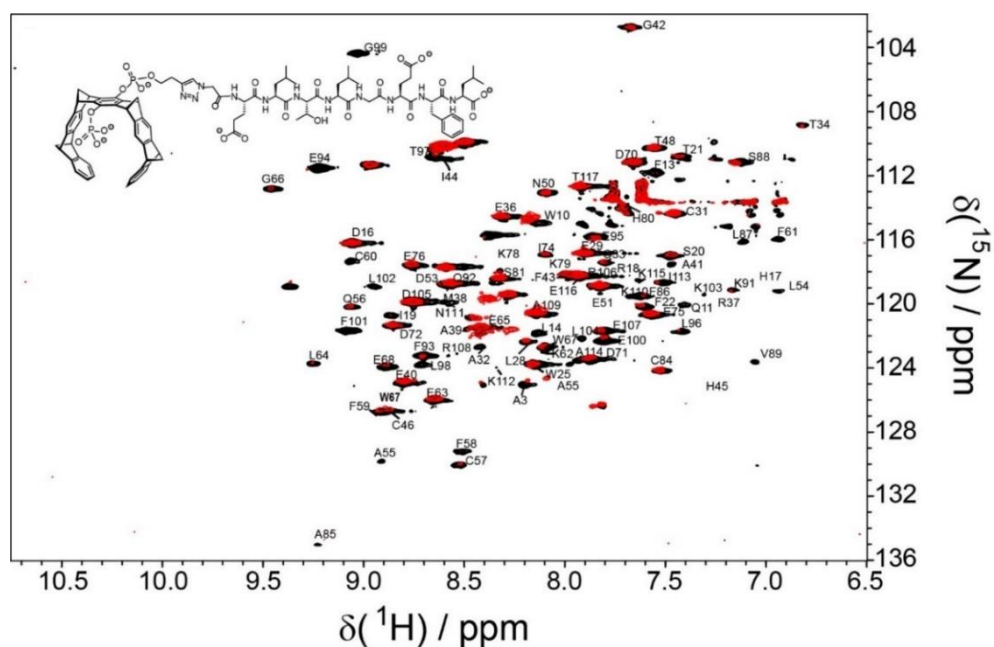
Figure A1: ^{15}N-HSQC NMR spectra of ^{15}N-labeled Survivin$_{120}$ WT in the absence (black) and presence (red) of TW-ELTLGEFL.

^{1}H-^{15}N-BEST-TROSY-HSQC spectra of 938 µM ^{15}N-labeled Survivin$_{120}$ before (black) and after (red) titration of 938 µM TW-ELTLGEFL. The purification of ^{15}N-labeled Survivin$_{120}$, NMR measurements and subsequent analyses were conducted by Dr. Christine Beuck (Bayer group, University of Duisburg-Essen). Assigned signals are labeled.

CONTACTS BETWEEN TW-ELTL AND THE SURVIVIN$_{120}$ PROTOMER
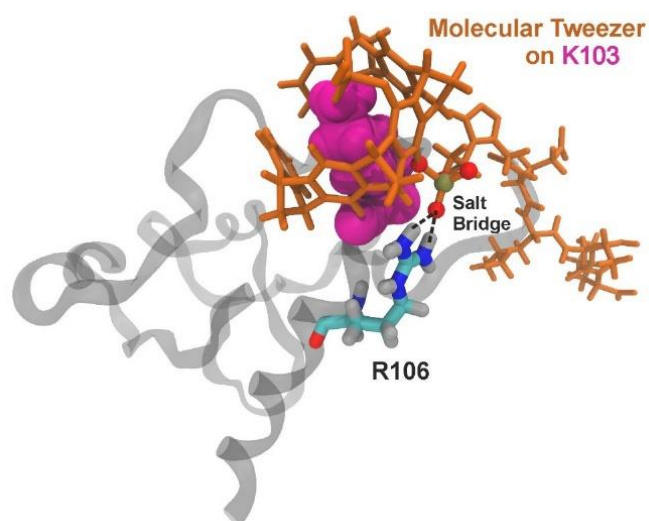
Figure A2: Representation of TW-ELTL binding to Survivin's NES region predicts several contacts.
The tweezer cavity (orange) encapsulates K103 (pink), while the peptide ELTL contacts the peptide fragment ^{95}ELTL^{98} on the Survivin$_{120}$ protomer. An additional salt bridge formed between the phosphate group of the tweezer and R103 stabilizes the peptide-modified tweezer at its position. The image was provided by Dr. Joel Mieres-Perez (Sánchez-García group, University of Duisburg-Essen).

NMR TITRATIONS OF ^{15}N-LABELED SURVIVIN$_{120}$ WT WITH TW-LFEEGLLT
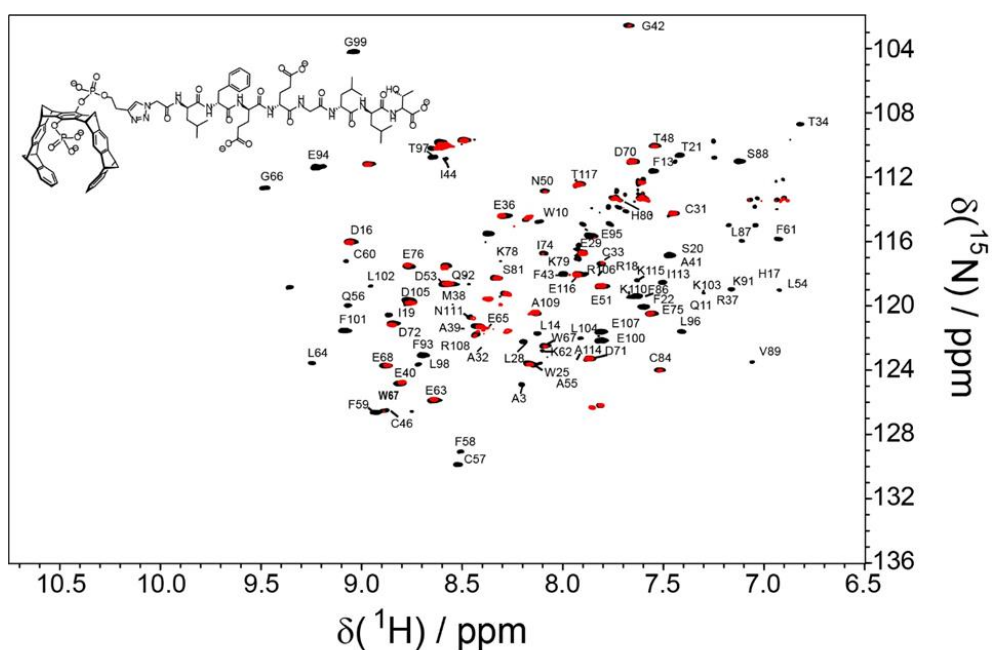
Figure A3: 15N-HSQC NMR spectra of 15N-labeled Survivin120 WT in the absence (black) and presence (red) of TW-LFEEGLLT.

^{1}H-^{15}N-BEST-TROSY-HSQC spectra of 938 µM ^{15}N-labeled Survivin$_{120}$ before (black) and after (red) titration of 938 µM TW-LFEEGLLT. The purification of ^{15}N-labeled Survivin$_{120}$, NMR measurements and subsequent analyses were conducted by Dr. Christine Beuck (Bayer group, University of Duisburg-Essen). Assigned signals are labeled.

NMR TITRATIONS OF ^{15}N-LABELED SURVIVIN${}_{120}$ **WT** WITH THE SHORT OLIGOMER D**TW**
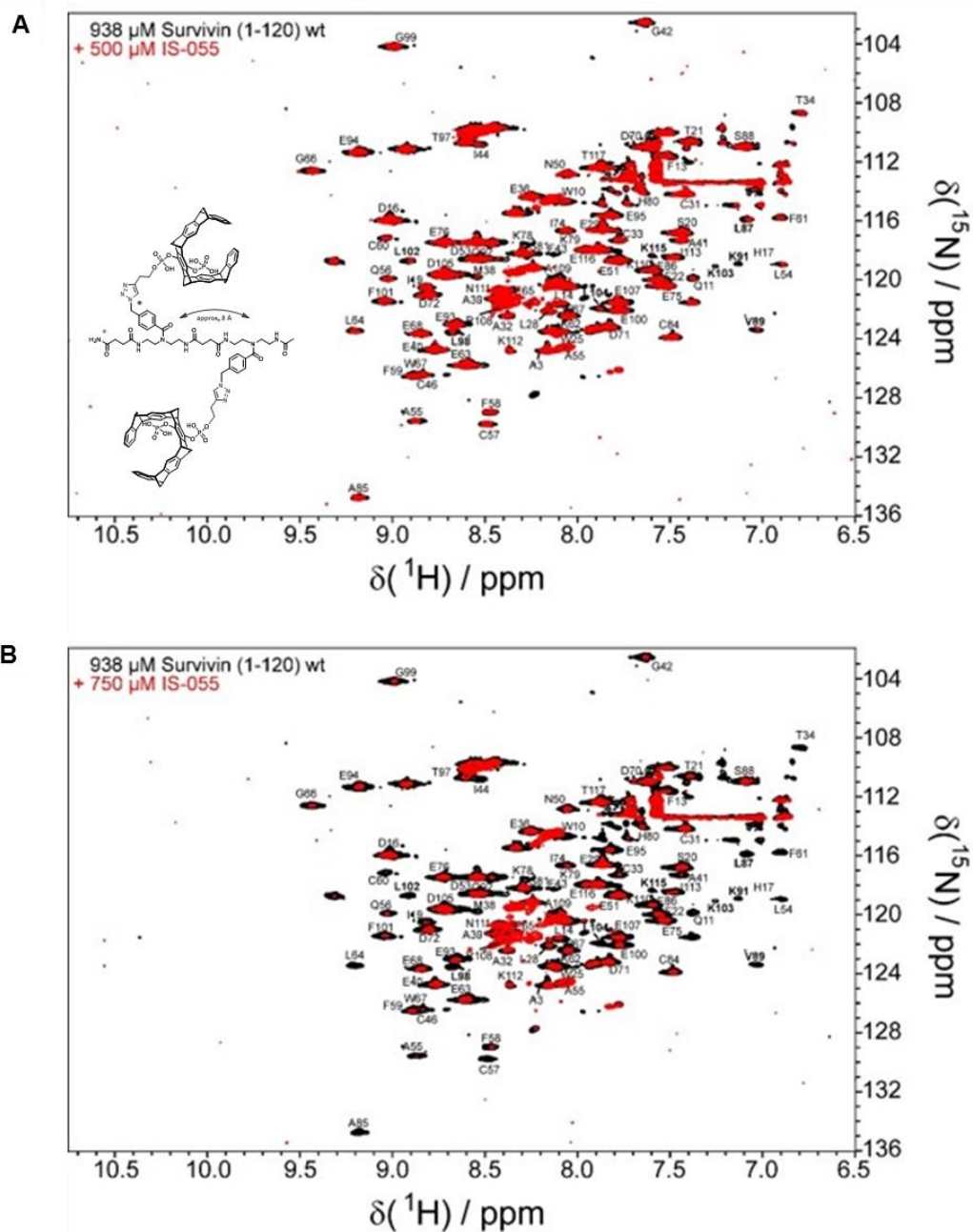
Figure A4: ^{15}N-HSQC NMR spectra of 15N-labeled Survivin120 WT in the absence (black) and presence (red) of short oligomer dTW.

^{1}H-^{15}N-BEST-TROSY-HSQC spectra of 938 µM ^{15}N-labeled Survivin${}_{120}$ before (black) and after (red) titration of 500 µM (A) and 750 µM (B) short oligomer double-tweezer. The purification of ^{15}N-labeled Survivin${}_{120}$, NMR measurements and subsequent analyses were conducted by Dr. Christine Beuck (Bayer group, University of Duisburg-Essen). Assigned signals are labeled.

VECTOR MAPS
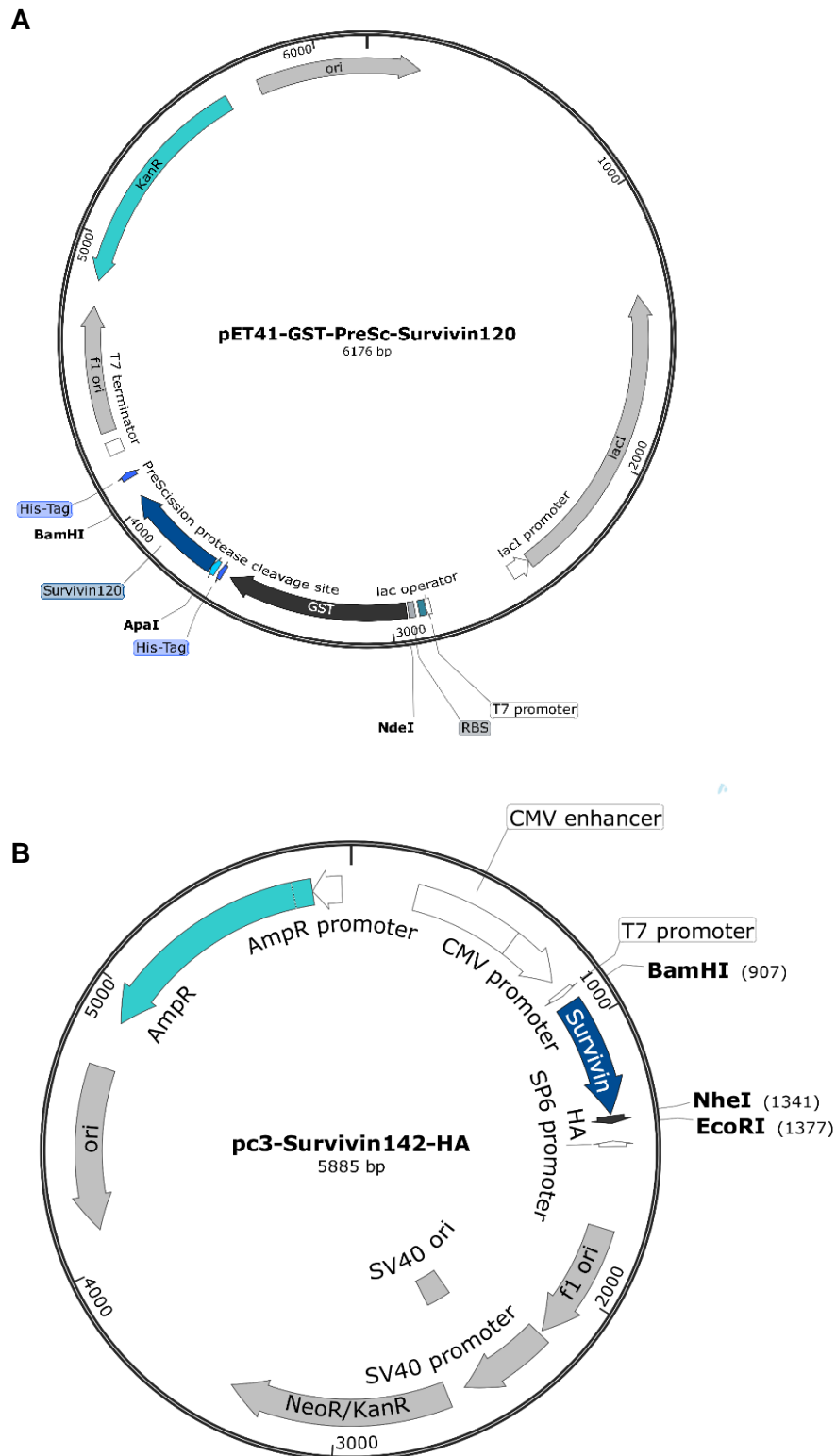
Figure A5: Vector maps of selected constructs.

A) Prokaryotic expression vector pET41. B) Eukaryotic expression vector pC3.

6.2 LIST OF ABBREVIATIONS

µ	Micro
A	Ampere
Å	Angström
aa	Amino acid
AML	Acute myeloid leukemia
Apaf-1	Apoptotic protease-activating factor 1
Approx.	Approximately
APS	Ammonium persulfate
BADS	p-(azidomethyl)benzoyl diethylenetriamine succinic acid
BAX	Bcl-2-associated X protein
Bcl-2	B-cell lymphoma 2
PDB	Protein Data Bank
BIR	Baculovirus IAP repeat
BIRC5	Baculoviral IAP Repeat Containing 5
BMRB	Biological Magnetic Resonance Data Bank
BRCA1	Breast cancer 1
BSA	Bovine serum albumin
c	Centi
Carb	Carbenicillin
CARD	Caspase recruitment domain
Caspase	Cysteinyl-aspartate specific protease
CD95	Cluster of differentiation 95
CDK	Cyclin-dependent kinase
CPC	Chromosomal passenger complex
CRC	Collaborative Research Centre
CRIME	Crm1, importin-β etc.
Crm1	Chromosome region maintenance 1
Da	Dalton
DIABLO	Direct IAP-binding protein with low pI
DMEM	Dulbecco's Modified Eagle Medium
DNA	Deoxyribonucleic acid
dNTP	Deoxynucleotide triphosphate
DPBS	Dulbecco's Phosphate-Buffered Saline

DTT	Dithiothreitol
dTW	Double tweezer
EDS	(Ethylenedioxy)bis(ethylamine) succinic acid (EDS)
EDTA	Ethylenediaminetetraacetic acid
EBI	European Bioinformatics Institute
EMBL	European Molecular Biology Laboratory
FADD	FAS-associated death domain
FCS	Fetal calf serum
FDA	Food and Drug Administration
FG	phenylalanine- and glycine rich
G	Gap
GCP	Guanidiniocarbonyl pyrrole
GDP	Guanosine diphosphate
GFP	Green fluorescent protein
GSH	glutathione
GST	Glutathione *S*-transferase
GTP	Guanosine triphosphate
H	HEAT repeat
h	Hour
HBXIP	Hepatitis B X-interacting protein
HEAT	Huntington elongation factor 3, regulatory subunit A of protein phosphatase 2A and the P3 kinase TOR1
His	Histidine
HLA	Human leukocyte antigen
HRP	Horseradish peroxidase
HSQC	Heteronuclear single quantum correlation
IAP	Inhibitor of apoptosis
IBM	IAP binding motif
INCENP	Inner centromere protein
ITC	isothermal titration calorimetry
k	Kilo
Kap	karyopherin
Kapβ1	karyopherinβ1
KLD	Kinase-Ligase-DpnI
l	Liter

LB	Luria-Bertani
LMB	Leptomycin B
M	Mitosis
M	Mol/liter
m	Meter
m	Milli
mRNA	Messenger RNA
n	Nano
NES	Nuclear export signal
Ni	Nickel
NLS	Nuclear localization signal
NMR	Nuclear magnetic resonance
NP40	Nonidet P40
NPC	Nuclear pore complex
NTA	Nitrilotriacetic acid
NUP	Nucleoporin
OD	Optical density
PAGE	Polyacrylamide gel electrophoresis
PBS	Phosphate-buffered saline
PCR	Polymerase chain reaction
pH	Potentia Hydrogenii
PMSF	Phenylmethanesulfonylfluoride
PPI	Protein-protein interaction
Ran	Ras-related nuclear protein
RanBP	Ran-binding protein
RanGAP	Ran-GTPase-activating protein
RanGEF	Ran guanine nucleotide exchange factor
RING	Really interesting new gene
RIPA	Radioimmunoprecipitation assay buffer
RNA	Ribonucleic acid
RT	Room temperature
S	Synthesis
SDS	Sodium dodecylsulfate
s.e.m.	Standard error of the mean
si	Small interfering

SINE	Selective inhibitor of nuclear export
Smac	Second mitochondria-derived activator of caspase
SOC	Super Optimal Broth with Catabolite repression
Surv	Survivin
TAE	Tris-acetate-EDTA
TBS	Tris-buffered saline
TBST	Tris-buffered saline/Tween
TEMED	N,N,N',N'-Tetramethylethylenediamine
TNF	Tumor necrosis factor
TRAIL	Tumor Necrosis Factor Related Apoptosis Inducing Ligand
Tris	Tris(hydroxymethyl)aminomethane
Tris-HCl	Tris hydrochloride
TW	Tweezer
UBA	Ubiquitin associated domain
UV	ultraviolet
V	Volt
Vs.	Versus
WT	Wildtype
XIAP	X-linked inhibitor of apoptosis protein
Zn	Zinc
°C	Degree Celsius

6.3 LIST OF FIGURES

6.4 LIST OF TABLES

6.5 LIST OF AMINO ACIDS

Table A.1: Amino acids and their one letter codes.

one letter code	amino acid
A	alanine
C	cysteine
D	aspartic acid
E	glutamic acid
F	phenylalanine
G	glycine
H	histidine
I	isoleucine
K	lysine
L	leucine
M	methionine
N	asparagine
P	proline
Q	glutamine
R	arginine
S	serine
T	threonine
V	valine
W	tryptophan
Y	tyrosine

DANKSAGUNG

Zuallererst möchte ich mich ganz besonders bei Prof. Dr. Shirley Knauer dafür bedanken, dass sie mir die Möglichkeit geben hat, meine Doktorarbeit in ihrer Gruppe anzufertigen und an diesem Thema und anderen spannenden Projekten arbeiten zu dürfen. Vielen Dank für deine Ratschläge und deine Unterstützung während meiner Promotion.

Ganz herzlich möchte ich mich bei Prof. Dr. Peter Bayer dafür bedanken, dass er mein zweiter Mentor im Rahmen des CRC-1093-Graduiertenkollegs war. Danke für die wissenschaftliche Unterstützung und für die Übernahme des Zweitgutachtens dieser Arbeit.

Herzlich möchte ich mich bei allen aktuellen und ehemaligen Kollegen der AG Knauer bedanken. Mein besonderer Dank gilt Cecilia und Elli für das Korrekturlesen meiner Arbeit!

Cecilia danke ich außerdem für die tolle Zeit in unserem gemeinsamen Büro, für die vielen Sporteinheiten und *Social Events*, die sie organisiert hat, die Gespräche über Katzen und Meerschweinchen und die stetige Versorgung mit Nervennahrung und Tee. Besonders danken möchte ich Elli dafür, dass sie immer alles im Blick hatte und mir mit Rat und Tat beiseite stand. Vielen Dank an Lisa, dass sie nicht nur ihre Labrotation und ihre Masterarbeit bei mir gemacht hat, sondern auch gleich noch für ihre Doktorarbeit in unserer Gruppe geblieben ist. Danke für die Aufmunterungen, wenn einmal etwas nicht klappte. Außerdem möchte ich mich bei Astrid für ihre hilfreichen Ratschläge und leckeren Backkünste bedanken. Großer Dank an Katha für das Organisieren von Grillpartys und für die Aufrufe zum Pubquiz. Alex danke ich dafür, dass ihm immer ein Witz einfällt und er sich um die Eis- und Kuchenreste kümmert. Vielen Dank an Paul für seine Hilfe bei Proteinreinigungen und die Übernahme des Survivin-Projekts. Des Weiteren danke ich Kay für die prompte Erledigung von Bestellungen, Reiseanträgen und das Lösen sonstiger Problemchen. Ein Riesendank an Sandra dafür, dass sie mich von Anfang an mit in das Survivin-Tweezer-Projekt einbezogen hat und ich auf ihrer tollen Vorarbeit aufbauen konnte.

Ich möchte mich auch bei allen Studenten bedanken, die während der letzten Jahre in unserer Gruppe waren und für Abwechslung gesorgt haben: Isa, Max, Lars, Pascal, Sebastian, Lara, Jessi, Marcel, Marina, Sarah, Daniela, Steffi, Philip, Jana…

Ein großer Dank geht an alle Kooperationspartner, mit denen ich während meiner Promotion zusammenarbeiten durfte. Allen voran danke ich Christine für die Unterstützung während der großen Survivin-Krise, für die Hilfe bei der Auswertung meiner Daten, für das Korrekturlesen und dafür, dass sie immer ein offenes Ohr für mich hatte. Herzlichen Dank an Inesa für die

PUBLICATIONS

2020

Vallet, Cecilia; Aschmann, Dennis; Beuck, Christine; Killa, Matthias; <u>Meiners, Annika;</u> Mertel, Marcel; Ehlers, Martin; Bayer, Peter; Schmuck, Carsten; Giese, Michael; Knauer, Shirley (2020): **Functional disruption of the cancer-relevant interaction between Survivin and Histone H3 with a guanidiniocarbonyl pyrrole ligand.** *Angewandte Chemie International Edition, 59(14)*, 5567-5571.

2017

<u>Meiners, Annika;</u> Meyer-Ács, Mira; Bondarenko, Elena; Steinhoff, Heinz-Jürgen; Mittmann, Karin (2017). **Conjugation of spin labeled proteins to fluorescent quantum dots.** *Materials Today: Proceedings*, *4*, S180-S187.

In revision

<u>Meiners, Annika;</u>‡ Bäcker, Sandra;‡ Heid, Christian;‡ Hadrovic, Inesa;‡ Beuck, Christine; Ruiz-Blanco, Yasser; Mieres-Perez, Joel; Pörschke, Marius; Grad, Jean-Noël; Vallet, Cecilia; Hofmann, Daniel; Bayer, Peter; Sanchez-Garcia, Elsa; Schrader, Thomas; Knauer, Shirley (2020): **Targeting a protein epitope: Specific inhibition of the Survivin-CRM1-interaction by peptide-modified Molecular Tweezers.** *Nature Communications*, in revision.
‡ equal contribution

Submitted

van der Meer, Selina; Hadrovic, Inesa; <u>Meiners, Annika</u>; Heggen, Marc; Loza, Kateryna; Knauer, Shirley K.; Bayer, Peter; Schrader, Thomas; Beuck, Christine; Epple, Matthias (2020): **New Tools to Probe the Protein Surface: Ultrasmall Gold Nanoparticles carry Amino Acid Binders**. Submitted to *Chemistry – A European Journal.*

In preparation

Zimmermann, Alexander; Vallet, Cecilia; <u>Meiners, Annika</u>; Aschmann, Dennis; Beuck, Christine; Brabender, Max; Killa, Matthias; Bayer, Peter; Knauer, Shirley; Voskuhl, Jens; Giese, Michael (2020): **Chemical modification of guanidiniocarbonyl pyrrole ligands to efficiently target the Survivin-Histone H3 interaction** (working title).

PRESENTATIONS AND AWARDS

PRESENTATIONS

CRC 1093 Bi-Weekly Seminar of the Integrated Graduate School, University of Duisburg-Essen (30th April 2020): **"Rational targeting of Survivin's nuclear export signal by supramolecular ligands"**; virtual presentation.

CRC 1093 International Symposium 2019 "Supramolecular Principles in Biological Systems", Essen (10–12th September 2019): **"Enhancement of supramolecular Survivin NES binder specificity"**; poster presentation.

Joint CRC 858 (University of Münster) and CRC 1093 (University of Duisburg-Essen) Graduate Student Symposium 2018 "Synergistic and Supramolecular Aspects of Chemistry and Biology", Billerbeck (29–31st August 2018): **"Rational targeting of intracellular protein transport signals by supramolecular ligands"**; poster presentation.

CRC 1093 Bi-Weekly Seminar of the Integrated Graduate School, University of Duisburg-Essen (12th June 2018): **"Rational targeting of intracellular protein transport signals by supramolecular ligands"**; oral presentation.

AWARD AND SCHOLARSHIP

06/2016 – 08/2016   PROMOS Internship abroad scholarship

06/2015   Hochschulpreis 2015 - Award for the excellent bachelor thesis "Konjugation von spin-markierten Proteinen mit fluoreszierenden Quantum Dots."

CURRICULUM VITAE

The curriculum vitae is not included for reasons of data protection.

EIDESSTATTLICHE ERKLÄRUNG

Erklärung:

Hiermit erkläre ich, gem. § 7 Abs. (2) d) + f) der Promotionsordnung der Fakultät für Biologie zur Erlangung des Dr. rer. nat., dass ich die vorliegende Dissertation selbständig verfasst und mich keiner anderen als der angegebenen Hilfsmittel bedient, bei der Abfassung der Dissertation nur die angegeben Hilfsmittel benutzt und alle wörtlich oder inhaltlich übernommenen Stellen als solche gekennzeichnet habe.

Essen, den _____   _____

Annika Meiners

Erklärung:

Hiermit erkläre ich, gem. § 7 Abs. (2) e) + g) der Promotionsordnung der Fakultät für Biologie zur Erlangung des Dr. rer. nat., dass ich keine anderen Promotionen bzw. Promotionsversuche in der Vergangenheit durchgeführt habe und dass diese Arbeit von keiner anderen Fakultät/Fachbereich abgelehnt worden ist.

Essen, den _____   _____

Annika Meiners

Erklärung:

Hiermit erkläre ich, gem. § 6 Abs. (2) g) der Promotionsordnung der Fakultät für Biologie zur Erlangung der Dr. rer. nat., dass ich das Arbeitsgebiet, dem das Thema *„Rational targeting of Survivin's nuclear export signal by supramolecular ligands – enhancement of NES binder specificity"* zuzuordnen ist, in Forschung und Lehre vertrete und den Antrag von *Annika Meiners* befürworte und die Betreuung auch im Falle eines Weggangs, wenn nicht wichtige Gründe dem entgegenstehen, weiterführen werde.

Essen, den _____   _____

Prof. Dr. Shirley Knauer

145